

**INVESTIGATION OF THERMALLY SPRAYED  $\text{Al}_x\text{CrCoFeNi}$   
HIGH-ENTROPY ALLOYS FOR HIGH-TEMPERATURE  
EROSION AND OXIDATION RESISTANCE**

Thesis Submitted for the Award of the Degree of

**DOCTOR OF PHILOSOPHY**

**in**

**Mechanical engineering**

**By**

**BALA GANESH REDDY MAJJI**

**Registration Number: 41900809**

**Supervised By**

**Dr. Hitesh Vasudev (24804)**

**Department of Mechanical Engineering  
(Professor)**

**Lovely Professional University, Punjab**

**Co-Supervised by**

**Dr. Amit Bansal**

**Mechanical Engineering (Assistant Professor)**

**IKGPTU, Jalandhar**



**LOVELY PROFESSIONAL UNIVERSITY, PUNJAB  
2025**

## DECLARATION

I, hereby declared that the presented work in the thesis entitled “INVESTIGATION OF THERMALLY SPRAYED  $\text{Al}_x\text{CrCoFeNi}$  HIGH-ENTROPY ALLOYS FOR HIGH-TEMPERATURE EROSION AND OXIDATION RESISTANCE” in fulfilment of degree of Doctor of Philosophy (Ph. D.) is outcome of research work carried out by me under the supervision Dr.Hitesh Vasudev, working as Professor, in the School Of Mechanical Engineering of Lovely Professional University, Punjab, India and Dr .Amit Bansal, IKGPTU, Hoshairpur. In keeping with general practice of reporting scientific observations, due acknowledgements have been made whenever work described here has been based on findings of another investigator. This work has not been submitted in part or full to any other University or Institute for the award of any degree.



**(Signature of Scholar)**

Name of the scholar: BALA GANESH REDDY MAJJI

Registration No.:41900809

Department/school: Mechanical Engineering

Lovely Professional University,

Punjab, India

## CERTIFICATE

This is to certify that the work reported in the Ph.D. thesis entitled “INVESTIGATION OF THERMALLY SPRAYED  $\text{Al}_x\text{CrCoFeNi}$  HIGH-ENTROPY ALLOYS FOR HIGH-TEMPERATURE EROSION AND OXIDATION RESISTANCE” submitted in fulfilment of the requirement for the reward of degree of **Doctor of Philosophy (Ph.D.)** in the School of Mechanical Engineering, is a research work carried out by Pardeep Singh, Registration No.41900809 is bonafide record of his/her original work carried out under my supervision and that no part of thesis has been submitted for any other degree, diploma or equivalent course.



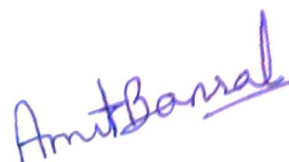
**Supervised By**

**Dr. Hitesh Vasudev (24804)**

**School of Mechanical Engineering**

**(Professor)**

**Lovely Professional University, Punjab**



**Co-Supervised by**

**Dr. Amit Bansal**

**Mechanical Engineering (Assistant Professor)**

**IKGPTU, Jalandhar**

## ABSTRACT

Power plants and the industry sector face losses to the components like super heaters, economizer, heat exchangers, piping and chimneys in petroleum industry. The continual advances in materials development will demand still higher operation temperatures for such components. The types of degradation phenomena that affect materials used in high-temperature applications can vary greatly depending on the application, including wear, solid particle abrasion, overheating, erosion-corrosion, high-temperature corrosion, and so on.

The plasma spray process was utilized extensively amongst processes and is popular as a viable technology for various applications. The plasma spray process gained popularity in many industries as it produces coatings of superior quality, flexibility, and cost-effectiveness. The high velocity and moderate temperature in this process result in lower porosity, high hardness, superior bonding between substrate and coating, high abrasion resistance, high density, fine finishing capability as compared to other coating processes, and lower oxide content. The capacity of materials to produce protective oxide scales on the surfaces is directly correlated with how well they operate in high-temperature aggressive situations. The coatings are anticipated to create protective oxides with a modest growth rate during service, which should prevent corrosive species from diffusing into the coating and subsurface of the coated material.

Al<sub>x</sub>CrCoFeNi high-entropy alloys coatings are applied for protection against oxidation and erosion wear at higher temperatures. The present research was conducted to explore the high temperature oxidation and erosion performance of SS-304 substrate and 3 different compositions of coatings viz. Al<sub>0</sub>CrCoFeNi (A1), Al<sub>0.5</sub>CoFeNi (A2) and Al<sub>1.0</sub>CoFeNi (A3) by plasma spray coating process. Here, the fraction  $x$  varies from 0 to 1 ( $x = 0$ ,  $x = 0.5$  and  $x = 1$ ) of Al in HEAs were studied; and three coatings are deposited. Thus, improving the life of the components made with SS-304 by applying such coatings protecting them against oxidation and erosion wear is our main aim behind developing this type of coatings. Spraying of plasma coatings have been done in M/S “Metallizing Equipment Corporation Pvt. Ltd(pf). Ltd.” (MECPL), Jodhpur, India.

The characterization of the deposited coatings has been carried out using techniques like EDS (“Energy Dispersive Spectroscopy”), SEM (“Scanning Electron Microscope”), XRD (“X-Ray Diffractometer”), OM (“Optical Microscope”), Micro-hardness Tester and Porosity Analyser. The thermal spray process of plasma spray was utilized to deposit coatings of different compositions of Al<sub>x</sub>CrCoFeNi powders on grey cast iron up to the thickness range of 200-230  $\mu\text{m}$ . The porosity in general, has been found to be less than 2.5% for all the coatings. A2 and A3 coated samples have shown the least value of surface porosity in order of 2.1 and 1.5, respectively. The plasma sprayed



coatings were discovered to have a micro-hardness that was more than the GCI. The A3 coating, which has a hardness of  $540 \pm 11 \text{ HV}_{0.3}$ , has enabled the hardness to be increased to its maximum value. The higher hardness ( $530 \pm 15 \text{ HV}_{0.3}$ ) of  $\text{Al}_1\text{CoCrFeNi}$  coating is attributed to the presence of the BCC phase in this coating.

All the plasma-sprayed  $\text{Al}_x\text{CrCoFeNi}$  coatings were found beneficial in increasing the resistance to oxidation and erosive wear.

According to ASTM-G76, erosion testing was done with an air jet erosion tester (“Model: TR-471-800, Make: Ducom Instruments Pvt. Ltd., Bangalore, India”). Additionally, the erosion behavior of uncoated and coated SS-304 has been evaluated at  $800^\circ\text{C}$  at impact angles of  $30^\circ$  &  $90^\circ$ . For both the SS-304 substrate and coated sample, the “erosive wear rate” ( $\text{g/g}$ )—defined as the ratio of “wear mass” loss in g to the supplied erodent mass in g—has been computed. The eroded samples were examined using the SEM (“Scanning Electron Microscopy”) method at both higher and lower magnifications. The main reason for the enhanced performance is the solid solution strengthening in high-entropy alloys (HEAs) due to a mismatch in atomic size differences among the elements, which is caused by the substantial lattice distortion caused by the higher aluminum content.

The eroded surface’s morphology shows the crack arrest by the coatings and micro-cutting and ploughing is responsible for the plastic deformation of coatings at a  $30^\circ$  impact angle, whereas the repetitive effect of erodent particles caused fatigue at a  $90^\circ$  impact angle and showed the brittle mode of erosion. The embedment of sand particles in the substrate was clearly revealed in the SEM micrographs. Based on the erosive wear rate, the erosion rates for the investigated coated and uncoated steel at  $90^\circ$  and  $30^\circ$  impact angles can be arranged in the following order:

**As-sprayed:**  $\text{Al}_{1.00}\text{CoFeNi}$  (A3) >  $\text{Al}_{0.50}\text{CoFeNi}$  (A2) >  $\text{Al}_0\text{CrCoFeNi}$  (A1), A718 > SS-304  
With the increase in Al content in  $\text{Al}_x\text{CrCoFeNi}$ , the erosion resistance significantly increased.

For 50 cycles, the high-temperature oxidation test was carried out at  $800^\circ\text{C}$ . Maximum oxidation resistance has been established by the  $\text{Al}_1\text{CrCoFeNi}$  coating. A maximum microhardness of  $540 \pm 11 \text{ HV}_{0.3}$  was reported for values of 1. Superior oxidation resistance has been demonstrated by the coating with an x value of 1, requiring a minimum weight gain of  $3.3 \text{ mg/cm}^2$ .

The primary cause of the improved performance in high-entropy alloys (HEAs) is the solid solution strengthening brought about by an imbalance in the atomic sizes of the constituent elements as a result of significant lattice distortion brought on by the increased aluminum content. The sliding wear resistance has been observed in the following sequence:

**As-sprayed:**  $\text{Al}_{1.00}\text{CoFeNi}$  (A3) >  $\text{Al}_{0.50}\text{CoFeNi}$  (A2) >  $\text{Al}_0\text{CrCoFeNi}$  (A1), A718 > SS-304

## ACKNOWLEDGEMENT

First and foremost, I am very much heartily thankful to my dissertation Supervisor, Dr. **Hitesh Vasudev**, Professor in School of Mechanical Engineering, Lovely Professional University, for his invaluable guidance and support during the present research work.

I wish to thank **Dr. Amit Bansal**, co-supervisor, Assistant Professor Mechanical Engineering, IKGPTU, Kapurthala.

I would like to thank my friends, **Mr. Pardeep Singh**, **Mrs. Satyavathi**, and all the fellows who helped me directly or indirectly during the entire period of this work.

I express my profound regards to my parents for their blessings and for being the main source of inspiration to succeed in my endeavours. I would like to express particular thanks to my father **Mr. M.A.R. Reddy**, my mother, **Mrs. Majji Leelavathi** for her advises, care and love. I would like to express particular thanks to my Guardian **Mrs. Nekkanti Madhuri** for his encouragement and financial support to pursue Higher studies, and my beloved Sister and brother-in-law **Mr.J. Ravindra Varma** and **Mrs. Majji Nuthan Soumya** for his love and care. I feel blessed for having Brother **Mr. Aashish Kumar** and thank for his constant support. I feel proud to my grandfather and grandmother **Mr. B. Gurumurthy Reddy** and **Mrs. Rajeswari Reddy** for their extensive love and supporting me in my entire life.

I would like to thank everyone who supported me for completing this work successfully and I express my apology that I could not mention everyone individually. Above all, I would like to express my sincere gratitude from the core of my heart to **ALMIGHTY** for giving courage, strength and patience to carry out my research out.

**(BALA GANESH REDDY.MAJJI)**

## TABLE OF CONTENTS

Title / Content	Page No.
<b>Declaration</b>	ii
<b>Certificate</b>	iii
<b>Abstract</b>	iv–v
<b>Acknowledgement</b>	vi
<b>Table of Contents</b>	vii–ix
<b>List of Figures</b>	x–xi
<b>List of Tables</b>	xii
<b>CHAPTER 1: INTRODUCTION</b>	1–13
1.1 Surface Degradation	1–2
1.2 High–Temperature Erosion	3
1.3 High–Temperature Oxidation	3–4
1.4 Preventive Measures	4–5
1.5 Coating Techniques	5
1.5.1 Thermal Spray Coating Methods	5–7
1.5.2 HVOF Process	7–10
1.5.2.1 Characteristics of Plasma Spray Process	10–11
1.5.2.2 Advantages of Plasma Spray Process	11–12
1.5.2.3 Applications of Plasma Spray Process	12–13
<b>CHAPTER 2: LITERATURE REVIEW</b>	<b>14–44</b>
2.1 Materials for High-Temperature Applications	14–16
2.2 Oxidation & Thermally Sprayed HEA Wear Behavior	16–17
2.3 HEAs Developed through Plasma Spray	17–19
2.4 HEAs Developed through Cold Spray	19–23
2.5 Protective Coatings	23–24

2.6	Emerging Methods to Control High–Temperature Wear Rate	24
2.6.1	Thermal Spray Coatings	24–25
2.6.2	Powder Thermal Spray Coatings	25–26
2.7	Behavior of Coatings at High Temperature	26–30
2.8	Oxidation Behaviour of HEAs	30–37
2.9	AlCoCrFeNi	37–42
2.10	Problem Formulation	42–43
2.11	Research Gaps	43
2.12	Objectives of Research Work	43–44
<b>CHAPTER 3: EXPERIMENTAL EQUIPMENT AND PROCEDURES</b>		<b>45–55</b>
3.1	Selection of Substrate	45
3.2	Deposit of Coatings	45
3.2.1	Preparation of Substrate Material	45–46
3.2.2	Coating Powder	46–47
3.2.3	Deposition of Coatings	47–49
3.3	Preparation and Testing	49
3.3.1	Preparation of Specimen	49
3.3.2	Coating of Specimen	49–50
3.3.3	Surface Roughness and Porosity Measurement	50
3.3.4	Microhardness Measurement	50
3.3.5	XRD Analysis	50
3.3.6	FE-SEM and EDS Analysis	51
3.3.6.1	Surface and Cross-Sectional Analysis	51
3.3.6.2	Elemental Mapping Analysis	51
3.4	High–Temperature Wear Behaviour	52
3.4.1	Air Jet Erosion Analysis	52–53

3.5	Oxidation Analysis	53–54
<b>CHAPTER 4: RESULTS AND DISCUSSION</b>		<b>56–81</b>
4.1	SS-304 Substrate	56
4.1.1	Chemical Composition of Substrate	56
4.2	SEM–EDS Examination	56–68
4.3	Porosity Analysis	68–69
4.4	Microhardness Evaluation	69–70
4.5	Discussion	70–72
<b>CHAPTER 5: OXIDATION ANALYSIS OF AlCoCrFeNi COATINGS</b>		<b>73–81</b>
5.1	Oxidation Test	73–74
5.2	Visual Inspection of Oxidized Samples	74–75
5.3	SEM–EDS and XRD Analysis	75–80
5.4	Summary	80–81
<b>CHAPTER 6: HIGH-TEMPERATURE EROSION TEST</b>		<b>82–89</b>
6.1	Results and Discussion	82
6.1.1	Erosion Test	82–85
6.1.2	SEM Analysis	85–88
6.2	Summary	88–89
<b>CHAPTER 7: CONCLUSION AND FUTURE SCOPE</b>		<b>90–92</b>
7.1	Conclusions	90–91
7.2	Future Scope	92
<b>Bibliography</b>		<b>93–110</b>
<b>List of Publications</b>		<b>111–113</b>

## TABLE OF FIGURES

FIGURE	CAPTION	PAGE NO.
1.1	Various classes of coatings techniques used for engineering applications (Goyal et al.2010)	6
1.2	Comparison of various thermal spray process (Tokarev,1996)	7
1.3	Schematic representative of the HVOF process and built-up mechanism of coatings (Mttews,2004)	8
2.1	Basic mechanics of HVOF spray process(Vasudevet.at.2021)	15
2.2	SEM micrographs of (a) AlSiTiCrEeCoNiMo0.5 and (b) AlSiTiCrEeNi-Mo0.5 (Haung et.al.2004)	17
2.3	SEM micrographs of AlCoCrFeNiTi0.5 coatings at (a) low and (b) higher magnifications (Anupam et.al.2019)	17
2.4	AlCoCrFeNiTi0.5 HVOF coatings Diffractograms (Anupam et.al.2019)	19
3.1	(a) front and (b) side view of shot blasting machine and (c) Blasting medium (Virgin Alumina)	45
3.2	PS apparatus used in the current research work	47
3.3	(a) Air jet erosion test ring (b) Panel of Air jet erosion test ring.	51
3.4	(a) silica tube furnace diagrammatical representation and (b) red hot oxidized sample in alumina boat	52
4.1	SEM micrographs of powder at various magnifications used for coatings 1 - AlCrCoFeNi	55
4.2	SEM -EDS of powder used for coatings AlCrCoFeNi	55
4.3	SEM micrographs of powder at various magnifications used for coatings 2 – Al0.5CrCoFeNi	56
4.4	SEM -EDS of powder used for coatings Al0.5CrCoFeNi	56
4.5	SEM micrographs of powder at various magnifications used for coatings 3 – Al1CrCoFeNi	57
4.6	SEM -EDS of powder used for coatings Al1CrCoFeNi	57
4.7	SEM Micrographs of a various magnification's coatings 1 Al0CrCoFeNi	58
4.8	X Ray maps coatings 1 Al0CrCoFeNi from surface	59
4.9	SEM cross sectional micrographs of a t various magnifications coatings 1 - Al0CrCoFeNi	60
4.10	X RAY maps coatings 1 – Al0CrCoFeNi from cross section	61
4.11	SEM micrographs of at various magnifications coatings 2 - Al0.5CrCoFeNi	61
4.12	X Ray maps coatings 1 Al0.5CrCoFeNi from surface	62
4.13	SEM cross sectional micrographs of a t various magnifications coatings 2 - Al0.5CrCoFeNi	62
4.14	X RAY maps coatings 1 – Al0CrCoFeNi from cross section	63
4.15	SEM micrographs of at various magnifications coatings 3 – Al1CrCoFeNi	63
4.16	X Ray maps coatings 1 Al0.5CrCoFeNi from surface	64
4.17	SEM cross sectional micrographs of a t various magnifications coatings 3 – Al1CrCoFeNi	64
4.18	X RAY maps coatings 1 – Al1CrCoFeNi from cross section	65
4.19	XRD of a deposited coating	66
4.20	(a&b) SEM micrographs of Al0crCiFeNi coatings (c&d) EDS mappings of Al0CrCoFeNi (e&f) SEM micrographs of Al0.5CrCoFeNi, (g&h) EDS mapping of Al0.5CrCoFeNi coatings (i&j) SEM micrographs of Al1FeCrCoNi coatings (k&l) EDS mappings of Al1CrCoFeNi	67

4.21	Microhardness Indents of all coatings	68
5.1	(a) Schematic of the tube furnace, and (b) oxidized sample in Al <sub>2</sub> O <sub>3</sub> Boat (c) Weight balance	72
5.2	Pictographs of Oxidized coating samples	74
5.3	Oxidized coatings at 900c subjected to 50 cycles of oxidation	75
5.4	(a) oxidized SS 304 substrate at high temperature and (b) area scan EDS of SS 304	75
5.5	(a) EDS mapping of oxidized SS 304 substrate at high temperature and (b) elemental distribution of oxidized SS - 304	76
5.6	oxidized surfaces of (a) C1, (b) C2 , (c) C3 coatings	78
6.1	Macrographs the SS 304 substrate specimens at (a) 30 and (B) 90 impacts angles	82
6.2	(a) Enclosed surfaces SEM micrographs of uncoated SS – 304 substrate (a) 30 and (B) 90 impact angles	83
6.3	Photograph of the various CI coated eroded samples (a) 30 and (B) 90 impact angles	83
6.4	SEM micrographs of the eroded surface of Al <sub>0</sub> CrCoFeNi (C1) coated SS 304 at 30 and 90 angle of impacts	85
6.5	SEM micrographs of the eroded surface of Al <sub>0.5</sub> CrCoFeNi (C1) coated SS 304 at 30 and 90 angle of impacts	86
6.6	SEM micrographs of the eroded surface of Al <sub>1</sub> CrCoFeNi (C1) coated SS 304 at 30 and 90 angle of impacts	87

## LIST OF TABLES

TABLE NO	CAPTION	PAGE NO
Table 1.1	Attributes for various thermal spray processes (Pawlowski, 1995).	9
Table 2.1	HEAs properties deposited using different thermal spray coating processes.	21
Table 2.2	Oxidation and Wear resistance of materials with reference to Table2.1.	22
Table 2.3	Compilation of various HEA compositions studied for their oxidation resistance in bulk form.	31 To 35
Table 3.1	Process parameters used for the Plasma spraying process.	47
Table 3.2	Air-jet erosion test parameters.	51
Table 4.1	SS-304 substrate's chemical composition.	54
Table 4.2	Designation system utilized for the coatings.	55
Table 4.3	Average coating roughness, porosity, and thickness for various coatings under investigation.	68
Table 4.4	Average microhardness of as-sprayed & post-processed coatings.	69
Table 5.1	Analyzing high temperature oxidation requires several parameters.	73
Table 6.1	Erosive wear rate of the as-sprayed AlCoCrFeNi coatings.	86



# CHAPTER 1

## INTRODUCTION

### 1.1 SURFACE DEGRADATION

Industrial sectors and power plants especially petroleum industries lose a lot of money because of wear and tear of important parts of these plants like superheaters, economizers, etc. This is particularly an issue on parts needing high oxidation and wear resistance because the service of such parts is heavily reliant on the surface integrity when operating under harsh conditions. To drive back such challenges, the advanced materials that possess superior surface characters are needed. In the latter respect, the High Entropy Alloys (HEAs) and Compositionally Complex Alloys (CCAs) or simply the multicomponent alloys were introduced specifically independently by Cantor et al. and Yeh et al. in 2004. In contrast to traditional alloys where one principal element is used (such as Ni-based superalloy), HEAs and CCAs are developed as multiple principal element alloys, either in equiatomic or nearly equiatomic proportions. The complexities of intermetallics that are otherwise created with conventional designs are avoided in this design approach which leads to their distinct and sometimes superior mechanical and chemical properties. The property tunability of these materials is very remarkable depending upon the variation in composition. Miracle et al. and Murty et al., in in depth reviews, have pointed out the enormous potential of HEAs, that in some compositions, they have the potential of performing better than traditional alloys in a wide variety of applications, particularly under harsh conditions.

As the industrial need of high-performance materials is increasing, High Entropy Alloys (HEAs) are being widely investigated with regards to oxidation resistance. The FCC+BCC/B2 phase structures have been reported in several HEAs, especially those with high nickel (Ni) and cobalt (Co) and low aluminum (Al) concentrations, which can be compared to traditional MCrAlY coatings to some extent (Tsao et al., 2016; Chen et al., 2018a; Kai et al., 2019). The higher the amount of aluminum, the better the oxidation resistance of such alloys, especially during high temperatures more than 1000 degrees Celsius (Butler et al., 2016a; Liu et al., 2019; Wang et al., 2019). Such improvement is basically credited to the fact that there was an increment in the production of a protective alumina ( $\text{Al}_2\text{O}_3$ ) layer at the early stages of oxidation.

Also, other oxygen-active inerts, including silicon (Si) and titanium (Ti) have been reported to improve oxidation resistance when alloyed in small proportions together with other materials (Zhang et al., 2013; Hsu et al., 2016). Nevertheless, the additions that are too high, i.e., approaching equiatomic concentrations, can lead to the appearance of non-protective oxides, hence reducing surface stability. The parabolic oxidation kinetics is common to most AlCoCrFeNi-based HEAs and the conventional MCrAlY and aluminide coatings (Butler et al., 2015; Daoud et al., 2015). Another study by Lu et al. also showed that further enhance oxidation resistance could be achieved by trace additions of rare earth (RE) elements (Tonelson et al., 2020).

Transferring these characteristics to thermal spray HEA coatings has also developed significant traction, motivated by the potential real-life application such as bond coats (Li et al., 2018a). Literature presents reports on several alloys based on the  $\text{Ni}_{0.5}\text{Co}_{0.5}\text{Fe}_{0.5}\text{Cr}_{1.5}\text{Si}_{0.5}\text{Al}_{0.2}\text{Ti}_{0.2}$  composition family, studied variously by casting-crushing followed by sintering (Hsu et al., 2016); casting – crushing followed by thermal spray (APS) (Hsu et al., 2017a) and high velocity oxy fuel spray (HVOF) (Hsu et al., 2017b); and gas atomization followed by thermal spray (APS, HVOF and warm spray) (Hsu et al., 2018). In terms of oxidation resistance, these compositions typically developed an underlying alumina layer and overlying less protective mixed oxides. Further, upon oxidation, Al-depleted zones were observed in the coating as well as the substrate, with severe interdiffusion between the two. Gas atomized and warm sprayed  $\text{NiCo}_{0.6}\text{Fe}_{0.2}\text{Cr}_{1.3}\text{SiAl}$  performed similarly to conventional MCrAlY alloys at 1100 °C and developed only a single protective alumina layer. Bhattacharya et al. (2016) used CALPHAD to determine Al-rich compositions that did not undergo phase changes in the temperature range of use, resulting in  $\text{Al}_{30}\text{Co}_{22}\text{Cr}_{23}\text{Ni}_{23}\text{Si}_2$  (at.%). Using mechanically alloyed feedstock, they synthesized coatings via APS and HVOF, with the latter exhibiting excellent oxidation resistance at 1050°C and 1150°C. Jadhav et al. (2019) also studied compositions of this family, with  $\text{FeCoCrNi}_2\text{Al}$  exhibiting the best oxidation resistance at 1050 °C for 300h of testing. These alloys were synthesized by mechanical alloying, mechanically activated sintering, and spark plasma sintering, and upon oxidation developed protective  $\alpha\text{-Al}_2\text{O}_3$ . Tsai et al. (2016) studied  $\text{Al}_{0.2}\text{Co}_{1.5}\text{CrFeNi}_{1.5}\text{Ti}_{0.3}$ , which showed improved oxidation resistance at 900 and 1000 °C after an aluminizing treatment, surviving without spallation for over 400h.

According to this research, HEAs have a bright future in oxidation-resistant applications as bond coatings. Since this is yet a growing field, the following three major gaps can be identified in the literature: (i) a mechanistic understanding of HEA coating development during thermal spray is required, diagnosing the dominating process parameters and microstructural features; (ii) the vast compositional hyperspace made available by the HEA concept demands exploration for novel compositions; (iii) the wide spectrum of thermal spray technologies remains to be traversed for

HEAs, providing the appropriate processing route for the potential next generation bond coats. These issues have been attempted to be tackled in this thesis, under a limited scope but in a detailed manner.

## **1.2 HIGH-TEMPERATURE EROSION.**

The erosion of the surface takes place owing to the striking of abrasive particles on the surface and this produces craters, pores, and detachment of material from the working area. Praveen et al. (2015) reported the formation of cracks and erosion at the surface of SS-304-graded stainless steel. Moreover, the different failure mechanisms have been studied at several impact angles. The unburned carbon and oxide particles at high temperatures strike the material's surface and this results in the surface failure of the component. A higher maintenance cost is required there and sometimes replacement of components is needed. These are stringent problems in industries and researchers have been continuously developing new materials for high-temperature applications.

The failure of the surface due to oxidation and erosive wear can be found in engineering components used in automobiles, aerospace, production lines, and the petrochemical industry. Corrosion and erosive wear both are common forms of surface degradation of engineering components.

Erosive wear is owing to the striking of hard particles on the surface (Finnie, 1960). The protection of surfaces is therefore required which can provide wear resistant in the type of coating and is a good solution to prevent the surfaces from wear (Ma et al. 2014; Balla et al. 2010; Gupta et al. 2011 and Oladijo et al. 2012).

## **1.3 HIGH-TEMPERATURE OXIDATION**

Dealing with high temperature oxidation poses a considerable challenge for various components in the petroleum industry. These include superheaters, economizers, heat exchangers, piping, and chimneys. This process involves a chemical reaction between metallic objects and atmospheric oxygen, resulting in the formation of metal oxides at high temperatures.

Superheaters, when exposed to high-temperature gases, are especially prone to corrosion caused by chlorine compounds. Economizer tubes are susceptible to corrosion from both the flue gas components and the corrosive elements they come into contact with. In addition, the heat transfer through boiler tubes is hindered by the corrosion products in the feedwater systems, leading to

excessive heat and eventual tube malfunction. This corrosion-induced damage can result in unexpected shutdowns, which can be financially burdensome for petroleum operations.

The petroleum industry relies on advanced coating technologies to mitigate the effects of high temperature oxidation. Diffusional coatings, such as chromium-rich and aluminide coatings, offer excellent defense against hot corrosion and oxidation. Overlay coatings, such as MCrAlY systems, provide superior protection against high-temperature corrosion and oxidation when compared to diffusion coatings. Thermal barrier coatings (TBCs) are utilized to lower substrate temperatures, improve engine efficiency, and minimize cooling airflow in vital components such as moving blades and combustion chambers.

When choosing metals and coatings for components in the petroleum industry that are exposed to high temperature oxidation, various factors are taken into consideration. These factors include strength, corrosion resistance, mechanical properties, and material availability. Alloys that possess excellent strength at high temperatures and are resistant to corrosion are highly favored. Coatings are carefully selected to ensure sufficient safeguard against oxidation and corrosion under the specific operating conditions.

When choosing high-temperature coatings, it's important to consider their resistance to oxidation, hot corrosion, thermal cycling, and their ability to adhere to the substrate. Advanced coatings have been engineered to withstand the demanding conditions in the petroleum industry, including elevated temperatures, increased pressures, and corrosive environments. Collaborations between coating manufacturers and the petroleum industry play a vital role in introducing innovative coating technologies to the market and promoting their widespread use.

#### **1.4 PREVENTIVE MEASURES.**

Prevention is required for life prolongation of the things Of course; corrosion and wear can't be eliminated altogether; but certainly, costs like these could have been reduced to a great extent. Countless protective techniques are training commercial industries and research is still ongoing to expand a few more areas, especially for high-temperature applications. There are some methods to reduce high-temperature wear and corrosion:

- Swapping out the bulk material for a substance that can resist extremely harsh environmental conditions is one way. With this procedure, the surface can be protected because the entire component has to be replaced.

- A surface modification of material through coating is also a way to attack the problem regarding failures of materials in high-temperature applications. A composite coating can give such a multi-set of properties at low cost by using the available coating techniques, whereas easy handling and good mechanical strength against erosion as well as sliding wear are also possible with this material (Li et al. 2013). 2003; Liu et al. (Carter and Foster, 2001; Sidky and Hocking, 1999)

The researchers have continued to work on developing new coating technology and worried about surface degradation issues of engineering applications. “Use of the coating in any of those products would increase its costs by 10%” (Matthews et al. 1998). There are certain methods to overcome the failure of material surfaces like use some ways such as shielding material, patterns of types of equipment, select alloys grades and putting protective coatings on the materials in order to aggressive environments (Stringer 1987 Heath et al. 1997). Coatings techniques offer a wide choice of materials, polymers to ceramics, and mechanical, thermal and electrical properties can be conveniently achieved for this protection ability (Sidky et al. 1999; Sidhu et al. 2005 and Chatha et al. 2012).

## **1.5 COATING TECHNIQUES.**

Coatings are utilized for room and high-temperature applications and even for aqueous conditions like seawater. The various classes of coatings that have been used for the deposition of engineering components are given in **Fig. 1.1** (Goyal et al. 2010).

The life of the material can be increased by using these techniques to prevent the formation of scales (Bala et al. 2009). Amongst the all-coating processes a thermal spray is an emerging technique to use with any class of engineering materials to achieve the relationship between multiple sets of properties.

### **1.5.1 Thermal spray coating methods.**

In the early 19<sup>th</sup> century, a scientist in Switzerland called Dr. Max Schoop designed a thermal spray process. Dr. Schoop got this idea in mind after observing his little son who was playing with toy cannon. Mr. Schoop after watching his son found that an idea if metal can be melted and then predicated in the form of spray could eventually build up and stick with that material.

In the 1970s, new techniques come in the area of thermal spray process to produce and develop high-temperature and wear-resistant materials due to the increase in demand of industry

(Knotek, 2001). The thermal spray coating approach is a widely utilized technique for surface modification in the form of coatings with a thickness even in microns.

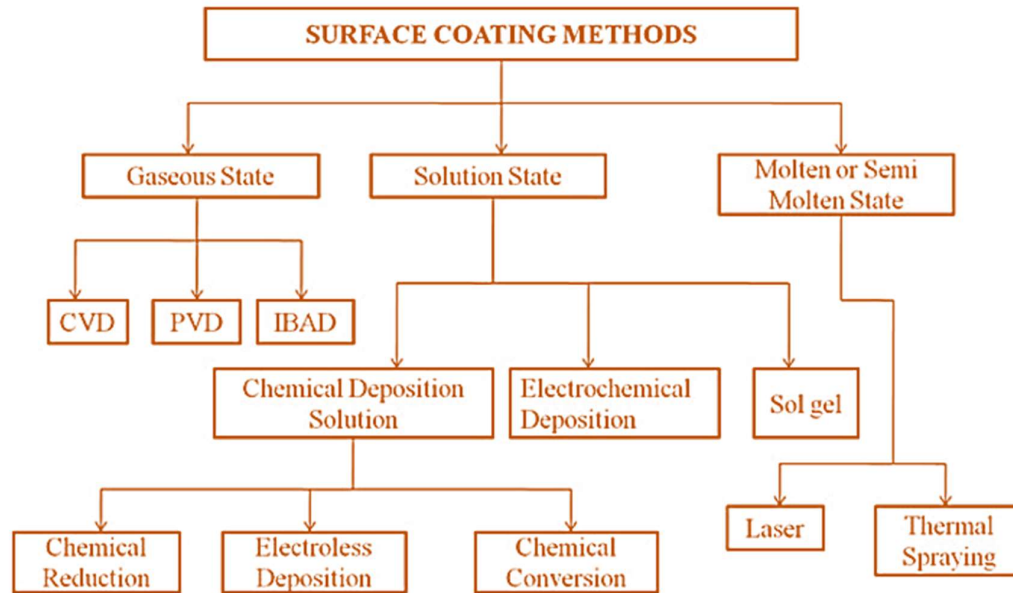


**Fig.1.1.** Various classes of coating techniques used for engineering applications (Goyal et al. 2010)

The components under erosive wear, oxidation, abrasive wear, and corrosion can be coated and protected using this technique (Ishikawa et al. 1993; Singh et al. 2015; Kumar et al. 2015; Goyal et al. 2012; Marceau and Adjorlolo; 1995; Groshart, 1995). Thermal spraying is a method for depositing any substance that does not disintegrate, or dissociate when heated, evaporate, or sublimate. The metallic and non-metallic classes include polymers, alloys, metals, ceramics, and cermet's can be sprayed by the process of thermal spray. The feedstock material is mostly used in the form of powders from nano to micron sizes. In the process of thermal spray, the feedstock material is heated and then sprayed to deposit on the semi-molten in substrate material state or molten, and on cooling this is plastically deposited on the surface in the type of splats. This approach is extensively utilized in high-temperature uses like in aerospace engineering, manufacturing processes, and space exploration (Nicoll, 1992; Nakagawa et al. 1994; Thakur et al. 2013). In particular, HVOF-sprayed coatings are utilized in engineering components for corrosion and wear resistance including engine and machine tool casings, superheaters, boiler steels, pump impellers, and pipe fitting applications (Tan et al. 2005). The thermal spraying coating techniques that are used for the deposition of the coatings for corrosion and wear resistance are given below and were reviewed by (Heath et al, 1997):

- HVOF
- Spray and fuse method
- D-Gun (Detonation Gun) spray
- Cold spraying (CS)
- Air and Vacuum plasma spraying
- Flame spraying with a wire or powder.

There are various spraying parameters of the HVOF process including particle speed, temperature of the flame are presented in **Fig.1.2**. The comparison shows that the PS (“Plasma Spray”) has a maximum temperature while cold spray has a minimum temperature. The HVOF covers both characteristics of high velocity and sufficient temperature for the coating deposition. The bond strength is achieved by good particle velocity and this results in good hardness and a coating with less porosity. HVOF was most effective for depositing cermet materials and especially corrosion-resistant alloys (hydroxyapatite, aluminium, nickel-based, stainless steels, and so on (Kuroda et al. 2008).

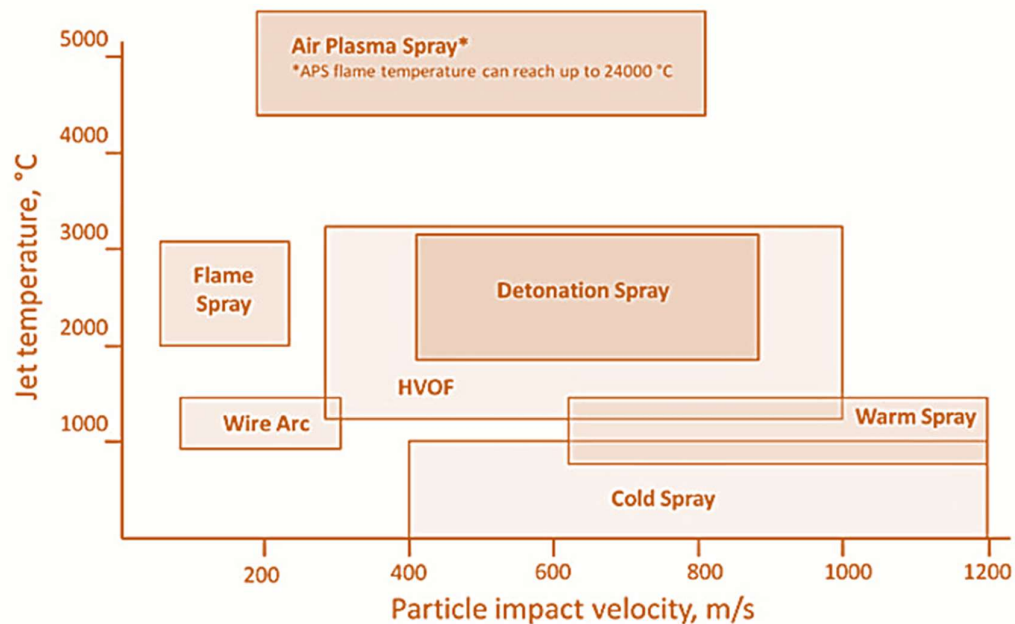


**Fig.1.2.** Comparison of various thermal spray processes (Tokarev, 1996).

### 1.5.2 HVOF process.

In a family of thermal spraying, a new technique called HVOF was introduced in the 1980s. A schematic diagram of the HVOF process is revealed in **Fig. 1.3** along with the built-up mechanism of coating. In the HVOF,  $O_2$  and liquid of gas fuel are burnt and combustion takes place to generate a flame this flame is accelerated with feedstock powder and sprayed on the substrate to

be coated. The hot gas at very high pressure near about 1 MPa flows via a nozzle having a converging-diverging cross-section. The powder particles' velocity or jet velocity reaches up to 1000 m/s. The feedstock powder is injected and it achieves a velocity of 800 m/s. The jet of powder and hot gas then mixes and accelerates toward the substrate materials. The jet of powder and gas strikes with the substrates then it forms splats and is finally plastically deposited on the substrate with mechanical bonding. The HVOF process produces a coating with very less porosity and higher bond strength [Brandt, 1995]. Bonding occurs mostly as a function of kinetic energy rather than thermal energy. The difference between HVOF from other spray processes is revealed in **Table 1.1**.

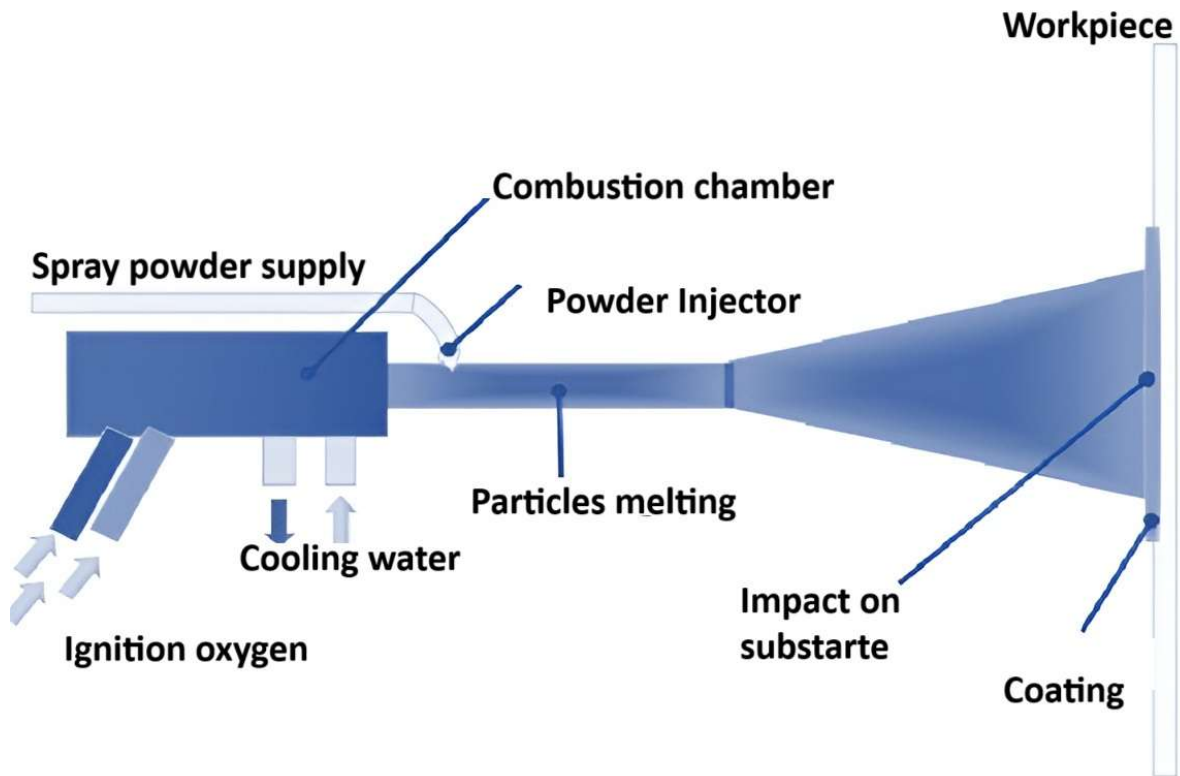


**Fig. 1.3.** Schematic representation of the HVOF process and built-up mechanism of coating (Matthews, 2004) .

In thermal spray coating approaches HVOF technique is gaining popularity for coating material, high velocity produces higher bond strength, lower porosity content, and dimensional restoration (Gill and Staia, 1999). The coating was used in this method, which can reach 1000 m/s (Lugscheider et al. 1998). Furthermore, the excellent coating quality (Liu et al., 2003 Sidhu et al. 2010) can be achieved. Compared to conventional thermal spray coating methods, the HVOF process can deposit coatings with higher levels of hardness, extremely low levels of oxidation,



strong abrasion resistance, reduced porosity levels, and higher levels of erosion resistance (Liu et al. 2003; Zhao et al. 2002; Mann et al. 2001; and Lee et al. 2000).

HVOF process can provide lower oxidation during the coating process owing to high velocity, high hardness of coating due to good bond strength, and high resistance to corrosion due to less porosity (Bala et al. 2010; Sidhu et al. 2006; Guilemany et al. 2006; and Matthews et al. 2004). High bonding coatings that have better hardness, reduced porosity, and higher density may be deposited thanks to high velocity's unique properties. The process of HVOF is a member of the family of thermal spraying techniques and can provide coatings with fewer pores, greater hardness, improved bond strength, as well as less decarburization as compared to thermal spraying techniques.

**Table 1.1** Attributes for various thermal spray processes (Pawlowski, 1995).

<b>Process of Coating</b>	<b>Heat Source</b>	<b>Feedstock material</b>	<b>Feedstock powder temp (°C)</b>	<b>Powder Velocity (m/s)</b>	<b>Deposition rates (Kg/hr)</b>
Flame spray	Oxy-acetylene	Powder or wire	3100	40	2-5
Plasma spray	Plasma arc	Powder	10000	200-400	3-8
LPPS	Plasma arc	Powder	11000	200-400	3-8
Detonation spray	O <sub>2</sub> acetylene-N <sub>2</sub> +gas detonation	Powder	4700	800	0.6
HVOF	Oxyfuel combustion	Powder	3000	800	2-4”

The fuel combustion takes place in a “combustion chamber” in the HVOF process and the burning of liquid with oxygen produces intense heat along with high pressure. In the case of the HVOF process, there is a feature of high velocity with a moderate temperature range which helps in the deposition of coating with lower porosity and produces a coating with good properties. This

method is extensively utilized for nickel deposition-based alloys. This is also used for depositing carbide coatings and stainless-steel feedstock powders.

#### *1.5.2.1 Characteristics of the plasma spray process*

The main factor in plasma spray success is the extremely high kinetic energy created and transmitted utilizing space-age rocket propulsion technology between the plasma spray unit and the substrate, finally leading to the high-velocity particles when practically embedded with substrate and forming an excellent coating with the required following features of a coating:

1. **Source of Heat at High Temperatures:** The plasma spray process utilizes a high-temperature plasma flame as the heat source to melt and spray the coating material, just as a metallurgist would expertly manipulate the elements to achieve the desired outcome. This plasma flame is capable of reaching temperatures exceeding 10,000°C, enabling it to effortlessly liquefy a diverse array of materials, such as refractory metals and ceramics, that pose challenges for alternative thermal spray methods.
2. **Utilizing powder injection and acceleration techniques:** The coating material is injected into the high-temperature plasma flame in the form of a fine powder. The powder undergoes rapid heating and is propelled to high velocities, usually ranging from 300-800 m/s. The high velocity enables the molten or semi-molten particles to strike the substrate surface with considerable kinetic energy.
3. **Formation of Substrate Coating:** As the particles collide with the substrate surface, they quickly change shape and solidify, creating flat, disk-like splats. The overlapping splats gradually accumulate to form the desired coating thickness and structure. The extremely fast cooling rate, reaching  $10^6$  K/s, results in the creation of coatings that possess distinct microstructures and properties.
4. **Diverse Coating Materials:** Various coating materials, such as metals, alloys, ceramics, cermets, and composites, can be applied using the plasma spray process. The versatility of this process enables its application in a wide range of industries and various uses. Plasma spray coating materials often consist of alumina, titania, chromium carbide, chromium oxide, and molybdenum-nickel-aluminum.
5. **Compatibility of Substrate Materials:** The plasma spray process is capable of coating a wide range of substrate materials, such as metals, ceramics, plastics, glass, and composites. This adaptability enables the process to be utilized for a wide variety of components and parts across various industries. The substrate material needs to have the capability to endure

the elevated temperatures of the process without experiencing any notable harm or distortion.

6. **Evaluating Thickness and Deposition Rates:** Plasma sprayed coatings can be applied in various thicknesses, ranging from 20 micrometers to several millimeters. The deposition rates for the plasma spray process can be quite high, enabling efficient and cost-effective coating application. The thickness and deposition rate are influenced by various factors, including the coating material, substrate geometry, and process parameters.
7. **Properties and Performance of Coatings:** Plasma sprayed coatings offer a variety of advantageous properties, such as wear resistance, corrosion protection, thermal barrier capabilities, electrical conductivity or resistivity, and oxidation resistance. Plasma sprayed coatings have a wide range of applications in various industries including aerospace, oil and gas, automotive, and energy.
8. **Process Complexity and Quality Control:** The plasma spray process can be quite intricate, necessitating the use of specialized equipment including the plasma torch, powder feeder, and process control systems. Ensuring a consistent coating quality necessitates meticulous management of various process parameters, such as gas flow rates, arc current and voltage, powder feed rate, and spray distance. Stringent quality control measures, including real-time process monitoring, non-destructive testing, and adhesion testing, are commonly used to guarantee the integrity and performance of the plasma sprayed coatings.<sup>2538</sup>

Essentially, the plasma spray thermal spray process involves the utilization of a high-temperature plasma flame to liquefy and propel a diverse array of coating materials onto various substrates. This process enables the formation of thick, high-performance coatings with distinct microstructures and properties. The intricacy of the process, though, requires meticulous control and quality assurance measures to ensure consistently dependable coatings.

#### *1.5.2.2 Advantages of the Plasma spray process*

- Plasma spraying offers a diverse selection of coating materials in powder form to cater to a wide range of needs. This encompasses a range of materials, including metals, alloys, ceramics, and refractory materials.
- Plasma spraying offers the advantage of being compatible with a wide variety of substrate materials. This versatile technique can effectively coat metals, ceramics, plastics, glass, and composites

- Plasma spraying is exceptionally well-suited for applying refractory coatings due to the high temperature plasma jet it utilizes.
- Plasma spraying offers a broader range of powder particle sizes, ranging from 5-100  $\mu\text{m}$ , compared to HVOF spraying.
- Plasma spraying is a coating process that has been thoroughly studied and is easily accessible.
- Plasma spraying is capable of creating coatings that exhibit excellent adhesion to the substrate and deliver consistent, reproducible performance.
- Plasma spraying has the potential to enhance and restore surfaces that have experienced wear or damage.

#### *1.5.2.3 Applications of the Plasma spray process*

- There are several advantages that make this process very promising for repair and for producing a wide range of industrial components. There are many examples like pipelines in oil refining industries, blades in turbines, cylinders, and rings; and bearing-related components, pump elements, pistons, sleeves, valves, shafts, and seals.
- This process has many applications for protection against corrosion and the lack of process-induced oxidation offers enhanced properties.
- In the electrical & thermal engineering field, there is an absence of process-induced oxidation and it offers enhanced conductivity in the coatings.
- This process is also used in the aerospace engineering field and it is mostly used for coatings in gas turbines and in the form of aluminium and coatings of its alloy.
- Retrieval and repair of the parts and the plate stocks that are mostly used in aircraft structures.
- Repair and maintenance of worn surfaces can be done for wear resistance and corrosion resistance coatings can also be produced.

Power plants and the industry sector often experience significant damage to various components such as super heaters, economizers, heat exchangers, piping, and chimneys within the petroleum industry. The current work investigates the evaluation of oxidation and erosive wear at higher temperatures and high-temperature erosive wear of substrate material, namely SS-304 and three different compositions of coatings viz.  $\text{Al}_0\text{CrCoFeNi}$  (A1),  $\text{Al}_{0.50}\text{CoFeNi}$  (A2) and  $\text{Al}_{1.00}\text{CoFeNi}$  (A3) deposited by plasma spray coating process. The air jet erosion test is carried out at high temperatures of at  $900^\circ\text{C}$ . for uncoated and coated materials. Moreover, the oxidation test

was also conducted to understand the behaviour of coatings and substrate at 900°C. The weight change data were analysed for comparison of various coating compositions. The weight change data after air jet erosion testing provides information on volume loss and hence the erosion resistance of the coating was calculated. The weight gain has been recorded in oxidation test for 50 cycles and kinetics of oxidation was analysed.

## **CHAPTER 2**

### **LITERATURE REVIEW**

This chapter offers a comprehensive study of the literature with a focus on the performance of engineering materials used in high-temperature applications. The different techniques of the coatings on the working surface and the effect of the surrounding environment were studied. The plasma spraying process has been studied and discussed with regard to oxidation and air jet erosion at high temperatures. The high temperatures are a subject of study that is now undergoing a lot of research. The relevant review literature by numerous researchers had been reviewed and particularly for the substrate material used and for high entropy alloys and other applications. The problem has been formulated and objectives were defined after a critical review of the literature survey.

#### **2.1 MATERIALS FOR HIGH-TEMPERATURE APPLICATIONS.**

Nowadays, different fields such as medicine, aerospace, and energy-transportation-industry production-require new materials with high capabilities. All sectors, including the creep resistant sector, temperature resistant, wear resistance level, ductility and toughness level, hardness, and optimal strength value, must meet minimal requirements for mechanical attributes (Miracle et al., 2014). Overall, we may conclude that a material's performance in industry is closely correlated with the quality of its surface. The broad availability of technologies that allow for the replacement of a bigger bulk with a low-grade base material that is suboptimal coated by a non-bulk coating with improved performance and surface qualities forms the basis of the cost-effective surface modification technique in this instance. Surface modification proved particularly helpful in high-stress circumstances, thermal insulation, wear prevention, and corrosive conditions. PVACs are extensively utilized in thermal barrier coatings (TBC), such as YSZ overlay protective coating and yttria-stabilized zirconia (YSZ), which are crucial in shielding cobalt or nickel-based superalloys from extremely high temperatures (ULTIMET). The technique of thermal spray coating (TSC) is a new, sophisticated, and adaptable approach to surface treatment. The majority of the examples

under examination include a line-of-sight process wherein a spray torch is introduced into molten or nearly molten feedstock material, heated to a near-molten or molten state, and then directed towards the base material. Davis and others, 2004. The basic operating concept of the HVOF high-velocity oxy-fuel thermal spray process is shown in Figure 2.1. The powder is melted and deposited on the substrate by being added to the burning fuel stream. This technique is the same as a thermal spray mechanism, with the exception of the feedstock material's capacity to adopt the shape of a wire or rod (Vasudev et al., 2021).

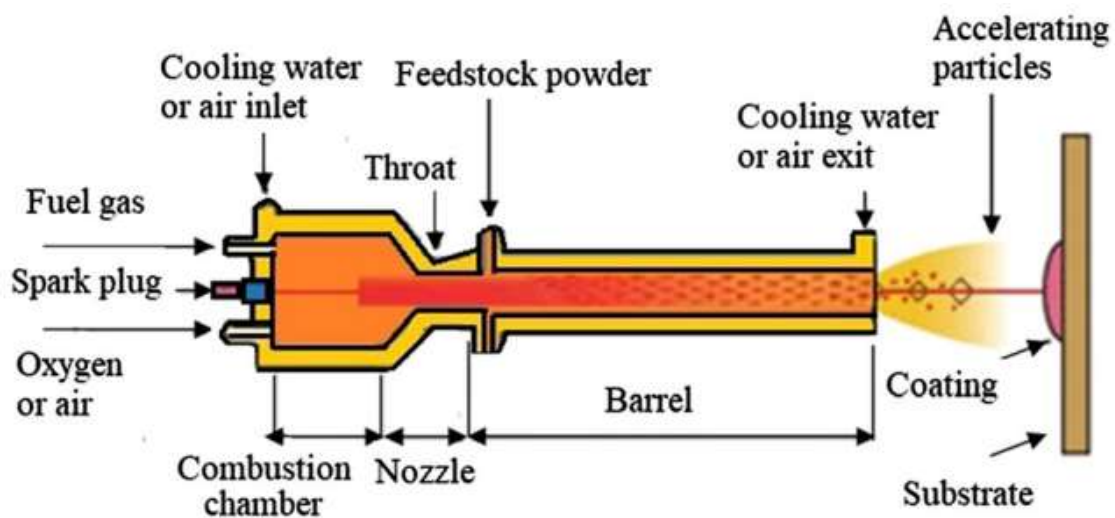


**Figure.2.1** Basic mechanism of HVOF thermal spray process (Vasudev et al, 2021).

The most important feedstock materials that are used in thermal spray coating techniques include conventional, nano, and bi-modal material besides a novel type of material which is termed high entropy alloys. Since solid solution alloys are composed of 5 near-equi/equi-atomic ratios elements, these have been termed HEAs (Cantor et al., 2004; Yeh et al., 2004; Murthy et al., 2019). Indeed, according to research (Glodovtaz et al., 2014; Pradeep et al., 2016), HEAs qualify the conventional material at cryogenic temperatures and more elevated levels of temperature as well as room temperatures are in close comparison. High entropy alloys tend to perform better than conventional materials. Solid solution phase stabilization at high temperature is due to the same

atomic characteristics (crystal structure, valency, and atomic field) combination higher in configurationally entropy and mixing enthalpy of for example BCC or FCC than inter-metallic compound (Hass et al., 2018; Zhang et al., 2014; Miracle et al. “Cocktail effects”, that is, promotion of different features previously described for HEAs, are contributed to the combined interactions of all basic elements present in such materials (Ranganathan et al., 2003). This is demonstrated by the development of bulk HEAs having better resistance to wear than traditional materials (Chaung et al.:2011; Verma et al., 2019)) and oxidation ((Butler et al.,2016), corrosion (chi et al, 2017) in addition to superior mechanical properties (Wang.et.al.,2008).

## **2.2 Oxidation and thermally sprayed high entropy alloys’ wear behavior**

In components that perform at high temperatures, oxidation resistance is essential. Recent research has revealed the creation of metal-ceramic-based coatings that can be utilized to battle high-temperature oxidation resistance. Boiler tubes, heat exchanger tubes, automotive parts, and furnace parts are typical technical components that must endure high temperature oxidation up to 1000°C (Vasudev et al., 2020). This section focuses on high-entropy alloys that have been created via thermal spray coating techniques. Three approaches have been considered in the development of oxidation-resistant coatings, which include aluminizing the surface through interaction between metal substrates and Al (Grisaffe et al., 1972) and overlayer coatings for example superalloys of MCrAlY (M=Ni, Co, Fe) (Wang et al., 2002) of thermal expansion. Aluminide or glass-ceramic at low temperatures, layers become stiff and brittle, and delamination from the substrate is easy due to a mismatch in coefficients of thermal expansion. Industry prefers MCrAlY alloys for overlayer coating to prevent high temperatures oxidation of structural components. Though, because of their lesser hardness (HRC 20–30), while particles or equivalents are present in the environment, they have poor wear resistance. As a result, standard coating materials are unable to offer an optimum covering that is both oxidation as well as wear resistant. In this research, a novel alloy design idea



called "multi-principle-element alloys" was investigated in order to develop alloys with exceptional qualities for crucial applications like turbine blades, moulds, and dies.

### 2.3 High-entropy alloys developed through plasma spray

For evaluating the multi-principle-element alloys like characteristics, microstructure, processing, AlSiTiCrEeNi-Mo<sub>0.5</sub> (labeled as 7E), and AlSiTiCrEeCoNiMo<sub>0.5</sub> (labeled as 8E) were explored. The characteristic micro-structural features constitute a lamellar structure created by plasma spraying, as seen in **Fig.2.2**. It suggests that the porosity and oxygen concentration were both very low. As shown in **Table 2.1**, the deposited coatings' oxidation performance showed better wear and oxidation resistance.

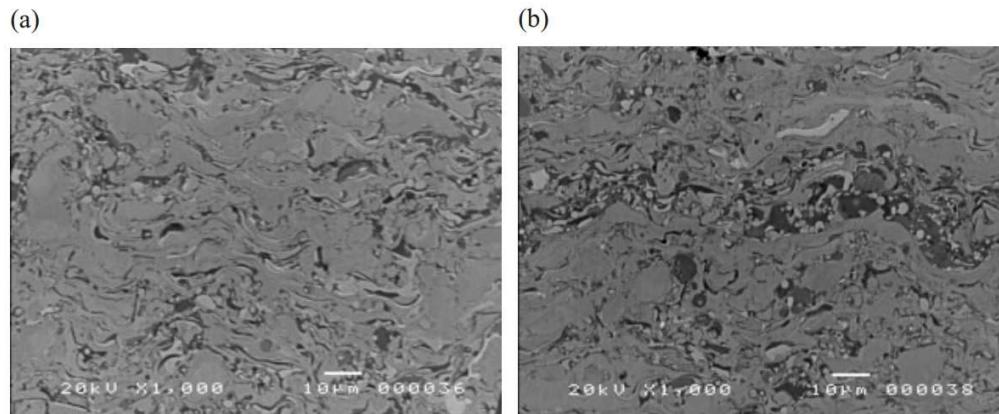


**Fig.2.2** SEM micrographs of [a]AlSiTiCrEeCoNiMo<sub>0.5</sub> and [b]AlSiTiCrEeNi-Mo<sub>0.5</sub> (Haung et al., 2004).

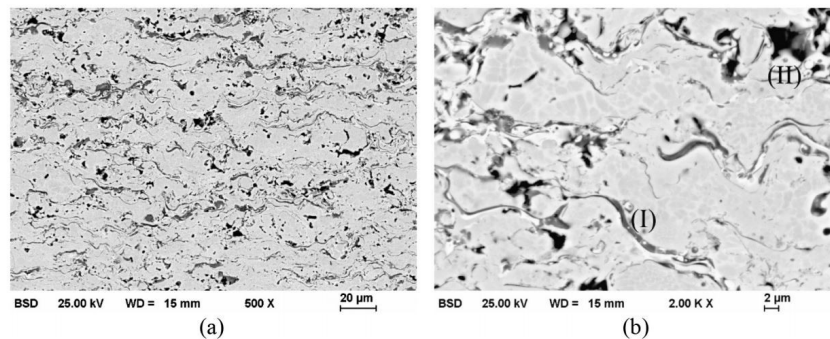


**Fig.2.3.** SEM micrographs of AlCoCrFeNiTi<sub>0.5</sub> coating at [a] low and [b] higher magnifications (Anupam et al., 2019).

Another recent work used the high velocity oxy-fuel technique [HVOF] to deposit AlCoCrFeNiTi0.5 powder. **Figure 2.3** shows the microstructure of the coating.

The powder was characterized and for the HVOF coating process utilized as a feedstock. A homogenous and lamellar coating structure may be seen in the overview image. Because of the reactive and tiny particles' increased quantity, within the coating oxidize lamellae may be observed. Additionally, porosity is seen within the covering (Anupam et al., 2019).

As shown in **Figure 2.4**, the HVOF coating diffractogram also shows bcc phase's large diffraction peaks with B2 structure. In comparison to the feedstock powder, the diffraction peaks enlarge which results in A2 structure overlapping with the bcc phase' diffraction peaks. There is suppression off cc phase production with A1 structure in the atomized powder. However, there are a few modest additional intensity maxima which can be attributed to a different bcc phase with B2 structure. The diffraction peaks have shifted significantly from the primary phase, indicating a change in lattice parameters. For the bcc (B2) phase, a3.58 lattice parameter was established, compared to for the bcc (B2) main phase 2.92 lattice parameter. The COF (coefficient of friction) in the wear test is also temperature dependent. The COF initially rises as the temperature rises. A drop in COF can be seen at temperatures below 650 °C. Though, a considerable standard deviation is exhibited by the measured values, particularly around 650 degrees Celsius. At the greatest temperature of 900 °C, the investigations yielded the 0.97 lowest average COF as well as a correspondingly lower standard deviation. The metallic coating's abrasive wear and the development of free oxides were seen at temperatures below 500 °C. As the temperature rises, so does the amount of oxides covering the surface. A dense oxide layer forms at temperatures above 800 °C. Grooves imply abrasive wear behavior and the primary material's protection, which results in effective wear resistance. Spinel could be the source of the produced oxides. For the maximum test temperature (900 °C), the production of extra phases is revealed by the phase analysis. In the

coating and gas atomization process, quick cooling prevented the formation of a tetragonal-phase and a small fcc phase. The findings show that for high-temperature applications, AlCoCrFeNiTi0.5 HEA coatings are suitable.

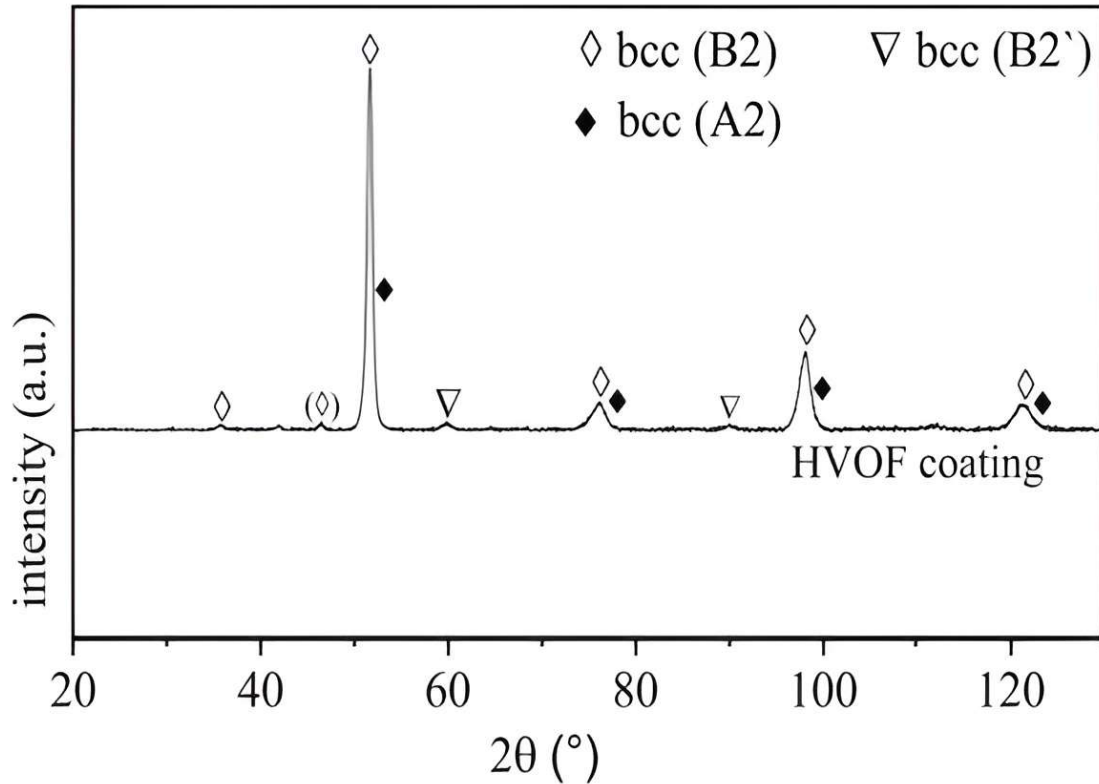


**Fig 2.4.** AlCoCrFeNiTi0.5 HVOF coating Diffractograms (Anupam et al., 2019).

## 2.4 High-entropy alloys developed through cold spray

Among the newest thermal spray processes, one is cold spray as well as it's already being utilized to create high-entropy alloys. Under various pressure and gas temperature settings, Ni-based and stainless-steel superalloy substrates were sprayed with AlCoCrFeNi alloy powder particles in the work by Anupam et al.,2019. Following that, on a superalloy substrate one optimal spraying condition was selected, for 25 hours at 1100 °C isothermal oxidation was carried out as well as for understanding the oxidation mechanism. In terms of oxidation, some research has been published on the well-studied AlCoCrFeNi equiatomic quinary alloy, which was manufactured through mechanical alloying as well

as with the help of atmospheric plasma spraying (APS) coated on substrates of steel (Berndt et al., 2015). During the spraying procedure, alloy powder's substantial oxidation and melting was detected, as well as in the coating concomitant alterations in the alloy phase. The resulting coating had a composite alloy–lower oxidation resistance oxide microstructure which makes the AlCoCrFeNi and APS combination impractical. To address this problem, the coating method was altered to cold spray with the help of similar alloy compositions as that of feedstock. As the name implies, cold spray, is a type of thermal spray method that operates at a lower temperature. A heated (1000 °C) high-pressure gas combination is used to introduce the powder particles and accelerate them. The gas is then forced into a converging-diverging nozzle of De-Laval type, which accelerates it to Mach 1 and higher speeds (Assadi et al., 2003). When particles strike the substrate at speeds over a particular "critical velocity" (typical of a feedstock– substrate combination, shape, and particle size), impact energy is resulted by their kinetic energy's transformation. Significant plastic deformation accompanied this entire process and localised heat generation at the particle-substrate contact, which allows the particle-substrate mechanical attachment (Assadi et al., 2003). It's worth noting that there is no direct heating of the particles, therefore any temperature-induced phase transitions are avoided. Furthermore, although the spraying is performed in the open air, the powder oxidizes very little, thus in the coating the alloy is accurately recreated (Stoltenhoff et al., 2002). After 5 hours of mechanical alloying, phase progression in AlCoCrFeNi is shown by the XRD patterns. Only peaks which belongs to a small FCC and a large BCC phases are evident after the fifth hour, with no residual elemental peaks visible. It has been suggested by the Al's significant negative mixing enthalpy with Fe, Co, and Ni that such elements provides contribution to the BCC lattice, however a Fe, Co, and Ni mixture that at high temperatures resulted in an FCC, is probably the FCC phase. The oxide stringers absence between the splats, low interplay porosity, discontinuous fractures across the coating parallel to the interface, a good interface between substrate and coating, a rough coating surface, and non-uniform coating thickness are all traits similar to all situations. This is well documented in the literature of HEA that Al works as a BCC stabilizer in oxidized coatings (Wang

et al., 2012), and the same is true in un-oxidized coatings. When this alloy is subjected to an oxidizing environment with high-temperature, however, Fe, Cr, and Al (in the Ellingham diagram's sequence of stable oxide production) tend to oxidize preferentially. From the BCC phase, Al simultaneous loss results in an FCC CoCrFeNi alloy under the oxide layers. Also, Cr oxidizes to  $\text{Cr}_2\text{O}_3$ , which then volatilizes to  $\text{CrO}_3$  at temperatures exceeding  $1000^\circ\text{C}$ . It's difficult for capturing/monitoring the process in tests like these, but it's plausible that it affects the HEA's oxidation behavior. For the production of 3D components, feedstock powders are now additively created using a novel process called "Cold Spray Additive Manufacturing" (Vasudev et al., 2020). This technology is intended to be used in the future for the usage of high-entropy alloys. **Table 2.1** shows the HEAs properties deposited using different thermal spray coating processes and **Table.2.2.** represents the high-temperature oxidation and wear behavior of high entropy alloys created utilizing thermal spray techniques with respect to Table 1.

**Table.2.1:** HEAs properties deposited using different thermal spray coating processes.

Material	Phases	Powder particle size [ $\mu\text{m}$ ]	Coating Technique	Hardness	Porosity	Ref.
AlSiTiCrEeCoNiMo <sub>0.5</sub>	1 BCC	160 $\mu\text{m}$	Plasma Spraying	486 $\pm$ 31 Hv	0.92	Haung et al., 2004
AlSiTiCrEeNi-Mo <sub>0.5</sub>	2 FCC	160 $\mu\text{m}$		486 $\pm$ 31 Hv	1.06	
AlCoCrFeNiTi <sub>0.5</sub>	BAA A2  BCC B2	-45 $\pm$ 15 $\mu\text{m}$	HVOF	610 $\pm$ 31 Hv	-	Lobel et al., 2020

AlCoCrFeNi	BCC	11 6	Cold	3.86±0.2GPa	-	Anupam et al, 2019
	FCC	1.0 nm	Spray			

**Table 2.2** Oxidation and Wear resistance of materials with reference to **Table2.1**.

Coatings	Oxidation rate [mg/cm <sup>2</sup> ]	No. of testing cycles[N]	Wear resistance/COF	Ref
AlSiTiCrEeCoNiMo <sub>0.5</sub>	900 °C- 2  1000 C- 4.5  1100 C- 8.7	150	11 m/mm <sup>3</sup>	Haung et al., 2004
AlSiTiCrEeNi-Mo <sub>0.5</sub>	900 °C-3  1000 °C-5  1100°C- 8.5	150	11 m/mm <sup>3</sup>	Haung et al., 2004

AlCoCrFeNiTi0.5	-	-	COF at 500°C- 1.4  COF at 650°C- 1.2  COF at 800°C-1.1  COF at 900°C- 0.9	Lobel et al., 2020
AlCoCrFeNi	1100 °C	-	-	Anupam et al, 2019

The following conclusions can be made from the current article: The most common thermal spray procedures for producing HEA coatings are HVOF and APS. For the development of HEAs, the cold spray approach has recently been introduced. While the primary application field is for high temperatures performance, one of the major research interests is the HEA feedstock which contains Ti, Si, and/or Al, with the CrFeCoNi base. Because of their thick microstructure, HVOF HEA coatings have the maximum hardness. However, wear resistance and hardness were generally higher in traditional materials because of the supersaturated multi-component phase as well as other strengthening processes' development. Thermal sprayed HEA coating has shown promise in traditional bond coat material replacement due to their excellent oxidation resistance.

## 2.5 PROTECTIVE COATINGS.

A material has to withstand aggressive conditions when working at high temperatures and is subjected to oxidation, erosion, and corrosion. The material fails due to these failures and therefore requires some surface modification to prevent the material from surface degradation (Pawlowski, 1995).

Many properties are required at the same time to avoid the failure of the material and the use of some combination of elements or different classes of coatings like composite coatings can fulfill this requirement and a coating enhances the service life of the component. They can be deposited

and sometimes used for decoration purposes to the component from an aesthetics point of view. The primary advantages of coatings were summarized by Heath et al. (1997) and are given below:

- Any material from polymer to metallic could be coated with coating processes. Material selection can be optimized according to particular conditions under which a particular component has to work like corrosion and erosion. Surface properties can be different from the bulk material property.
- Functionally graded materials could be by combining for required corrosion and erosion resistance. Multi-layered coatings can also be helpful in some applications. For instance, a bond coat is used between the top coat and substrate to avoid the mismatch of the thermal coefficient of expansion for two different materials. Therefore, coating materials can be tailored according to the particular requirement for any material.
- Unique microstructures and alloys can be achieved with thermal spray techniques which are impossible with bulk materials. These comprise composites and coating corrosion-resistant phases.
- The coating cost is lower than the bulk material and a coating provide improved service life of a component. Therefore, the cost/performance ratio of the coating in thermal spray coatings is interesting.
- The thermal spray coatings can even use on-site for repair and maintenance purposes with equipment. Hence, this technique has gained popularity for surface protection against corrosion

## **2.6 SOME EMERGING METHODS TO CONTROL HIGH-TEMPERATURE WEAR RATE .**

There are various techniques that have been used for the surface modification process and they can help to attain the desired properties at the surface. Some of the techniques are discussed in this section.

### **2.6.1 Thermal spray coatings**

This process has many variants which are HVOF, plasma spraying, and detonation gun spray. These processes can easily provide very hard, dense, and smooth coatings with accuracy and these processes are used for high-precision components like aeronautical components, steam turbine blades, and die (Holmberg and Mathews, 2009).

TiO<sub>2</sub>-13Al<sub>2</sub>O<sub>3</sub> coatings were used for resistance against wear corrosion with the plasma spray. In this process, the powder is sprayed in the form of liquid droplets on the substrate and this



finally plastically deformed after condensation. These coatings provide higher bond strength. The plasma spraying technique is used for ceramic coating due to the high temperature which completely melts at high velocity prevents the decomposition of powder particles they do not interact with the oxygen and unwanted phases are avoided (Priyantha et al., 2003).

Composite coatings provide some phases which prevent the surface of the cast iron (Hock et al., 2003) Zirconia coatings with plasma spraying technique have been used on gas engine components for increasing their strength at high temperatures (Liang and Ding, 2005) Zirconia is a light element and it goes into the grain boundaries and makes the structure denser.

Grain boundaries are open-structured and when zirconia diffuses it provides a barrier for the dislocations to move. It has also a great role in  $\text{Ni}_3\text{Al}$  single phase when added to it provides strength.  $\text{Ni}_3\text{Al}$  single phase not only provides strength to the coating but also decreases the corrosion rate. For this purpose,  $\text{Ni}_3\text{Al}$  plasma sprayed coatings were used on boiler steels. This coating showed very effective results against high-temperature corrosion (Sidhu and Prakash, 2003). Apart from zirconia, there are some other light elements like carbon and boron that can be used with  $\text{Ni}_3\text{Al}$  single-phase coating to increase its strength.

The actual environmental conditions in the case of boilers in thermal power plants are not very different from the die used for glass manufacturing. In thermal power plants, steam is generated through boilers and that is obtained by heating water with the help of coal. Heating of coal produces ash particles known as soot and which is in the form of black powder it contains similar elements which are present in glass material like silica, alumina, and magnesia and this further contains carbon and oxygen to form gases that rapidly damages the surface of heat exchanger walls, soot blowers' regions and the boiler surface of heating zone surface area.

The presence of these constituents accelerates the corrosion rate and results in premature failure of the surface of components. The ni-20Cr coating has been applied with a "high-velocity oxy-fuel" technique on boiler steels and thermal power plant (Sidhu et al., 2006). The use of such coatings provides wear and corrosion resistance at high-temperature conditions.

## **2.6.2 Powder thermal spray coatings**

The study of high-temperature coatings reveals that nickel-based coatings have a great effect on the working surface's performance. Conventional powders having an size of 74 microns & nanopowders having size of 67 nm were deposited by a thermal spray coating technique called cold gun spray method and their results have shown a higher resistance to wear and increase in hardness as well (Kaur et al., 2015).

Thermal spray coatings techniques have shown good results for high wear resistance which also include the  $\text{Cr}_3\text{C}_2$ -NiCr and WC-Co coatings sprayed with the detonation gun spray method and this coating showed good adhesion to the base metal in high-temperature wear with no evidence of spalling and the oxide scale that forms in this aggressive environment (Kaur et al., 2011).

## **2.7 BEHAVIOUR OF COATINGS AT HIGH-TEMPERATURE SETTINGS.**

This aims the review the latest wear resistance coatings for elevated temperature by using the HVOF technique with Nickel based powders, Nickel plus various reinforcements, and also post-heat treatments of the developed coatings.

Parveen et al. [2015] examined a 60-weight percent NiCrSiB-40 weight percent  $\text{Al}_2\text{O}_3$  composite coating that was applied via atmospheric plasma spraying on AISI 304 substrate material. SEM, an optical microscope, and an XRD have been utilized to analyze the coating surface. We assessed the coating's density, porosity, microhardness, and surface abrasiveness. An adhesion tester that pulls off was used to gauge the coating's adhesive strength. At  $30^\circ$  &  $90^\circ$  erodent impact angles, the erosion rate of samples that were coated and uncoated was assessed. To analyze the erosion mechanism, eroded sample SEM images were collected. According to the test findings, the coating shields the substrate from impacts at both  $30^\circ$  and  $90^\circ$ .

**Premkumar. K, et al. [2018]** examined the behavior of nanocomposite coatings. HVOF sprayed nanocomposite and traditional 27%  $\text{Cr}_3\text{C}_2$  to “23% Ni- 50% Cr” coatings were deposited onto SA 210 Gr C. Erosion testing conducted at  $450^\circ\text{C}$  temperatures and on impact angles of 30, 60 &  $90^\circ$ . Therefore, it can be inferred from this that the nanocomposite was relatively superior to both the conventional and the uncoated substrates owing to a  $\text{Cr}_2\text{O}_3$  layer formation which acted as an obstacle for approaching erodent particles. The less porosity of nanocomposite was also the reason for low erosion rates. For all ductile materials, there was a higher erosion rate at oblique angles. Furthermore, erosion resistances of both nanocomposite & conventional coatings offer 7.5 times and 3.5 times higher values at bleak ( $30^\circ$ ) impact angle as compared with that of uncoated substrate.

**H. Vasudev et al. [2019]** used the HVOF method to integrate a bilayer of the 718 alloys into the NiCrAlY coating. The behavior of coated and naked samples under high-temperature oxidation as well as erosion was investigated. According to the authors, alloy-718 is more resistant to erosion and corrosion. High hardness and the development of stable oxides ( $\text{Al}_2\text{O}_3$  &  $\text{Cr}_2\text{O}_3$ ) are linked to improved resistance.

**Vasudev. H, et al. [2019]** In a different investigation, the influence of microwave-based post-processing on microstructure and ‘mechanical properties’ of HVOF-deposited alloy-718 coating was studied. The authors noted that significant improvement of microstructure was achieved post processing where porosity and micro-cracks having been healed (Iddi et al., 2020). ‘There will be un-melted particles and pores evident in the SEM micrographs of a sprayed coating, although post-processing, as a result of material flow in microwave processing healing may occur within some of these pores.’ Moreover, micro-hardness, fracture toughness and surface roughness were also enhanced.

**Daram. P, et al [2019]** also examine the effect of post-treatments on corrosion and microstructure performance of NiCrMoAlY alloy coating. The authors concluded that there is a reduction of pores after “heat treatment” that results in enhancing corrosion resistance.

**Singh, et al. [2019]** investigated the “high-temperature tribological performance” of a 65 percent (“NiCrSiFeBC”)-35 percent (WC-Co) coating sprayed at high velocity with Oxyfuel at temperatures ranging between ambient to 800°C. The coating has been created on the “AISI H11” and “AISI H13”. The as-sprayed coatings' microstructural properties, microhardness, porosity, surface roughness, as well as bond strength were assessed. Pin-on-disc tribometer tribology examination was carried out. The outcomes showed that the created coating performed significantly better than the untreated specimens, exhibiting decreased porosity and increased microhardness. At normal temperatures, the coated specimens wore mostly by abrasive processes. The predominant processes at high temperatures were found to be adhesive and oxidative wear.

**Praveen. A. S, et al [2020]** In another investigation authors deposited two weight compositions 1.4wt & 0.17wt % of nano  $\text{Al}_2\text{O}_3$  with NiCrSiB by HVOF technique. Authors reported that with the addition of 1.4wt percent nano  $\text{Al}_2\text{O}_3$  micro hardness increases from 576 Hv to 748Hv.

**Chhabra et al [2020]** Wear and surface degradation of tools (“die materials”) in the sector of hot metal forming is a key issue that has a negative impact on the process economics. Interaction between the tool along with workpiece at greater temperatures causes the issue. Nevertheless, there is still a lack of data regarding the wear & friction of dies. The goal of the current inquiry was to investigate the potential of “ $\text{Cr}_3\text{C}_2$ -NiCr” surface coating using tribological (wear and friction) experiments. The coatings were made using an HVOF spraying process. The coated specimens' microhardness, bond strength, surface roughness, and porosity were discovered and examined. The uncoated and coated samples were then studied in the lab for elevated-temperature wear and friction. 25 N & 50 N loads were used in the investigation. At all test parameters, the coated samples demonstrated an improvement in wear resistance. At 400 °C, the coated sample indicated the lowest

COF value and specific wear rate. The SEM method was used to investigate wear processes. The wear processes for the  $\text{Cr}_3\text{C}_2$ -NiCr-coated samples were found to be adhesive at room temperature and a mix of adhesive/ oxidative/abrasive at greater temperatures.

**Chhabra et al [2020]** focused on analyzing the wear and friction properties of  $\text{Cr}_3\text{C}_2$ -NiCr coatings used on the die steel material's surface by atmospheric plasma spraying. The specimens that had been sprayed were described. We assessed the microhardness, bond strength, and coating porosity values. At room temperature,  $400^\circ\text{C}$ , &  $800^\circ\text{C}$  under 2 loads of 25N & 50N, wear tests on the high-temperature “pin-on-disc” tribometer were conducted in the laboratory. The SEM method was used to examine the wear processes of each worn-out sample. Analysis was done on the particular wear rates along with friction coefficient values. The newly created coating outperformed its uncoated equivalent in terms of wear resistance. At high temperatures, the “friction coefficient” values for coated specimens declined. The wear mode has been seen to be adhesive at room temperature, and at higher testing temperatures, it was seen to be a mix of oxidative, adhesive, as well as abrasive.

**Sun et al., [2021]**, studied atmospheric plasma sprayed NiAl-20 wt%  $\text{Bi}_2\text{O}_3$  coatings with varying  $\text{Cr}_2\text{O}_3$  contents. The findings revealed that  $\text{Cr}_2\text{O}_3$  greatly improved the coatings' mechanical strength without compromising their plasticity. In addition to this  $\text{Cr}_2\text{O}_3$  also improves the wear coatings behaviour owing to high hardness and plastic deformation resistance.

**Dhzurinskiy et al., [2021]**, In the research plasma, sprayed  $\text{Cr}_3\text{C}_2$ -NiCr-based coatings have been deposited on “SS-304” L substrate and investigated its erosion performance. The coating developed features a dense microstructure with few flaws like micro-cracks and pores, as well as high hardness and toughness. Enhanced erosion resistance will be attributed to the high value of fracture toughness and hardness in developed coatings.

**P.K. Huan get al. [2004]** studied the alloys  $\text{Al}_{0.5}\text{CoCrCuFeNi}$  with the effect of the electromagnetic stirring provides that it has effective grins for alloys and as well as excellent mechanical properties. With the Investigation proves that the electromagnetic stirring with  $\text{Al}_{0.5}\text{CoCrCuFeNi}$  of the both compressive strength and tensile strength was higher than without electromagnetic stirring of  $\text{Al}_{0.5}\text{CoCrCuFeNi}$ . It also states that oxidized  $\text{AlSiTiCrFeCoNiMo}_{0.5}$  and  $\text{AlSiTiCrFeNiMo}_{0.5}$  at  $900^\circ\text{C}$ ,  $1000^\circ\text{C}$ ,  $1100^\circ\text{C}$  and observed good oxidation resistance up to 1000c over 100H substrate.

**Karin A. Dahmen [2014]** discussed the special features of high wear resistant HEAs,  $\text{Co}_{1.5}\text{Cr}_{0.5}\text{FeNi}$  as follows: (a) thermal property; (b) physical property including density( $\rho$ ),

atomic radius( $r$ ), lattice parameter( $a/d$ ), melting temperature( $T_m$ ); magnetic properties include; saturation magnetization, standard deviation, and entropy change  $TSM S_{sxn} 8(i+j) - nRT4M i^*$ .  $5CrFeNi1.5Ti$  and  $Al0.2Co1.5CrFeNi1.6$ . In comparison with  $5Ti$  alloys, high entropy bulk metallic glasses have investigated remarkable using eutectic composition, dense atomic packing and entropy of mixing points of view. This work also demonstrates that HE bulks metallic possess glass forming ability and plastic properties.

**A. S Ming et al. [2015]** analyzed the plasma sprayed high entropy alloys and properties of  $AlCoCrFeNi$  and  $MnCoCrFeNi$  by ball milling and then plasma sprayed, Minor oxide peels were detected which attributed to high temperature.

**W.L. Hsu et al, [2018]** studied the oxidation resistance at  $1100^\circ C$  that makes excellence at elevated temperature,  $TheNiCo0.6Fe0.2Cr1.5SiAlTi0.2$  and  $NiCo0.6Fe0.2Cr1.3$  alloys are investigated with high velocity oxy fuel spraying (HVOF), warm spraying (WS) and plasma spraying (PS) process. It was observed that thermal barrier coating showed better oxidation resistance over substrate at high temperature i.e with  $FeCoCrNiAlx$  high entropy alloy coating.

**A.Anupam et al.[2019]** The cold sprayed  $AlCoCrFeNi$  high entropy alloys were invested and isothermal oxidation experiments were performed at  $1100^\circ C$  for 25h on the coating at  $400^\circ C$  and pressure of 10 bar, Ni-base superalloy substrate cold sprayed no coating. The interface between the coating and substrate remained intact after oxidation treatment, all of the mechanical property results were measured.

**Y.K. Mu [2019]** studied nano oxides reinforced high entropy alloy coating synthesized by atmospheric plasma spraying of microstructure, surface morphology, hardness and wear resistances. The crystal structure of the  $CoCrFeNiAl$  and  $CoCrFeNiMo$  are checked and their good hardness ( $573 \pm 19$  Hv0.1) and that of coefficient of friction (COF) is  $0.49 \pm 0.04$ .

**Y. Cai, L. Zhu et al. [2019]** evaluated the microstructure and properties of  $FeCoCrNiAl0$ . Not much changed on the cladding layer after compared with before high temperature. Image by Francillon from Wikimedia the formation of BCC solid solution at the grain boundary occurred due to high-temperature condition when Al element content was as much as 14.89% (0.7mol). Which improved micro-hardness and tribological behavior but reduced the corrosion resistance.

**A. Sekhar et al. [2019]** investigated the TiAlNiCo, TiAlNiFe and TiAlNiCoFe alloys with mechanical properties, microstructure, Compressive strength and hardness had been studied and observed the good hardness of the more than 700Hv1.0 and compressive strength more than 2.5Gpa and state that all the alloys having microstructure of single BCC and observed very good mechanical properties .

**Yo.Mu et al. [2020]** have examined the wear and corrosion behavior of AlCoCrFeNi high entropy alloy coatings produced by atmospheric plasma spraying. This has led to an increase in the power of atmospheric plasma spraying as well as discussions of efficiency, hardness, surface morphology, mechanical properties, and microstructures .

**Y. Cai et al. [2020]** analyzed the effect of high-temperature conditions on the microstructure and properties of FeCoCrNiAl<sub>0.3</sub> and FeCoCrNiAl<sub>0.7</sub> high alloy coatings. The investigation on the microstructure, microhardness, tribological behavior and corrosion resistance of a coating have been done test and micro-hardness test was carried out. The coating has Little change in the morphology of the structure and properties of FeCoCrNiAl<sub>0.3</sub> before and after high temperature oxidation test, while enhanced corrosion resistance, porosity, micro hardness against 488° C×10 h, were also mitigated .

These days, thermal spray coatings are widely employed by producers of heavy machinery, machine tools, power plants, and the automotive industry (Praveen et., 2015; Grewal et al., 2015). When it comes to creating coatings that are resistant to wear and corrosion, these methods are quite dependable.

## **2.8 Oxidation Behaviour of HEAs**

As the HEA materials hyperspace is being explored for potential bond coat compositions, it is worthwhile to review studies already conducted on the oxidation behaviour of HEAs.

All the HEAs whose oxidation behaviour has been studied can be categorized into three major groups: (i) low temperature alloys (targeting applications up to 600– 900 °C) usually relying on Cr for protection (Holcomb *et al.*, 2015; Laplanche *et al.*, 2016); (ii) high temperature alloys (targeting applications in the 900–1100 °C range), usually depending on Al/Cr/Si/Ti for protection; and (iii) refractory alloys, relying on Ta/Al/Cr (Lo *et al.*, 2019; Liu *et al.*, 2014), in

which formation of volatile oxides is a major issue. Focussing on functioning as bond coats, in the temperature range of 900 – 1100 °C, group (ii) alloys: the AlCoCrNiX (where X = Fe/Si/Ti/Cu) HEAs are usually favoured. In each case, the alloy composition, phase constitution, as well as phase fraction and morphology play a vital role in the alloy's oxidation behaviour. This is directly connected to the synthesis route and thermal treatment accorded to the alloy before oxidation testing.

A complete list of literature on oxidation studies of HEAs of the AlCoCrFeNi family of HEAs is presented in Table 2.3.

**Table 2.3:** Compilation of various HEA compositions studied for their oxidation resistance in bulk form.

<i>Composition</i>	<i>Synthesis route/phases</i>	<i>Oxidation conditions</i>	<i>Oxides; Rate</i>	<i>Reference</i>
AlCoCrFeNi	As-cast; FeAl+NiCoCr+FeCr	850 –1050 °C; dry air	<ul style="list-style-type: none"> <li>•850 °C: <math>\theta</math>-Al<sub>2</sub>O<sub>3</sub> + spinel;</li> <li>•950 °C: <math>\alpha</math>- Al<sub>2</sub>O<sub>3</sub>+spinel;</li> <li>•1050 °C: spinel (FeCr<sub>2</sub>O<sub>4</sub>) + discontinuous alumina</li> <li>•850–950 °C: parabolic; 1050 °C: breakaway;</li> <li>•Al-depleted layer;</li> <li>•AlN</li> </ul>	(Sung <i>et al.</i> , 2013)
Al <sub>0.5</sub> FeCoCrNiSi <sub>0.2</sub> , Al <sub>0.5</sub> FeCoCrNi, and Al <sub>0.5</sub> FeCoCrNiTi <sub>0.5</sub>	As-cast;	900 °C	<ul style="list-style-type: none"> <li>•1,2: Cr<sub>2</sub>O<sub>3</sub> + AlN;</li> <li>•3: complex CoFe<sub>2</sub>O<sub>4</sub> spinel + mixed oxide scales + AlN</li> </ul>	(Zhang <i>et al.</i> , 2013)
Al <sub>10</sub> (CoCrFeNi) <sub>90</sub> (Al10F), Al <sub>20</sub> Cr <sub>25</sub> Co <sub>25</sub> Ni <sub>25</sub> Si <sub>5</sub> (Al20S) and Al <sub>15</sub> Cr <sub>10</sub> Co <sub>35</sub> Ni <sub>35</sub> Si <sub>5</sub> (Al15S)	As-cast; Ni-Al + Fe-Cr; dendritic segregation; Al10F and Al15S: Ni- Co-CrFCC+ Ni-Al B <sub>2</sub> ; Al20S: BCC+B <sub>2</sub>	Interrupted isothermal@ 1050 °C- 1000h	<ul style="list-style-type: none"> <li>•External Cr<sub>2</sub>O<sub>3</sub> + internal Al<sub>2</sub>O<sub>3</sub> in all</li> <li>•Al-depleted FCC below</li> <li>•Parabolic, Wt change: Al15S&lt;Al20S&lt;Al10F</li> <li>•More Al: better oxd resis</li> </ul>	(Butler <i>et al.</i> , 2015)
Al <sub>8</sub> Co <sub>17</sub> Cr <sub>17</sub> Cu <sub>8</sub> Fe <sub>19</sub> Ni <sub>33</sub> (FCC), Al <sub>23</sub> Co <sub>15</sub> Cr <sub>23</sub> Cu <sub>8</sub> Fe <sub>15</sub> Ni <sub>15</sub> (BCC) and AlCoCuCrFeNi (R)	As-cast; AlCoCrFeNi dendritic+ Cu <sub>2</sub> D FCC: FCC+L12 BCC, R: Ni-Al BC+ Fe-Cr BCC	800–1000 °C	<ul style="list-style-type: none"> <li>•Multiple oxide layers: innermost Al<sub>2</sub>O<sub>3</sub>, intermediateCr<sub>2</sub>O<sub>3</sub>, outermost NiO, Fe<sub>2</sub>O<sub>3</sub>, Fe<sub>3</sub>O<sub>4</sub></li> <li>•800: parabolic</li> <li>•1000: spallation</li> <li>•Relative ratios of Al, Cr important</li> </ul>	(Daoud <i>et al.</i> , 2015)
Al <sub>0.5</sub> CoCrFeNi	As-cast	800, 900, 1000, 1100°C – 100h	<ul style="list-style-type: none"> <li>•Complete compact oxides @ 800, 900 °C</li> <li>•Thicker, cracked oxides at 1000, 1100 °C</li> <li>•Inner spinels : NiCr<sub>2</sub>O<sub>4</sub>, CoCr<sub>2</sub>O<sub>4</sub>,</li> </ul>	(Hong, <i>et al.</i> , 2015)



			Fe(Cr,Al) <sub>2</sub> O <sub>4</sub> + AlN	
AlCoCrFeNiTi0.5	Vacuum induction levitation melting	800, 900, 1000, 1100 °C	<ul style="list-style-type: none"> <li>• Good at all but 1000 °C;</li> <li>• Phase specific oxidation: Al<sub>2</sub>O<sub>3</sub> in dendritic, TiO<sub>2</sub> + Fe<sub>2</sub>O<sub>3</sub> + FeCr<sub>2</sub>O<sub>4</sub> in the interdendritic and eutectic</li> </ul>	(Wu <i>et al.</i> , 2015)
Al <sub>x</sub> (CoCrFeNi) <sub>100-x</sub> , x=0, 8, 10, 12, 15, 20, 30	As-cast FCC→FCC+BCC/B2→ BCC +B2; transition @ Al15 Al20,30: Ni-Al matrix + Cr-Fe ppt	1050 °C interrupted isothermal	<ul style="list-style-type: none"> <li>• Al8,10: External Cr<sub>2</sub>O<sub>3</sub>+ internal discontinuous Al<sub>2</sub>O<sub>3</sub> + AlN particles</li> <li>• Al12,15: external Cr<sub>2</sub>O<sub>3</sub>+ external Ni<sub>2</sub>Cr<sub>2</sub>O<sub>4</sub> +discontinuous internal Al<sub>2</sub>O<sub>3</sub></li> <li>• Al20,30: external Cr<sub>2</sub>O<sub>3</sub> and internal continuous Al<sub>2</sub>O<sub>3</sub></li> </ul>	(Butler <i>et al.</i> , 2016A)

<i>omposition</i>	<i>Synthesis route/phases</i>	<i>Oxidation conditions</i>	<i>Oxides; Rate</i>	<i>Reference</i>
			<ul style="list-style-type: none"> <li>• Al-depleted layer below oxide</li> <li>• Parabolic kinetics</li> <li>• 10<sup>-12</sup> to 10<sup>-13</sup> g<sup>2</sup>/cm<sup>4</sup>-s; lowest for Al30</li> <li>• Al8,15: GP1; Al12,15: GP2; Al20,30: GP3</li> </ul>	
Al8(CoCrFeNi)92, Al15(CoCrFeNi)85 and Al30(CoCrFeNi)70	As-cast ; annealed at 1050°C Al8: FCC+B2 Al15: FCC+BCC+B2 → Ann: Cr-Fe BCC+ B2 Al30: Cr-Fe BCC+ Ni- Al B2 → Ann: ppt free B2 + BCC wppts	1050 °C – 120h	<ul style="list-style-type: none"> <li>• As cast:</li> <li>• Al8: external Cr<sub>2</sub>O<sub>3</sub>+ sublayer of oxygen-enriched metal + internal semi-continuous Al<sub>2</sub>O<sub>3</sub></li> <li>• Al15: external NiCr<sub>2</sub>O<sub>4</sub> + underlying Cr<sub>2</sub>O<sub>3</sub>+ internal semicontinuous Al<sub>2</sub>O<sub>3</sub> + AlN</li> <li>• Al30: external Cr<sub>2</sub>O<sub>3</sub>+ underlying continuous Al<sub>2</sub>O<sub>3</sub>, with no spinels and very few AlN</li> <li>• Annealed:</li> <li>• Al8: Al<sub>2</sub>O<sub>3</sub> + (Al,Cr)<sub>2</sub>O<sub>3</sub> + Fe,Cr,Ni rich spinel</li> <li>• Al15: external Al<sub>2</sub>O<sub>3</sub> + underlying Fe,Cr,Ni</li> </ul>	(Butler <i>et al.</i> , 2016B)

			rich spinels • Al <sub>3</sub> O: only single continuous Al <sub>2</sub> O <sub>3</sub> with no internal oxidation • All had Al-depleted layer below oxide	
AlCo <sub>0.6</sub> Cr <sub>1.5</sub> Fe <sub>0.2</sub> NiSiTi <sub>0.2</sub>	Arc melt – crush – spark plasma sinter BCC+Cr-Ni-Co FCC + Cr <sub>3</sub> Si	1100 °C	• external mixed oxide and an internal Al <sub>2</sub> O <sub>3</sub> • parabolic, comparable to MCrAlY	(Hsu <i>et al.</i> , 2016)
Al <sub>0.2</sub> Co <sub>1.5</sub> CrFeNi <sub>1.5</sub> Ti <sub>0.3</sub>	Cast : FCC Aluminised: Al(CoCrFeNiTi) + Al <sub>3</sub> Ti + Al <sub>3</sub> Ni + NiTi; Homog @ 1100°C – 6h – water quench	900, 1000, 1100 °C – 100h	• Cast: Cr <sub>2</sub> O <sub>3</sub> + TiO <sub>2</sub> + Al <sub>2</sub> O <sub>3</sub> + NiTi • Aluminised: Al <sub>2</sub> O <sub>3</sub>	(Tsai <i>et al.</i> , 2016)
44Ni-3.9Al-22.3Co-11.7Cr-11.8Fe-6.3Ti (H1) 51Ni-5Al-18Co-7Cr-9Fe-5Ti-2Ta-1.5Mo-1.5W (H2)	Bridgman solidification + optimized ageing treatment γ + γ', 50% γ' in H1, 70% in H2	900, 1100 °C	• 900 °C: H1, H2 similar wt gains • 1100 °C: H1=8x H2 • H1: (Ni,Co)O, CoFe <sub>2</sub> O <sub>4</sub> , Fe <sub>3</sub> Ti <sub>3</sub> O <sub>10</sub> , Cr <sub>2</sub> O <sub>3</sub> , TiO <sub>2</sub> , Al <sub>2</sub> O <sub>3</sub> • H2: (Ni,Co)O, CoFe <sub>2</sub> O <sub>4</sub> , (Ni,Ti) <sub>3</sub> O <sub>4</sub> , CrTi <sub>2</sub> O <sub>5</sub> , CrTaO <sub>4</sub> and Al <sub>2</sub> O <sub>3</sub>	(Tsao <i>et al.</i> , 2016)
AlCoCrCu <sub>x</sub> FeNi alloys, where x=0,0.5, 1	x-0: BCC x-1,1.5: Cu in ID	1000 °C	• More Cu = less oxidation resis • Al <sub>2</sub> O <sub>3</sub> ; adherence worse with Cu	(Dąbrowa <i>et al.</i> , 2017)

<i>Composition</i>	<i>Synthesis route/phases</i>	<i>Oxidation conditions</i>	<i>Oxides; Rate</i>	<i>Reference</i>
			• Al depleted zone	
CoCrFeNiX alloys, where X=Al/Mn/Si	Arc melting + anneal @ 900°C – 48h	at 700, 800, 850 and 900 °C TGA	• Oxd res: AlCoCrFeNi > CoCrFeNiSi > CoCrFeNiMn • 800, 900 °C: $\alpha$ - Al <sub>2</sub> O <sub>3</sub> + $\gamma$ - Al <sub>2</sub> O <sub>3</sub> + FeAl <sub>2</sub> O <sub>4</sub> + $\theta$ - Al <sub>2</sub> O <sub>3</sub> : compact, continuous oxide layers • No distinct Al-depleted layer reported	(Kai <i>et al.</i> , 2017)
Al <sub>0.6</sub> CoCrFeNi (H) Al <sub>0.6</sub> CoCrFeNiSi <sub>0.3</sub> (HS)	As-cast H: FCC+BCC HS: FCC+BCC+ Cr <sub>15</sub> Co <sub>4</sub> Si <sub>6</sub>	800, 900 and 1000 °C for 100h	• Al <sub>2</sub> O <sub>3</sub> , Cr <sub>2</sub> O <sub>3</sub> and spinel • Parabolic	(Chen <i>et al.</i> , 2018a)
CoCrFeNiAl <sub>x</sub> Ti <sub>y</sub>	Induction melting No Al: Co- Ti and Fe-Ni based FCC High Al: only B2 Med Al: BCC+B2	1000 °C – 5, 25, 50, 100h	• CoCrFeNiAl <sub>0.5</sub> : lowest wt gain • CoCrFeNiAlTi <sub>0.5</sub> , CoCrFeNiAl <sub>0.5</sub> : continuous alumina • Rest: alumina + Cr <sub>2</sub> O <sub>3</sub> , TiO <sub>2</sub> , spinels, Fe <sub>2</sub> TiO <sub>5</sub>	(Erdogan <i>etal.</i> , 2019)
Al <sub>0.3</sub> CoCrCuFeNi	First principles		• Competition between alumina, chromia	(Hong <i>et al.</i> , 2019)
Ni <sub>2</sub> FeCoCrAl <sub>0.5</sub>	Arc melt FCC	900 °C, different O <sub>2</sub> partial pressures	• Exclusive alumina at higher O <sub>2</sub> partial pressures	(Kai <i>et al.</i> , 2019)
Al <sub>x</sub> CoCrCuFeNi alloys, where x=0,0.5, 1, 1.5, 2	Arc melt	1000 °C 100h	• all alloys formed Al <sub>2</sub> O <sub>3</sub> , Cr <sub>2</sub> O <sub>3</sub> and spinel oxides • Al <sub>1.5</sub> and Al <sub>2</sub> lowest wt gains • For higher Al: internal Cr <sub>2</sub> O <sub>3</sub> , external Al <sub>2</sub> O <sub>3</sub>	(Liu <i>et al.</i> , 2019)
Al <sub>x</sub> CoCrFeNiTi <sub>0.5</sub> , where x=0.5, 1, 1.5.	Arc melting B2, BCC; with FCC and $\sigma$ phases being observed for Al <sub>0.5</sub>	1100 °C	• Al <sub>0.5</sub> : spinel + discontinuous internal Al <sub>2</sub> O <sub>3</sub> • Al <sub>1</sub> : Cr <sub>2</sub> O <sub>3</sub> + semicontinuous internal Al <sub>2</sub> O <sub>3</sub> • Al <sub>1.5</sub> : TiO <sub>2</sub> + continuous internal (Al,Cr) <sub>2</sub> O <sub>3</sub>	(Wang <i>et al.</i> , 2019)

Al <sub>x</sub> CoCrFeNi, where x=0.7, 1, 1.3 +0.02at.%Y,Hf each	As-cast Al0.7: FCC+BCC Al1, Al1.3: BCC+B2	1100 °C – 100h	<ul style="list-style-type: none"> <li>• Al0.7: α- Al<sub>2</sub>O<sub>3</sub>+ non-protective spinels</li> <li>• Al1, Al1.3: primary α- Al<sub>2</sub>O<sub>3</sub></li> <li>• HfO<sub>2</sub>, Y<sub>2</sub>O<sub>3</sub> at grain boundaries</li> <li>• Al-depleted layer</li> </ul>	(Lu <i>et al.</i> , 2020a), (Lu <i>etal.</i> , 2020b)
--	--	----------------	---	--

The following sections will summarize oxidation behaviours reported for variants of the AlCoCrFeNi family of HEAs:

## 2.9 AlCoCrFeNi

Among the alloys examined the most in the HEA community is Al<sub>x</sub>CoCrFeNi, with research focussed on deciphering its phase constitution, thermal stability, and their connection to the alloy's physical and mechanical properties. Equiatomic AlCoCrFeNi is characterized by a dual phase microstructure, comprised of Ni-Al based B2 and Fe-Cr based BCC, with Co distributed uniformly between the two phases (Manzoni *et al.*, 2013). In the as-cast form these phases are usually present in both dendritic and interdendritic regions, with the BCC phase occurring as precipitates in B2 matrix, attributed to spinodal decomposition during solidification from melt. Lower Al content alloys ( $x \leq 0.375$ ) usually present with single phase FCC, whereas those with excess Al ( $x \geq 1.25$ ) are reported to have single phase B2 structures (Chou *et al.*, 2009; Kao *et al.*, 2009). This is due to the more negative mixing enthalpies between Al-Ni/Co/Fe pairs, leading them to constitute the B2 phase (Li *et al.*, 2008). On the other hand, Cr segregates to the BCC phase with little Al and Ni content.

Sung *et al.*, (2013) reported the earliest studies on as-cast equiatomic AlCoCrFeNi oxidized in the temperature range of 850–1050 °C. They observed parabolic oxidation kinetics for 850–950 °C and breakaway oxidation kinetics at 1050 °C. In terms of oxidation products, at 850 °C,  $\theta$ -Al<sub>2</sub>O<sub>3</sub> + spinel; at 950 °C,  $\alpha$ -Al<sub>2</sub>O<sub>3</sub>+spinel; and at 1050 °C, spinel (FeCr<sub>2</sub>O<sub>4</sub>) + alumina, with a loss in the latter's integrity were observed.

The advantages of higher Al content on improved oxidation resistance were reflected in the results reported by Butler (2016a; 2016b), who studied the oxidation behaviour of  $\text{Al}_x\text{CoCrFeNi}$ , where  $x=8, 10, 12, 15, 20, 30$  at.% in as-cast and annealed forms, oxidized at 1050 °C. Higher Al content ( $x=20, 30$  at.%) compositions were observed to develop continuous alumina layers with overlying chromia, as opposed to lower Al content alloys which had a semi continuous  $\text{Al}_2\text{O}_3$  and overlying chromia and spinels. They observed oxidation rates of the order of  $10^{-12}$  to  $10^{-13}$   $\text{g}^2/\text{cm}^4\text{-s}$ , on par with conventional bond coat alloys. Further, they also demonstrated that the classification provided by Giggins and Pettit (1971) for oxidation of Ni-Cr-Al alloys could be applied to these HEAs with slight modification. The effect of annealing was also observed in their studies (Butler *et al.*, 2016b), where the same composition  $\text{Al}_{30}(\text{CoCrFeNi})_{70}$  after annealing showed growth of exclusive alumina scale, whereas the as-cast alloy had developed a dual  $\text{Cr}_2\text{O}_3$ -internal  $\text{Al}_2\text{O}_3$  layer. This was attributed to Al being redistributed across phases after annealing, making it available for easy formation of alumina.

Lu *et al.*, (2020a; 2020b) also did seminal work on understanding the fundamental oxidation mechanisms operating in  $\text{Al}_x\text{CoCrFeNi}$  ( $x=0.7, 1, 1.3$  mol), concluding that for higher Al containing alloys,  $\alpha$ -alumina forms even in the transient stages of oxidation, instead of  $\theta$ - $\text{Al}_2\text{O}_3$ , whose transformation to  $\alpha$ - $\text{Al}_2\text{O}_3$  is one of the prime reasons for strain induced spallation. More importantly, they also studied the effect of adding trace quantities of rare earths on the oxide layer adherence of HEAs. The rare earth element effect is established in bond coat literature, as mentioned in Section 2.2.4.1. Addition of 0.02 at.% each of Y and Hf was observed to improve oxide adherence remarkably, attributed to formation of  $\text{Y}_2\text{O}_3$  and  $\text{HfO}_2$  at alumina grain boundaries. They also demonstrated the dual (outer columnar and inner equiaxed) grain

structure of alumina layer, indicating that oxidation in these HEAs is governed by inward diffusion of oxygen. Finally, the nano-scale phase precipitation that is characteristic of these alloys, attributed to spinodal decomposition, was credited for providing nucleation sites for quick development of the alumina scale.

All the studies report development of an Al-depleted layer below the oxides, also characteristically seen in MCrAlY and aluminide alloys post oxidation. The Al content of this layer is critical to the oxide layer growth, since if it falls below a critical value, the available Al would be insufficient to replenish the alumina layer in case it is damaged. Lu *et al.*, (2020b) calculated this value for AlCoCrFeNi to be 4 at. %.

Another branch of the AlCoCrFeNi family is where the effect of addition of Cu was studied. In terms of phase formation, the as-cast alloys always exhibited segregation of Cu to the interdendritic region, while AlCoCrFeNi made up the dendritic region. The effect of this was observed in the oxidation behaviour of the alloys as well. Daoud *et al.* (2015) studied non-equiatomic compositions Al<sub>8</sub>Co<sub>17</sub>Cr<sub>17</sub>Cu<sub>8</sub>Fe<sub>19</sub>Ni<sub>33</sub> (FCC) and Al<sub>23</sub>Co<sub>15</sub>Cr<sub>23</sub>Cu<sub>8</sub>Fe<sub>15</sub>Ni<sub>15</sub> (BCC) and compared them to the equiatomic counterpart. In the temperature range of 800–1000 °C, all the alloys developed multiple oxide layers, with innermost alumina, intermediate chromia and sometimes external NiO and Fe<sub>2</sub>O<sub>3</sub>. Poor scale integrity and adherence were reported for specimens tested at 1000 °C.

Dabrowa *et al.* (2017) specifically studied the effect of Cu content on oxidation behaviour of AlCoCrCu<sub>x</sub>FeNi (x=0,0.5,1 mol). They reported formation of  $\alpha$ -Al<sub>2</sub>O<sub>3</sub> on oxidation at 1000 °C, whose adherence worsened with increasing Cu content. Cu was postulated to increase the CTE of the alloy, making the thermal strains generated during

cooling more severe, prompting oxide scale spallation. In their 2019 study, Liu *et al.* examined the oxidation behavior of  $\text{Al}_x\text{CoCrCuFeNi}$  alloys ( $x=0, 0.5, 1, 1.5$ , and  $2$  mol). They found that Cu segregated to interdendritic areas and that Al addition stabilized the BCC phase.  $\text{Al}_{1.5}$  and  $\text{Al}_2$  alloys had the lowest weight increases, indicating the advantageous effect of Al concentration on oxidation resistance.

Using a different approach, Hong *et al.*, (2019) studied the oxidation behaviour of  $\text{Al}_{0.3}\text{CoCrCuFeNi}$  using first-principle methods and calculated the adsorption energy for oxygen adhesion to alloy interfaces for various planar surfaces. They observed that it was lowest for sites with more neighbouring Cr atoms and second lowest for more neighbouring Al atoms. This contrasts with the calculated cohesive energies of oxides, which indicate  $\text{Al}_2\text{O}_3$  to be more stable than  $\text{Cr}_2\text{O}_3$ . They thus concluded that there was a competition between  $\text{Cr}_2\text{O}_3$  and  $\text{Al}_2\text{O}_3$  formation.

The other set of alloying additions to the  $\text{AlCoCrFeNi}$  family is of Ti and Si, added to improve the alloy's oxidation and wear resistance. The first to do this were Zhang *et al.* (2013), who studied  $\text{Al}_{0.5}\text{FeCoCrNiSi}_{0.2}$ ,  $\text{Al}_{0.5}\text{FeCoCrNi}$ , and  $\text{Al}_{0.5}\text{FeCoCrNiTi}_{0.5}$ , oxidized at  $900^\circ\text{C}$ . Owing to their lower Al contents, none of these alloys developed an alumina layer, instead,  $\text{Cr}_2\text{O}_3 + \text{AlN}$  oxidation products were observed for the first two alloys, while the final alloy developed complex  $\text{CoFe}_2\text{O}_4$  spinel + mixed oxide scales along with AlN. Chen *et al.*, (2018a) added minor quantities of Si to  $\text{Al}_{0.6}\text{CoCrFeNi}$  and studied their oxidation behaviour at  $800\text{--}1000^\circ\text{C}$ . They observed formation of FCC+BCC phases in the base alloy, with an additional  $\text{Cr}_{15}\text{Co}_4\text{Si}_6$  phase in the Si-containing alloy. Both alloys  $\text{Al}_2\text{O}_3$ ,  $\text{Cr}_2\text{O}_3$  and spinel scales after oxidation, with parabolic oxidation kinetics. Butler *et al.*, (2015) studied three compositions:  $\text{Al}_{10}(\text{CoCrFeNi})_{90}$  ( $\text{Al}_{10}\text{F}$ ),  $\text{Al}_{20}\text{Cr}_{25}\text{Co}_{25}\text{Ni}_{25}\text{Si}_5$  ( $\text{Al}_{20}\text{S}$ ) and



Al<sub>15</sub>Cr<sub>10</sub>Co<sub>35</sub>Ni<sub>35</sub>Si<sub>5</sub> (Al<sub>15</sub>S) in the as-cast state, comparing the efficacy of Fe vs. Si addition to the AlCoCrNi system upon oxidation at 1050 °C. In the compositions lean in Al (Al<sub>10</sub>F and Al<sub>15</sub>S), FCC+B2 phases based on Ni-Co-Cr and Ni-Al respectively were observed, while BCC+B2 phases were found in Al<sub>20</sub>S. Post oxidation at 1050 °C for 100h, external Cr<sub>2</sub>O<sub>3</sub> and underlying  $\alpha$ -Al<sub>2</sub>O<sub>3</sub> were found to form in all cases, along with an Al-depleted FCC phase region below the oxide layers. In terms of oxidation kinetics, the overall weight gain followed the trend: Al<sub>15</sub>S < Al<sub>20</sub>S < Al<sub>10</sub>F, exhibiting initial transition followed by parabolic stages. It has been noted that alloys with more Al concentration form thinner, more protective oxide scales. It was hypothesized that the solubility and diffusion of oxygen, as well as the concentration and diffusion of Al and/or Cr inside the alloy, would determine how HEAs would oxidize.

Wu *et al.*, (2015) added Ti to AlCoCrFeNi and oxidized AlCoCrFeNiTi<sub>0.5</sub> at 800–1100 °C, reporting formation of phase specific oxides: alumina in the dendritic and TiO<sub>2</sub> + Fe<sub>2</sub>O<sub>3</sub> + FeCr<sub>2</sub>O<sub>4</sub> in the interdendritic and eutectic regions. Al<sub>x</sub>CoCrFeNiTi<sub>y</sub> alloys with various Al and Ti contents were studied by Erdogan *et al.*, (2019), oxidized at 1000 °C, and reported lowest weight gain for the composition with zero Ti. As well, CoCrFeNiAl<sub>0.5</sub> and CoCrFeNiAlTi<sub>0.5</sub> exhibited continuous alumina formation, while the remaining alloys also formed other oxides such as Cr<sub>2</sub>O<sub>3</sub>, TiO<sub>2</sub>, spinels, Fe<sub>2</sub>TiO<sub>5</sub>. Wang *et al.*, (2019) studied Al<sub>x</sub>CoCrFeNiTi<sub>0.5</sub> (x=0.5,1,1.5 mol) oxidized at 1100 °C, and reported the formation of spinel + discontinuous internal Al<sub>2</sub>O<sub>3</sub>; Al<sub>1</sub> formed Cr<sub>2</sub>O<sub>3</sub> + semicontinuous internal Al<sub>2</sub>O<sub>3</sub>; and Al<sub>1.5</sub> formed TiO<sub>2</sub> + continuous internal (Al,Cr)<sub>2</sub>O<sub>3</sub> layers

Combining expected advantages of Si and Ti additions, Hsu *et al.*, (2016) synthesized AlCo<sub>0.6</sub>Cr<sub>1.5</sub>Fe<sub>0.2</sub>NiSiTi<sub>0.2</sub> *via* arc melting followed by crushing and subsequent consolidation by spark plasma sintering. The as-sintered alloy was

composed of major BCC phase, along with minor Cr-Ni-Co rich FCC and Cr<sub>3</sub>Si phases. After oxidation at 1100 °C, it was observed to form a dual oxide layer: an external mixed oxide and an internal Al<sub>2</sub>O<sub>3</sub> layer. The external oxide layer was further observed to thicken and spall with time at temperature, while the Al<sub>2</sub>O<sub>3</sub> layer thickened and adhered to the substrate. The oxidation kinetics was parabolic and comparable to MCrAlY alloys at that temperature.

Yet another way of improving oxidation resistance was proposed by Tsai *et al.*, (2016), where they aluminized Al-lean HEA Al<sub>0.2</sub>Co<sub>1.5</sub>CrFeNi<sub>1.5</sub>Ti<sub>0.3</sub>, followed by annealing and water quenching. The base alloy exhibited FCC structure and oxidized to form Cr<sub>2</sub>O<sub>3</sub> + TiO<sub>2</sub> + Al<sub>2</sub>O<sub>3</sub> + NiTi phases. In contrast, the aluminized HEA exhibited Al(CoCrFeNiTi) + Al<sub>3</sub>Ti + Al<sub>3</sub>Ni + NiTi phases, which resulted in the formation of stable alumina without spallation for over 400h.

Tsao *et al.*, (2016) developed two other variants of AlCoCrFeNi: 44Ni-3.9Al-22.3Co-11.7Cr-11.8Fe-6.3Ti (H1) and 51Ni-5Al-18Co-7Cr-9Fe-5Ti-2Ta-1.5Mo-1.5W (H2) (all in wt.%), termed as high entropy superalloys. Both alloys were synthesized *via* Bridgman solidification and exhibited  $\gamma + \gamma'$  phases. Upon oxidation at 1100 °C, H2 showed 8 times lower weight gain than H1, corresponding to its ability to develop continuous alumina scales although with external oxides.

## 2.10 PROBLEM FORMULATION.

The review of the literature was a critical stage for formulating the research problem and surface degradation of SS-304 at elevated temperatures has been formulated after extensive review. The erosion and oxidation of the surface are serious problems for the surface of the components like super heaters, economizer, heat exchangers, piping and chimneys in petroleum industry made of SS-304. The continual advances in materials

development will demand still higher operation temperatures for such components. These all-engineering applications are subjected to elevated temperatures. In a cyclic and repeating way, hot air impacts the component's surface, and this air includes some undesirable dust particles. The severity of such particles and the harsh climate are the 2 main causes of surface deterioration caused by erosion and oxidation. Some stringent steps were required to combat these problems. So, there is a need to use some protective method to avoid the failure of the surface.

## **2.11 Research Gaps**

- From available literature it is observed that very few attempts have been made to investigate the thermal spray coatings composed of  $\text{Al}_x\text{CrCoFeNi}$  high entropy alloys. Since, the  $\text{Al}_x\text{CrCoFeNi}$  high entropy alloys coatings deposition by using thermal spraying techniques is still in the research and development stage and therefore has been selected in the present research work.
- Research attempts are also required to determine the mechanical and microstructural properties of  $\text{Al}_x\text{CrCoFeNi}$  thermal spray coatings.
- All those types of substrate materials indicated above for the present study are considered based on further investigations of the literature survey and also considered past work done, future work that can be carried out, which is possible in today's life conditions to make some social welfare. Substrate: SS-304 stainless steel — this substrate is chosen because it is widely used in high-temperature applications [25].
- Furthermore, the plasma spraying thermal spray technique has been used for the present work as it offers the smoothest, hardest; well bonded coatings with the lowest porosity and most homogeneous microstructure.

## **2.12 OBJECTIVES OF THE RESEARCH WORK.**

The following are the objectives of the current study:

1. To develop various compositions of  $\text{Al}_x\text{CrCoFeNi}$  high entropy alloys coatings on stainless-steel SS-304) through thermal spray coating techniques i.e., plasma spraying.
2. To examine the as-sprayed  $\text{Al}_x\text{CrCoFeNi}$  high entropy alloys coatings for

comparison in terms of mechanical and micro-structural characteristics.

3. To investigate the high temperature erosive wear behavior of base material and developed coatings at 900°C.
4. To investigate the high temperature oxidation behavior of base material and developed coatings at 900°C.
5. To propose the best combination of coatings for the base metal.

## CHAPTER 3

### EXPERIMENTAL EQUIPMENT AND PROCEDURES

In this chapter, the deposition method of the coatings has been reported along with the process parameters of the equipment used for depositing the coating. The various tools used for the characterization of uncoated & coated samples at different stages of the research work have been described. The procedures of sliding wear tests and erosion tests at elevated temperatures have also been mentioned. The various characterization techniques utilized for erosion and corrosion analysis formed during various tests.

#### 3.1 SELECTION OF SUBSTRATE.

SS-304 was chosen as a substrate material for the present research study. This material is widely used for Power plants and the industry sector faces losses to the components like superheaters, economizers, heat exchangers, piping, and chimneys in the petroleum industry. The substrate material was procured from Baharat Aerospace Limited, Mumbai, India. The chemical composition of the SS-304 substrate was ascertained using an optical spectrometer (Make: "Metal Vision, Model: 1008i").

#### 3.2 DEPOSITION OF COATINGS.

##### 3.2.1 Preparation of Substrate Material.

SS-304 was procured in the form of a flat plate with measurements of  $300 \times 200 \times 5$  mm<sup>3</sup>. After that, the plate was further sliced with a WEDM ("Wire-Cut Electro Discharge Machine") to provide a substrate sample for the testing of "air-jet erosion" ( $25 \times 25 \times 5$  mm<sup>3</sup>) and oxidation ( $20 \times 15 \times 5$  mm<sup>3</sup>). Subsequently, the specimens were machine-polished using alumina powder particles until they achieved an emery paper grade of 1200. The polished samples were subjected to abrasive grit blasting using virgin brown alumina grit of a 16-mesh size. The tools and media used for grit blasting are shown in **Fig.3.1**.



**Fig.3.1.** (a) Front and (b) side view of shot blasting machine and, (c) Blasting medium (Virgin alumina).

### 3.2.2 Coating Powder.

There were three different combinations of powders consisting of  $Al_xCrCoFeNi$  that were deposited using the plasma process on SS-304 substrate. The various powders combinations are  $Al_0CrCoFeNi$  (A1),  $Al_{0.50}CoFeNi$  (A2) and  $Al_{1.00}CoFeNi$  (A3), the morphology and particle powders size and their compositions have been given in chapter 4 of the present study.

The choice of the contents of Al 0, 0.5 and 1.0 in the  $Al_xCrCoFeNi$  alloys system is based on the strategic selection because allows examining the different aspects of phase changes and property variations that occur by the change in concentration of aluminum in the alloy. The corresponded critical points of the phase evolution of the alloy are reflected by the respective compositions. Al-free alloy at  $x = 0$  gives a stable FCC single-phase alloy case which is highly ductile and low hardness which is used in a reference baseline. At  $x = 0.5$  the alloy undergoes a transition regime in which both FCC and BCC phases exist and the study of two-phase microstructures which commonly gives an optimum combination of strength and ductility. Lastly, at  $x = 1.0$  alloy turns Al-rich and also facilitates the formation of BCC or ordered B2 phases based on the decrease in the concentration of valence electrons giving rise to the markedly higher level of hardness

and wear resistance at the cost of ductility. The systematic variation covers the entire range of microstructural and mechanical properties - spanning soft, ductile FCC and to hard, brittle BCC - and is in line with understood phase stability windows of HEAs.

### **3.2.3 Deposition of Coatings.**

APS is a thermal spray process that uses a plasma jet to melt and propel material onto a surface. It is used to create thin, dense coatings that have excellent adhesion, corrosion resistance, and thermal and electrical insulation properties. The process is versatile and can be used to apply a wide range of materials, including metals, ceramics, and polymers. It is an effective and economical choice for applications such as wear-resistant coatings and TBCs. The plasma jet melts the material to a molten state, which is then accelerated onto the surface of the substrate. The molten material subsequently solidifies as well as coalesces with the substrate, forming a strong bond. “This leads to a thin, highly dense and high-quality coating,” the company says. Whether or not using H<sub>2</sub> as the carrier gas, enough Ar must be used to maintain a flat meniscus within the APS coating. The gases penetrate from the hole of electrode and are warmed and then pulverized by the arc to form plasma. During this process, the nozzle controls the plasma jet by varying the speed at which it burns gases as well as its flow rate. the process heavily depends on carrier gases consisting mainly of such burnt gases. The quality of the deposited coating is mainly affected by thermal spray process parameters. The speed and flow rate of the gases also affect the spray rate, which in turn affects the deposition rate. The optimal parameters should be adjusted to obtain the desired coating properties.

These parameters include the stand-off distance maintained between the substrate material and the gun during deposition, as well as the current, voltage, and gas flow rate. The thickness of the coating is an important parameter because it affects the amount of heat that can be absorbed and the amount of stress that the coating can withstand. Thicker coatings provide better protection but may also increase thermal conductivity and reduce thermal insulation. The morphology of the powder particles and the powder itself are two of the factors that determine whether APS can generate a specialised coating with a certain powder. It is recommended that the layer-forming powder have a particle size of around 40  $\mu\text{m}$ . The melting process is often interrupted when larger particles are involved. Particles with a size less than 10  $\mu\text{m}$ , on the other hand, are unable to break through the plasma jet, move at a slower speed, and do not reach the surface of the substrate.

Plasma spraying (PS) is performed for the deposition of coatings using a 9 MB plasma gun. It is used for spraying metallic and ceramic coatings. It offers advantages such as a high deposition rate, good adhesion, and abrasion resistance. As the PS process involves a very high velocity of around 250 m/s, the samples are held using different fixtures according to the different sizes of the samples. The fixture's main advantage is that the coating's uniformity is maintained. The fixtures are sample holding devices used during the deposition process to ensure the quality of the coating. 2700 gun at “M/s Metalizing Equipment Corporation, Jodhpur, India”). As the HVOF process involves a very high velocity of around 1000m/s, therefore the samples were held by using different fixtures according to the different sizes of the samples. The main advantage of a fixture is that the uniformity of the coating is maintained. The fixtures are sample-holding devices used during the process of deposition to ensure the quality of the coating. The parameters of process in coatings are listed in **Table 3.1**. The same parameters of process have been adopted for the deposition of all powder combinations. However, the skilled and experienced operators performed the coating operation. The deposition of coating includes the initial trails in the form of some passes. The average particle size of the feedstock powder and the number of passes decides the approximate coating thickness to be deposited. Therefore, the deposition of coating with 40  $\mu\text{m}$  average particle-sized powder requires approximately 6 passes for 200 $\mu\text{m}$  thickness of the coating. The PS equipment is presented in (**Figure 3.2**).

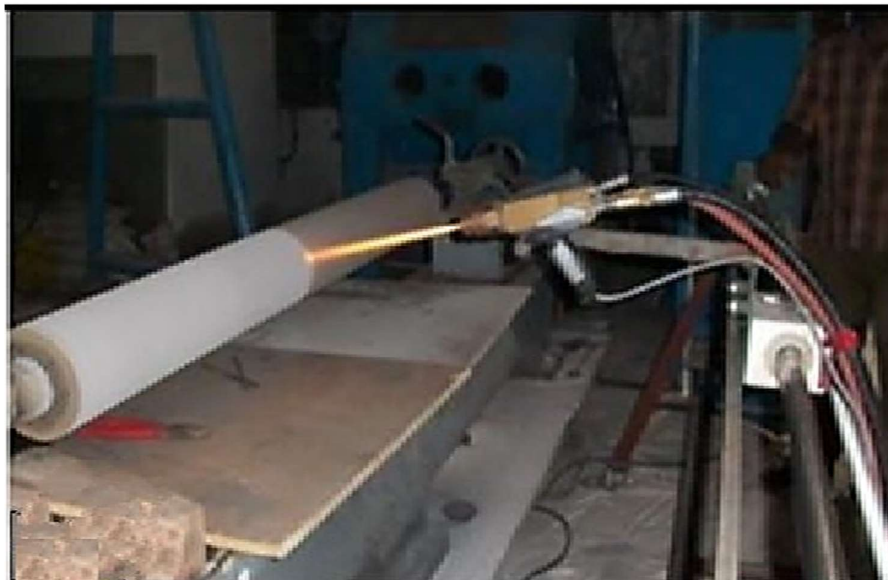


**Fig 3.2** PS apparatus used in the current research work.



**Table 3.1** Process parameters used for the Plasma spraying process.

Parameters selected for spraying/units	Values for composite coatings
Argon gas flow rate/slp <sub>m</sub>	40
Spray angle/degree	90
Powder feed rate (pfr)/g min <sup>-1</sup>	30
Hydrogen gas flow rate/slp <sub>m</sub>	2
Nozzle size/mm	6
Spraying distance of substrate from gun/mm	101.6

### 3.3.1 Preparation of Specimen.

Slow-speed metallurgical diamond saw (“Model: MS-10, Make: Ducom Instruments Private Limited Bangalore, India”) the cutting was done by using Maintaining ‘around’ 200 RPM of speed in the diamond saw. The detail of this diamond saw is presented in Appendix A (see Fig. A-6). The polished was done slowly with the “200,400,600,800,1000 and H1200 pumice grade of emery paper before mirror like images were gotten from the cloth polishing with diamond paste to the 4/0 grade of finest emery papers”. The specimens were ultrasonically cleaned and dried in air for moisture removal. The detail of the ultrasonic cleaner is presented in Appendix A (Fig. A-5).

### 3.3.2 Coating Thickness Measurement.

The thickness has been measured in the deposition process using a thickness gauge used for thin films (Model: Minitest 2000; Make: “Elektro-Physik Koln Company, Germany”), having a precision of  $\pm 1 \mu\text{m}$ . The measured values of thickness were further verified by mounting and sectioning of deposited coatings according to the procedure given in section 3.3.1.

A FE-SEM (“Field Emission Scanning Electron Microscope”) (Make: JEOL, Japan; Model: JSM-6610LV) equipped with an EDS (“Energy Dispersive Spectroscopy”) was used for obtaining the cross-sectional BSE (“Back Scattered Electron”) images. The detail of the SEM equipment is presented in Appendix A (Fig. A-3). The average coating

of the thickness was obtained and seen from the BSE images. The values of the deposited coatings' average thickness from the cross-section are given.

### **3.3.3 Measurement of Surface Roughness and Porosity**

The plasma-sprayed samples were polished prior to the measurement of porosity. The as-sprayed coating surface has been polished down to emery papers of 1200 grit size for microstructure analysis. This involved the measurement of porosity on Dewinter inverted optical microscope (Model: LT-2B, Make: Chennai metco Pvt. Ltd, Chennai, India) using image analyzer software (Dewinter Material Plus, Version4.3) according to STM B276 standard. The detail of the Dewinter inverted optical microscope is presented in Appendix A (Fig. A-2). Ten values of porosity were taken and their averages have been reported. The porosity values and surface roughness of the deposited coatings are the average of the ten measurements and are given in Chapter 4 of the current research study.

### **3.3.4 Measurement of Micro-hardness**

The coatings' micro-hardness has been found with Vickers's micro-hardness tester (Model: Economet VH1 MD, Make: Chennai metco Pvt Ltd, Chennai, India) at 300g load with a dwell time of 10s. The detail of Vickers's micro-hardness tester is presented in Appendix A (Fig. A-4). The sample with the sprayed coating's micro-hardness was measured along the layer thickness. A total of 10 indents were made at two separate locations over the coating's cross-section. Five indentations were taken along the layer thickness at each place. Finally, their average value is reported and the distribution of micro-hardness values is presented in Chapter 4 of the current study.

### **3.3.5 XRD Analysis**

The feedstock powder and as-sprayed coatings' XRD patterns were taken. The XRD patterns of the surfaces after exposure to various tests were also reported to analyse the phases created on the surface of the coated and uncoated samples. XRD was conducted with a scanning rate of 1°/min and a step range (2- $\theta$  range) of 10°-100° on Bruker AXS diffractometer. The XRD has been conducted with a "Cu-K $\alpha$  radiation" source formed at 40mA & 40kV. The detail of XRD is presented in Appendix A (Fig. A-1).

### **3.3.6 FE-SEM and EDS Analysis**

#### **3.3.6.1 Surface Morphology /Cross-sectional Analysis/EDS Analysis**

An FE-SEM (“Make: JEOL, Japan; Model: JSM-6610LV”) acceleration with a voltage of 15kV and equipped with an EDS has been utilized for the study of the morphology of the powders and as-deposited coatings. The coated specimens were initially silver pasted between the samples and stub for having conductivity, thereafter, gold coated for obtaining elemental maps for the analysis of different elements present. The as-sprayed coatings have been studied to comprehend the coatings’ surface morphology and for the identification of melted splats, partially melted, un-melted particles, as well as pores formed on the surface of as-sprayed coatings. The EDS analysis provides the elemental compositions (weight %) at the selected region in the form of point and line analysis were taken at any region of the coating. Samples were made according to the process presented in section 3.3.1 for the cross-section analysis of the coating before and after the testing. The SEM/EDS analysis was conducted using an FE-SEM equipped with an EDS attachment. EDS study has been performed for the composition of elemental across the cross- at different regions of the substrate, bond coat, and top coats as well. SEM/EDS study of the as-coated and uncoated sample was presented in Chapter 4 of the current research work study.

#### **3.3.6.2 Elemental Mapping Analysis**

The different elements represented in the feedstock powders and their proper distribution were obtained by EDS maps and for this; the specimens have been cut over the cross-section and then further polished to achieve the elemental mapping. The procedure for sample preparation is already given in section 3.3.1. The coated specimen was sectioned, and polished, as well as silver was pasted between the samples & stub for conductivity, thereafter, gold for obtaining an elemental-mapping study of several elements represented on the as-sprayed and across the coating’s cross-section. The selected area represents the regions which are the substrate, bond coat, and coating regions. Elemental mappings for all deposited coatings were reported in this research study. The mappings give information about the elemental distribution in the deposited coatings. It concentration of the elements in the coatings can easily be seen with the help of X-ray mappings of deposited coatings. The cross-section of all coatings can give the distribution of elements and also helps to understand the difference between all coatings.

### 3.4 HIGH-TEMPERATURE WEAR BEHAVIOUR.

#### 3.4.1 Erosion Analyses in Air Jet Erosion Test Rig.

When high temperature air-jet erosion test was performed. Erosion testing was conducted using air jet erosion tester (“Model: TR-471-800, Make: Ducom Instruments Pvt. Ltd., Bengaluru.”) Nanotechnology (IJRAN)” and “Manufacturing Lab at Guru Nanak Dev Engineering College, Ludhiana, India”). Ltd., Bangalore, India). Detail of air jet erosion tester. Fig 3.3 Shall be Listed in Table (3.2): Test conditions of the temperature for air-jet erosion test at high temperatures: Following each test, the samples were re-weighed on a scale that was accurate to 0.01mg.

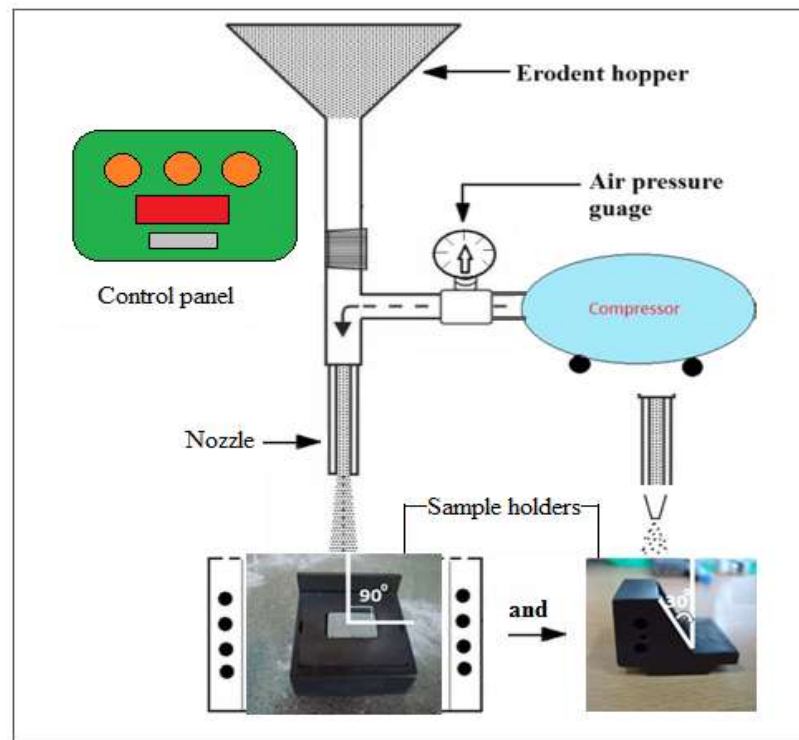


**Fig.3.3.** (a) Airjet erosion test rig (b) Panel of Airjet erosion test rig.

**Table 3.2** Air-jet erosion test parameters.

Parameters	Units	Values
Nozzle diameter	mm	1.5
Exposure time	min	10
Temperature	°C	800
Impact angle(degrees)	degrees	30° and 90°

Powder feed rate	g/min	6
Erodent size	μm	60
Erodent powder	-	Aluminium oxide

### 3.5 ANALYSIS OF OXIDATION

2: Tube Furnace. For oxidation studies the prepared samples were analyzed under simulated boiler condition in tube furnace at 900°C temperature. 3. 4). Each test sample was coated from all the faces to ensure the same condition and reduce measurement error. The simulated studies were conducted a total of 50 cycles; every alternate cycle comprises of 1hr of exposure to temperature 900°C and faced air cooling at room temperature for (20min). The selected cyclic oxidation conditions used in this work simulate closely the real industrial environment which experience shutdowns most of the time\_ *ibid*. Cyclic studies resulted more worse testing constraints which might be same as similar to industrial real world condition for repeated break downs and shutdowns (Verma and Kaushal, 2021; Kaushal et al., 2010; Kaushal et al., 2012; Kaushalet.al, 2014).

The weight change was measured by etc electronic balance (Model: ML-220) with a sensitivity 0.01mg after each cycle to observe that the samples were too much exposed to find and present oxidation kinetics. Average reading of three samples in each cycle was checked and recorded for further analysis. Colour changes were visual observation of the surface morphology in all samples. Measurement started immediately after and also was continued during cyclic oxidation study recorded colour changes (before spalling) to scale spalling.

The specimens after oxidation run were analyzed using XRD, SEM, and EDAX for surface analysis

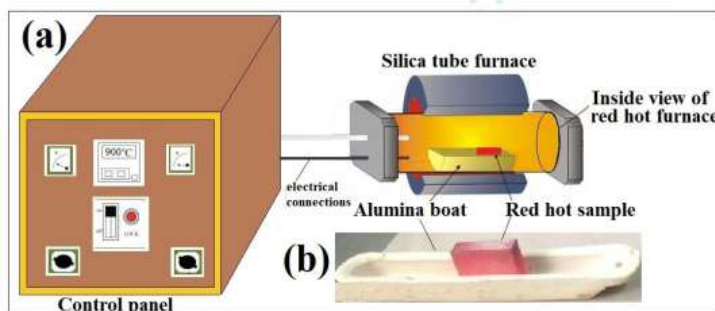


**Fig. 3.4** (a) silica tube furnace diagrammatical representation and b) red hot oxidized sample in alumina boat.

### 3.5.2 XRD Analysis.

The XRD patterns of as-sprayed and uncoated GCI after exposure were taken to identify the phases formed on the coatings. XRD has been with a scanning rate of  $1^\circ/\text{minute}$  and a step range ( $2\theta$  range) of  $10^\circ$ - $100^\circ$  on Bruker AXS diffractometer. The radiation source of Cu-K $\alpha$  generated at 40mA & 40 kV was used for the XRD. At the “Indian Institute of Technology” in Mandi, India, the XRD analysis was completed.

### 3.6.3 FE-SEM/EDS ANALYSIS.

#### 3.6.3.1 Cross-sectional Analysis.

The specimens exposed to cyclic oxidation test were analysed from cross-section by FE-SEM (“Make: JEOL, Japan; Model: JSM-6610LV”) with an EDS. The exposed specimens were initially silver pasted between the samples and stub for having conductivity, thereafter, gold coated for obtaining elemental maps for the analysis of various elements present. The effect of oxidation along the coated and uncoated samples cross-section was studied. The EDS analysis provides the elemental compositions (weight %) at the selected region in the form of point and line analysis were taken at any region of the coating across the cross-section. Samples were prepared according to procedure given in section 3.3.1. EDS study was performed for the elemental composition across the cross- at various regions of the substrate and coatings as well. SEM/EDS study of the as-coated and uncoated sample was represented in Chapter 4 of the current research work study.

### **3.7.2 FE-SEM Analysis**

#### **3.7.2.1 Surface Morphology**

After being subjected to a high-temperature solid air-jet erosion test, the surface morphology of the eroded samples was examined at various magnifications using a FE-SEM (“Make: JEOL, Japan; Model: JSM-6610LV”) fitted with an EDS.

## CHAPTER 4

### CHARACTERIZATION OF AS-SPRAYED COATINGS

The chapter deals with the characterization of the deposited coatings on SS-304 substrate by the process of plasma spraying. The SEM/EDS analysis from surface and cross-section along with elemental mappings of the coatings are reported.

#### 4.1 SS-304 SUBSTRATE

##### 4.1.1 Chemical Composition of Substrate

SS-304 has been chosen as substrate material and its composition has been examined with an optical spectrometer (Make: “Metal Vision, Model: 1008i”). The SS-304 compositions are provided in **Table 4.1**.

Table 4.1. SS-304 substrate’s chemical composition.

Elements	Actual composition
Cr	17.50-19.50
C	0.07
Mn	2.00
Si	1.00
P	0.045
S	0.015
Ni	8.00-10.50
Fe	Bal.

#### 4.2 SEM-EDS EXAMINATION OF SUBSTRATE AND COATINGS

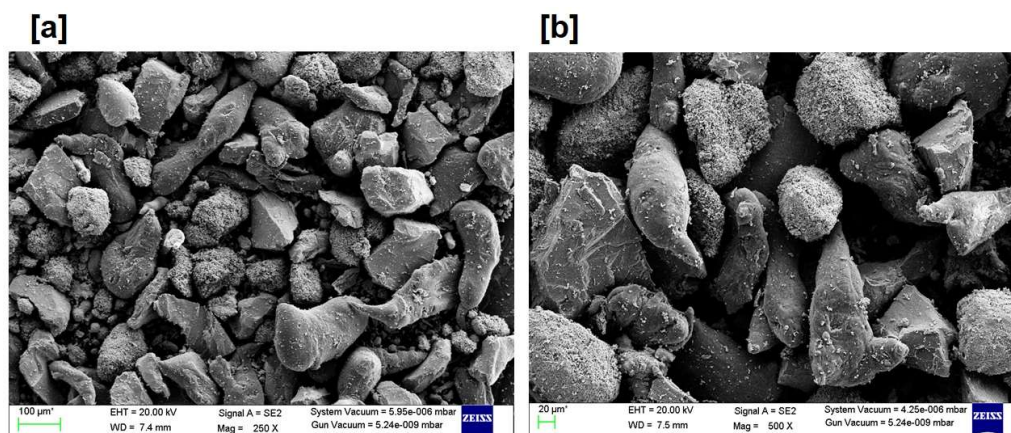
There were two different coatings that were deposited using the plasma spray process on the SS-304 substrate. The various coatings used in the present work along with the designation system used are exhibited in **Table 4.2**. The coatings powders morphology was determined using SEM/EDS. A standard SEM micrograph that shows the morphology of the  $Al_xCrCoFeNi$  powder is presented in **Fig. 4.1(a)**. The EDS of the  $Al_xCrCoFeNi$  powder is presented in **Fig.4.2**.

Table 4.2 Designation system utilized for the coatings.

Coatings	Al	Co	Cr	Fe	Ni
$Al_0CrCoFeNi$ (A1)	0	27.12	23.74	23.99	25.14
$Al_{0.50}CoFeNi$ (A2)	5.59	25.25	22.13	22.80	24.22
$Al_{1.0}CoFeNi$ (A3)	10.02	23.84	21.11	21.99	23.03



The SEM-EDS analysis of the powders used in the present work has been represented in the Fig. 4.1 to Fig .4.6. The average particle size of the used powders was in the range of 40-70  $\mu\text{m}$  as shown Fig.4.1, 4.3 and 4.5, respectively.



**Fig.4.1** SEM Micrographs of powders at various magnifications used for Coating 1-  $\text{Al}_0\text{CrCoFeNi}$ .

All coating powder powders have shown the proper blending of elements in the SEM micrographs. Moreover, the composition selected for the powders have been confirmed with the help EDS analysis. The coating composition has been represented with the SEM-EDS analysis of powders in Fig.4.2, 4.4 and 4.6, respectively. The EDS has conformed the presence of all elements except Al in C1 powder as shown in Fig. 4.2(b).

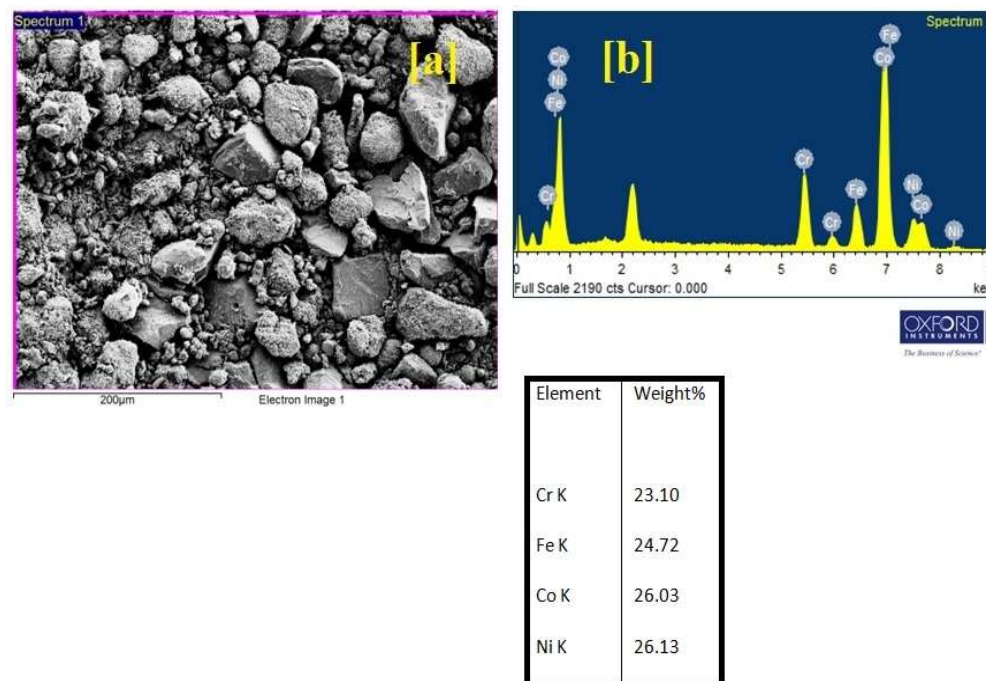


**Fig.4.2** SEM -EDS of powder- used for Coating 1-  $\text{Al}_0\text{CrCoFeNi}$ .

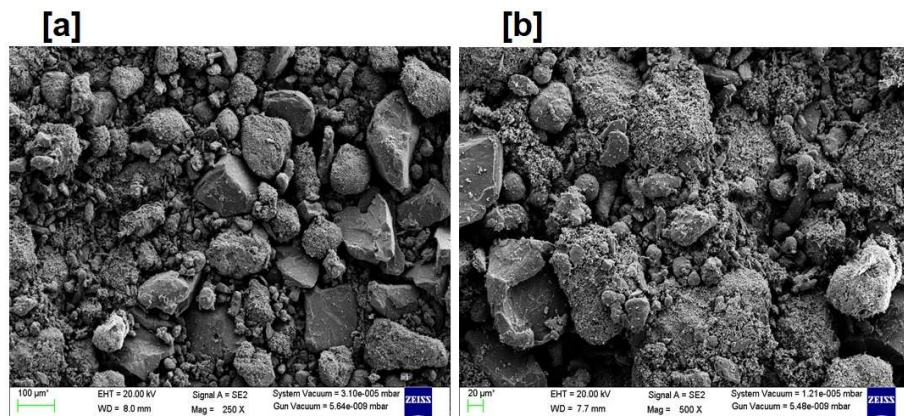


**Fig.4.3** SEM Micrographs of powders at various magnifications used for Coating 2- $\text{Al}_{0.5}\text{CrCoFeNi}$ .

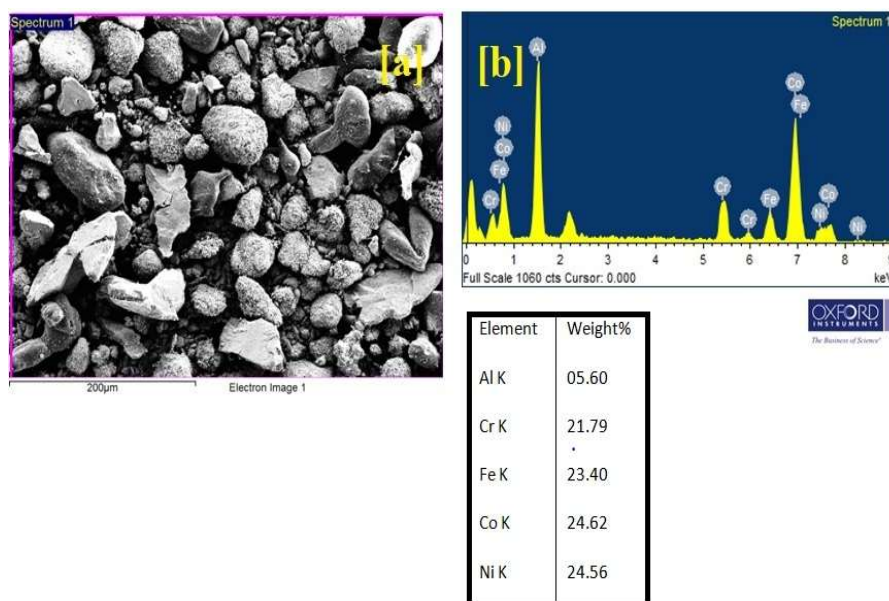


**Fig.4.4** SEM -EDS OF POWDER- Coating 2-  $\text{Al}_{0.5}\text{CrCoFeNi}$ .

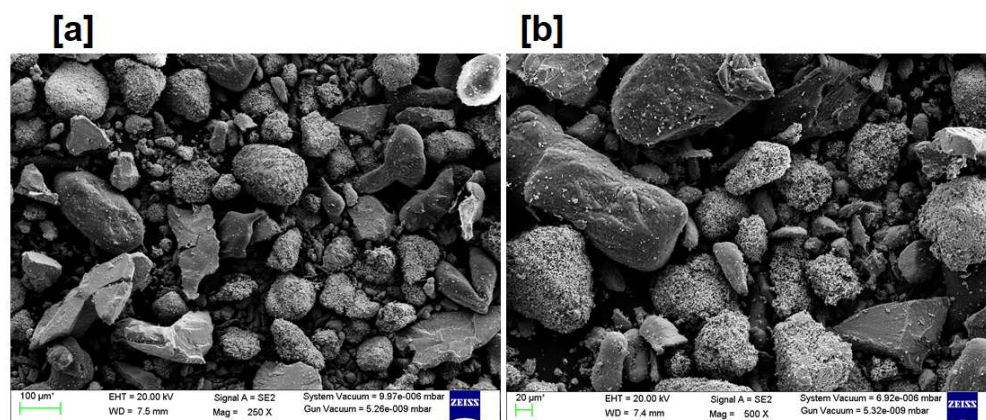


**Fig.4.5** SEM Micrographs of powders at various magnifications- Coating 3- $\text{Al}_1\text{CrCoFeNi}$ .



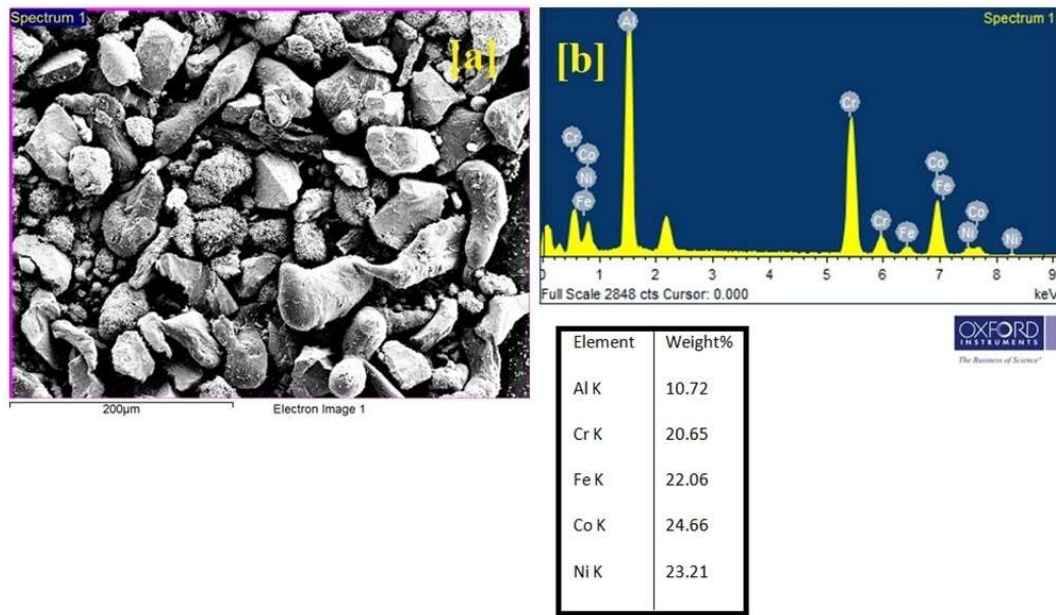


**Fig.4.6 SEM -EDS OF POWDER- Coating 3-  $\text{Al}_1\text{CrCoFeNi}$ .**

The  $\text{AlCrCoFeNi}$  high-entropy alloy powder commonly utilized in thermal spray coatings showcases a remarkably smooth surface and a tightly controlled particle size distribution, with an average particle size of approximately 50 microns. This particular powder morphology offers significant advantages in thermal spray processes, as it enhances the flowability and deposition efficiency of the feedstock material. The composition and microstructure of this high-entropy alloy powder contribute to its potential for improved mechanical properties, corrosion resistance, and wear resistance when used as a thermal spray coating.

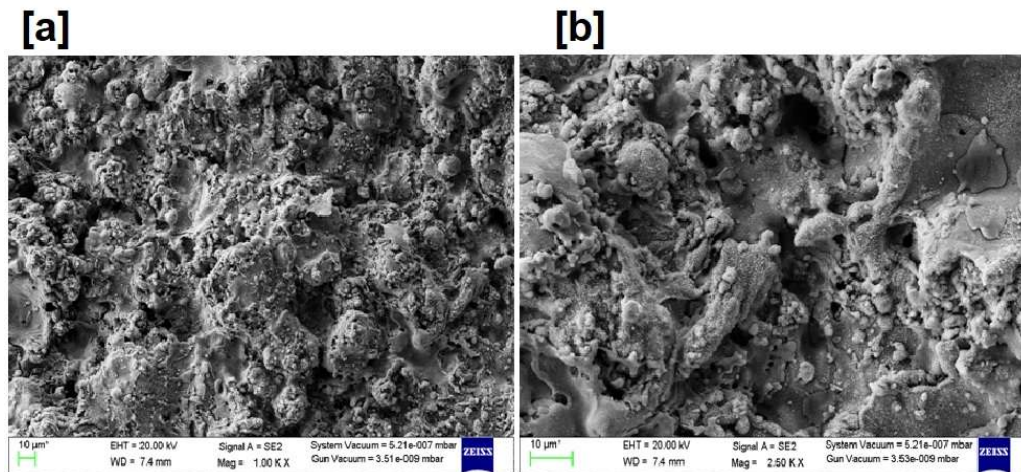


**Fig. 4.7 SEM Micrographs of at various magnifications- Coating 1-  $\text{Al}_0\text{CrCoFeNi}$**

The AlCrCoFeNi high-entropy alloy possesses desirable characteristics that make it highly sought after for a wide range of industrial applications that demand durable and protective coatings. The surface analysis of the coatings has been conducted to understand the surface features of the coatings with the help of SEM images as shown in Fig. 4.7, 4.11 and 4.15, respectively.

The surface of the coatings mainly consisted of melted, un-melted and partially-melted regions, which are typical features of HVOF sprayed coatings.

The surface analysis of the coatings was assisted by EDS mapping of the coated surfaces as shown in Fig. 4.8, 4.10 and 4.12, respectively. The surface of the coatings has showed the distribution of elements on the surface.

The concentration of elements was corresponding to the composition of the deposited coatings. EDS-mapping revealed the increased the concentration of Al in the deposited coatings, where higher concentration was observed the EDS maps of Al<sub>1.00</sub>CoFeNi coating.

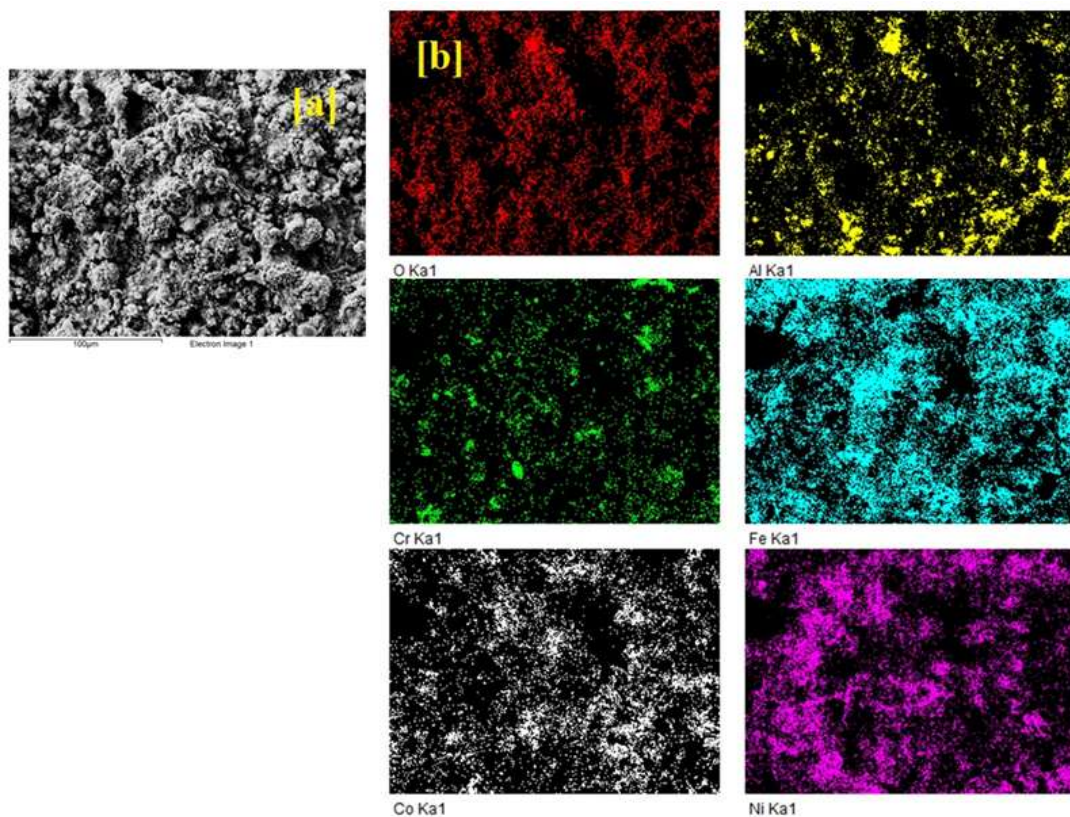


**Fig. 4.8** X-ray maps- Coating 1- Al<sub>0</sub>CrCoFeNi from surface.

The surface analysis of the coatings was further assisted with the cross-sectional analysis of the deposited coatings as shown in Fig. 4.9, 4.11 and 4.13, respectively. The cross-sectional SEM images revealed the well bonded coatings to the substrate materials and free from any cracks. The splat-by-splat formation of coatings is expected in any well bonded coatings and same has been observed in the cross-sections of the deposited coatings. Moreover, the inter-splat bonding can also be observed in the SEM images with higher magnification level.

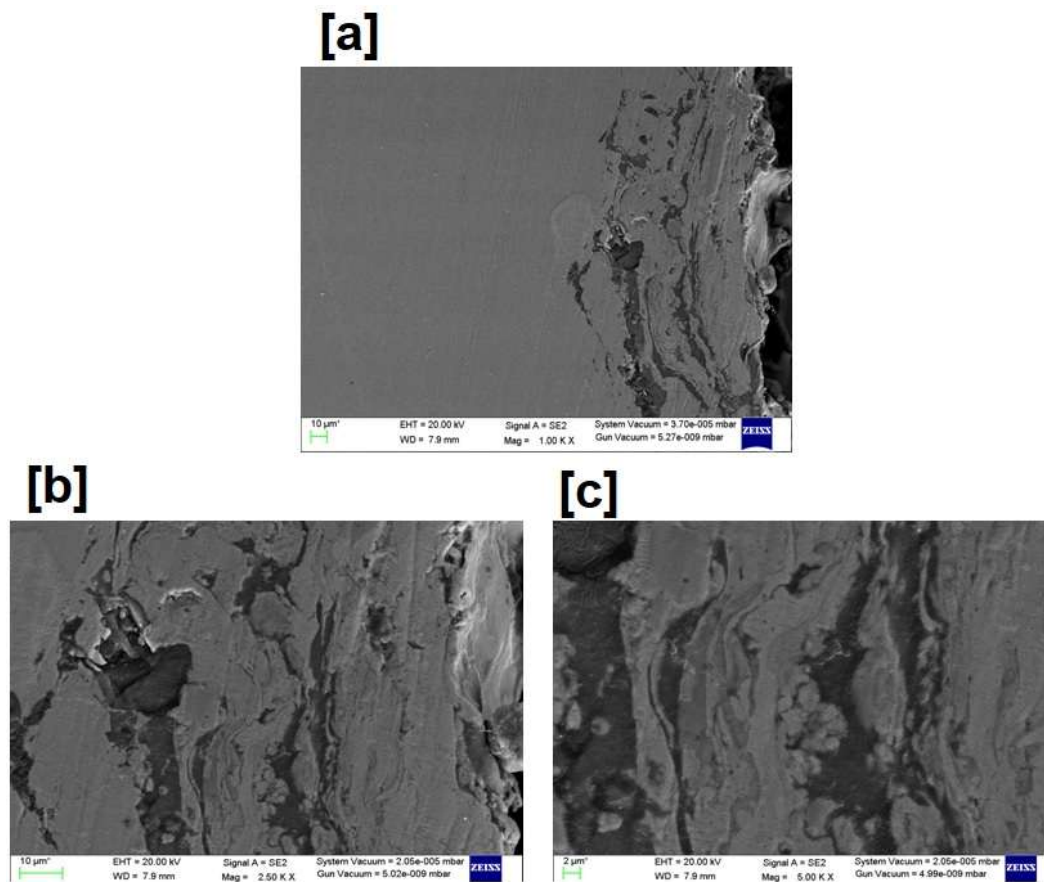


**Fig. 4.9** SEM cross-sectional Micrographs of at various magnifications- Coating 1-  $\text{Al}_0\text{CrCoFeNi}$ .

The cross-sectional analysis of the deposited coatings also included the EDS-mapping to understand the distribution of the elements across the cross section of the deposited coatings as shown in Fig. 4.10, 4.14 and 4.18, respectively. The cross-sectional SEM images revealed the well bonded coatings to the substrate materials and free from any cracks. The concentration of the elements was observed in-line with the composition of powders used for the deposition of the coatings. The maximum concentration of the Al was observed in the  $\text{Al}_{1.00}\text{CoFeNi}$  coating.



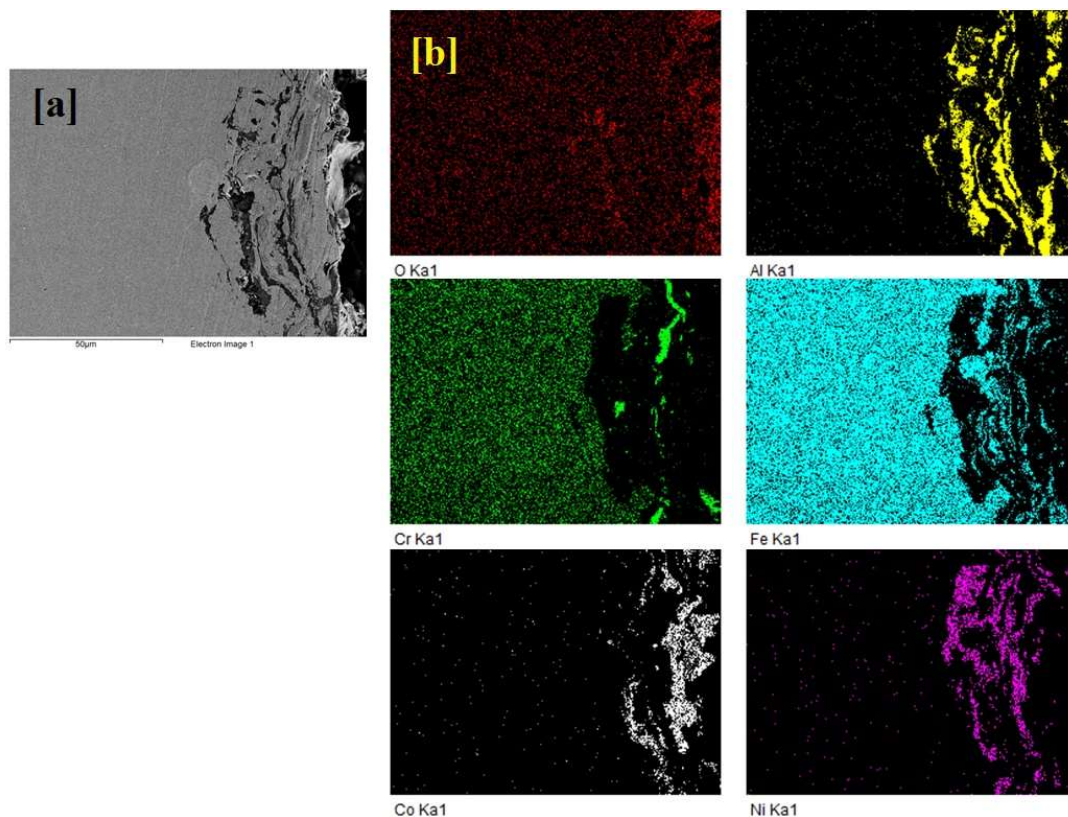


**Fig. 4.10** X-ray maps- Coating 1-  $\text{Al}_0\text{CrCoFeNi}$  from cross-section.

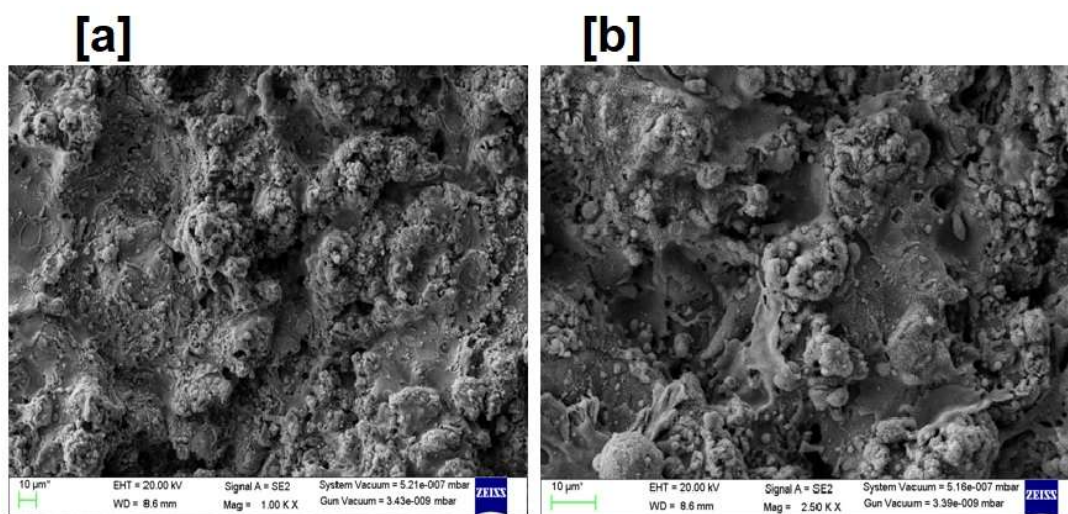


**Fig. 4.11** SEM Micrographs of at various magnifications- Coating 2-  $\text{Al}_{0.5}\text{CrCoFeNi}$ .

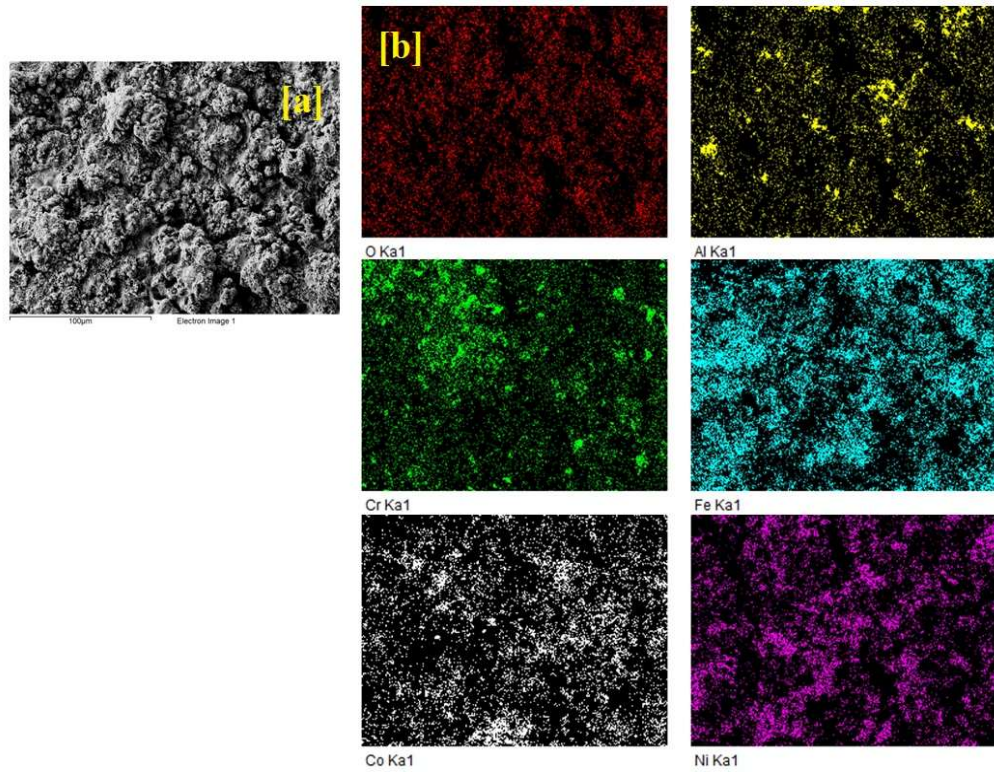


**Fig. 4.12** X-ray maps- Coating 2-  $\text{Al}_{0.5}\text{CrCoFeNi}$  from surface.

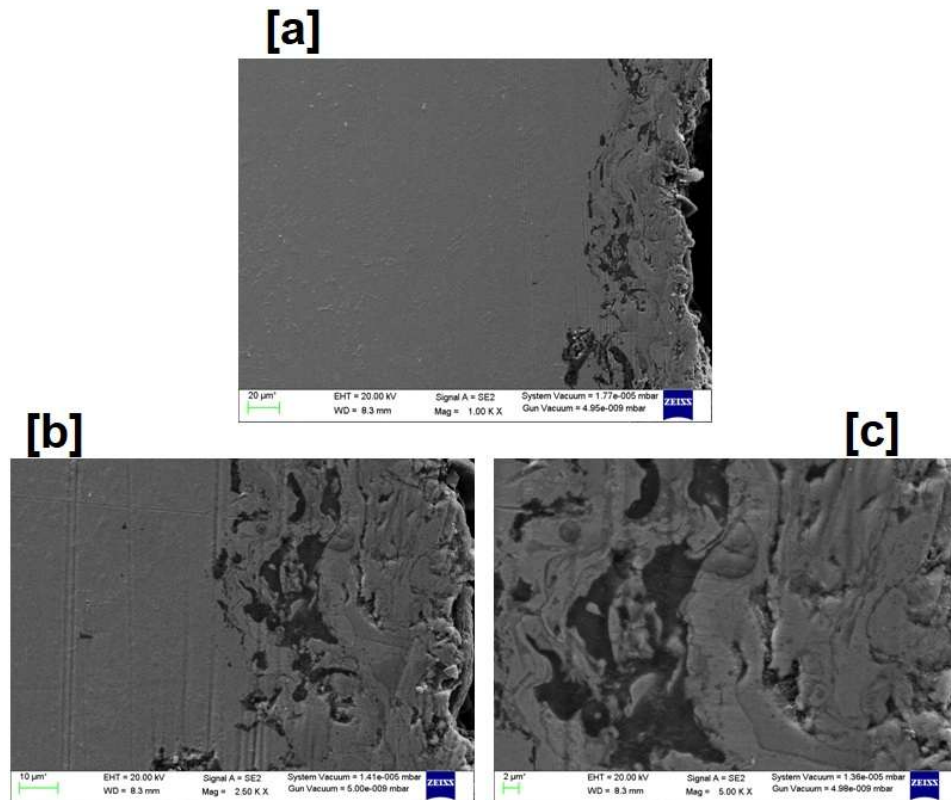


**Fig. 4.13** SEM cross-sectional Micrographs of at various magnifications- Coating 2-  $\text{Al}_{0.5}\text{CrCoFeNi}$ .



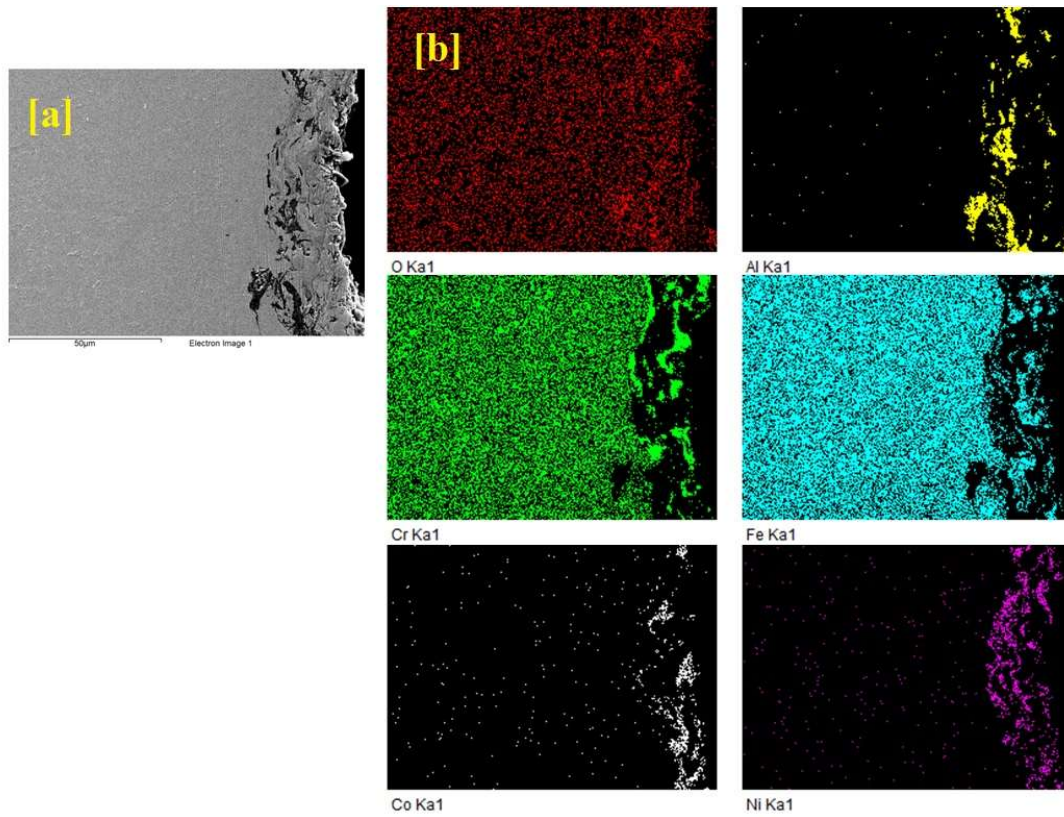


**Fig. 4.14** X-ray maps- Coating 2-  $\text{Al}_0\text{CrCoFeNi}$  from cross-section.

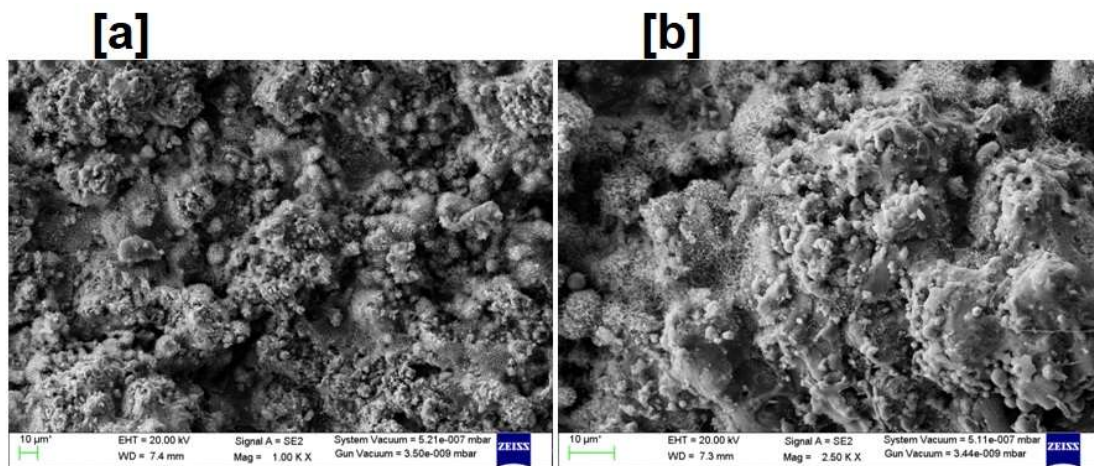


**Fig. 4.15** SEM Micrographs of at various magnifications- Coating 3-  $\text{Al}_1\text{CrCoFeNi}$ .



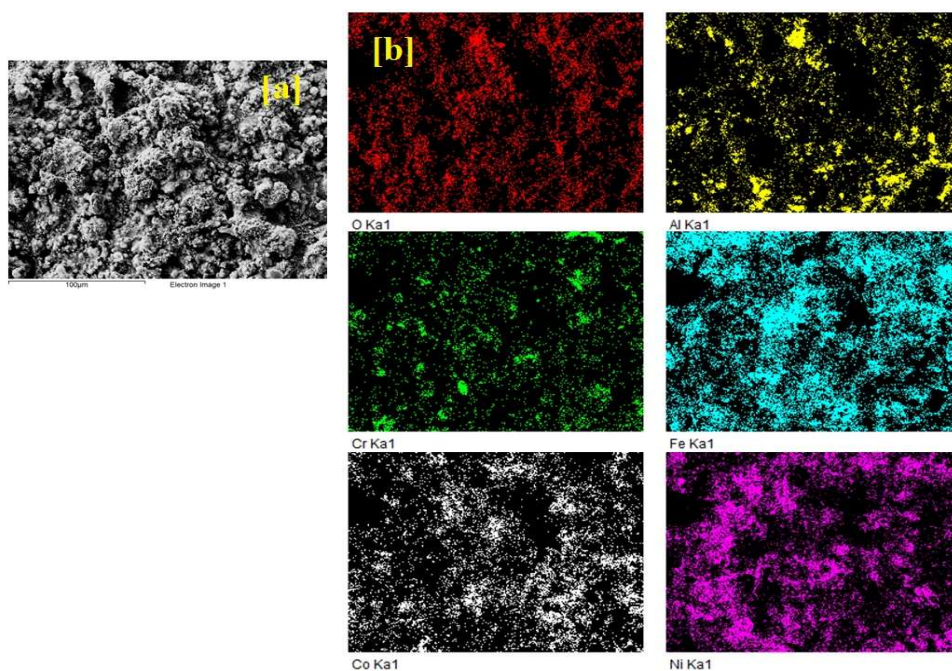


**Fig. 4.16**X-ray maps- Coating 3-  $\text{Al}_1\text{CrCoFeNi}$  from surface.

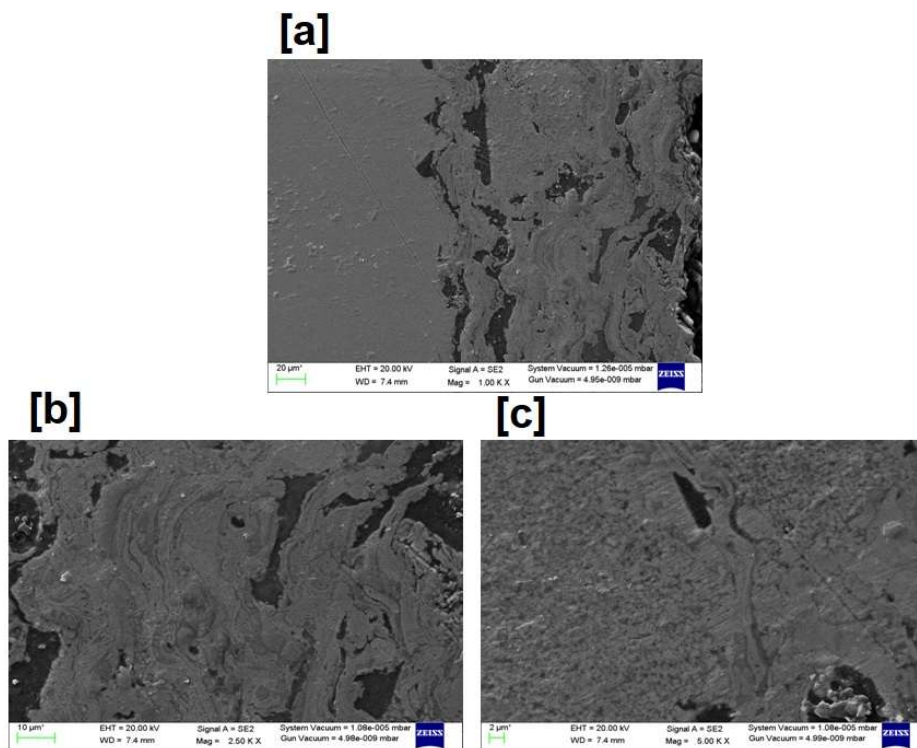


**Fig. 4.17**SEM cross-sectional Micrographs of at various magnifications- Coating 3-  $\text{Al}_1\text{CrCoFeNi}$ .

The XRD analysis of the deposited was performed to know the phases present in the deposited coatings as shown in Fig.3.23

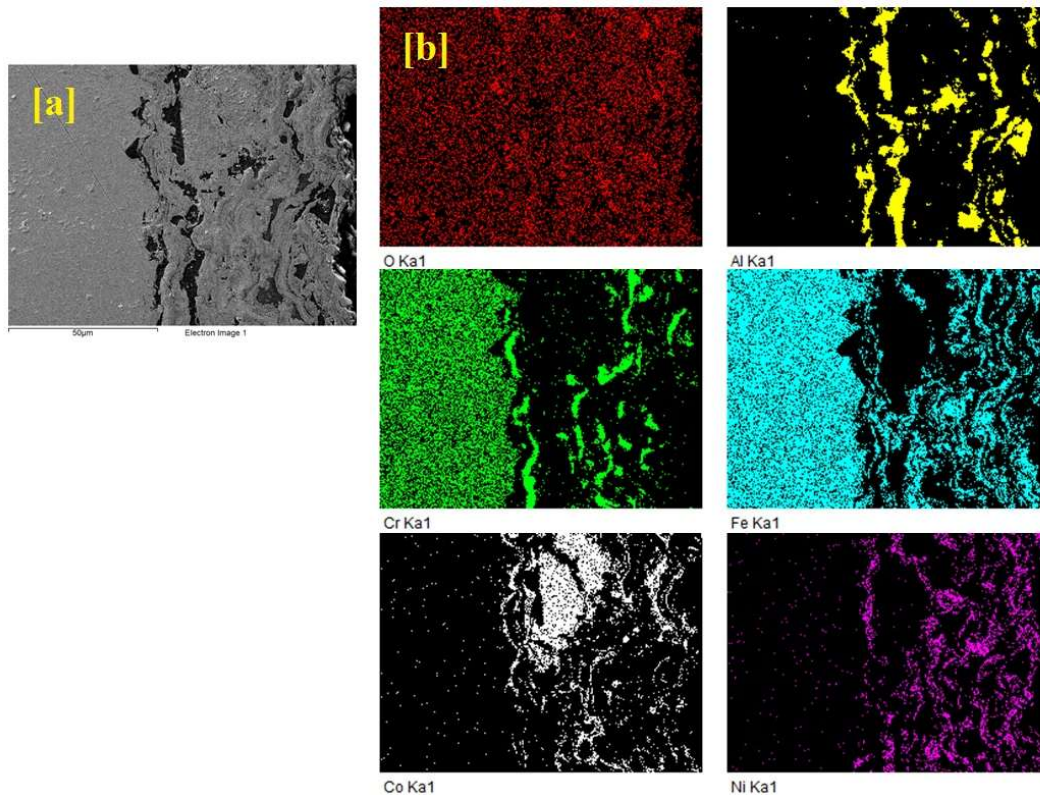


**Fig. 4.18** X-ray maps- Coating 3-  $\text{Al}_1\text{CrCoFeNi}$  from cross-section.

The XRD patterns of plasma sprayed coatings are presented in Fig. 4.19. Fig. 4.19, the coating has three diffraction peaks near  $2\theta = 39^\circ, 44^\circ, 52^\circ, 65^\circ, 76^\circ, 82^\circ$  and  $94^\circ$  corresponding to BCC phases, FCC phases, and spinels formed during the coating deposition. The increase in the Al concentration can be observed in these XRD patterns. Phase B corresponds to the BCC structure, which has major phases of Fe-Cr and Al-Ni. Phase F corresponds to the FCC structure, with the major phase consisting of Ni-Co-Cr. The phase S corresponds to the spinels  $\text{NiAl}_2\text{O}_4$ .

The surface analysis of the coatings was further assisted with the cross-sectional analysis of the deposited coatings as shown in Fig. 4.9, 4.11 and 4.13, respectively. The cross-sectional SEM images revealed the well bonded coatings to the substrate materials and free from any cracks. The splat-by-splat formation of coatings is expected in any well bonded coatings and same has been observed in the cross-sections of the deposited coatings. Moreover, the inter-splat bonding can also be observed in the SEM images with higher magnification level.

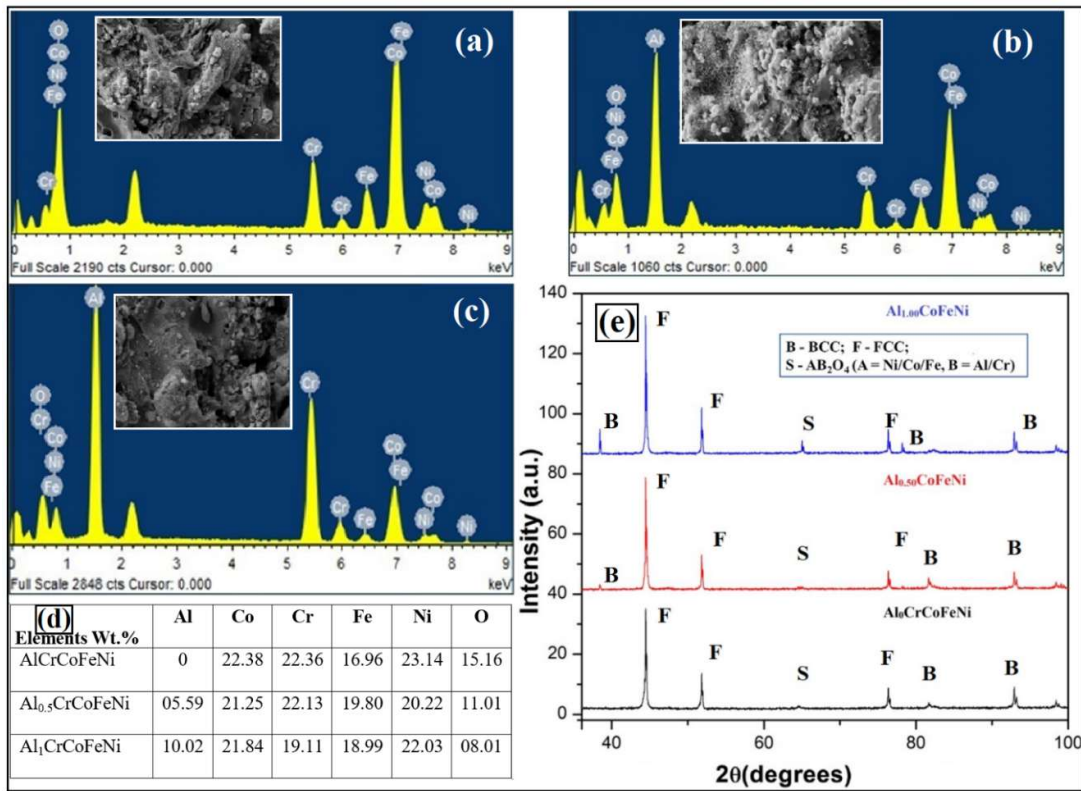


**Fig. 4.19 XRD of all deposited coatings.**

The SEM micrographs of  $\text{Al}_x\text{CoCrFeNi}$  coatings along with EDS mapping are shown in Fig.4.20. In Fig. 4.20 (a), the cross-section of the  $\text{Al}_0\text{CoCrFeNi}$  coatings shows substrate and coating regime separated by interface. A good mechanical bonding can be observed at the interface of substrate and coating and forming a homogenous composite layered structure in all coatings. In the coating region solid solution (Fig. 4.20b) can be seen in all coatings and the composition for Al is differentiated with the help of EDS mapping as shown in Fig. 4.20 (d), (h), and (l), respectively. The enlarged view of a cross-section of all coatings is represented in Fig. 4.20 (b), (f) and (j), respectively. The cross-section has shown three different shaded zones i.e., white, grey, and black phase. During EDS mapping it has been found that the black phase corresponds to aluminum and oxygen and the grey phase refers to rich in Al-Cr-Fe. The white phase corresponds to the depletion in Al content with a low oxygen level, resulting in aluminum depleted FCC+BCC phase.



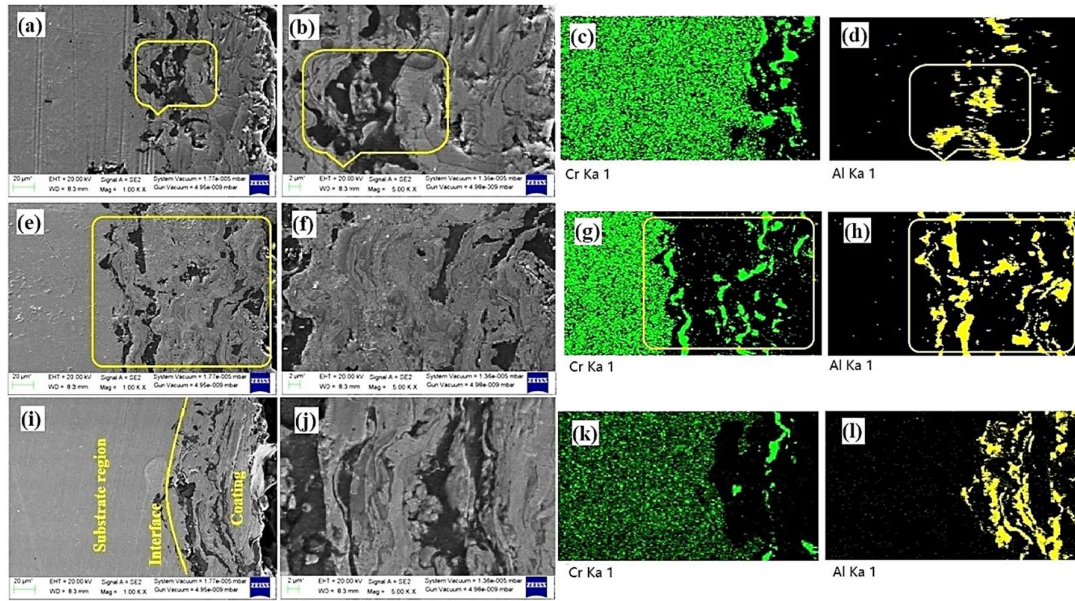


**Fig.4.20** (a&b) SEM micrographs of  $\text{Al}_0\text{CoCrFeNi}$  coating, (c&d) EDS mapping of  $\text{Al}_0\text{CoCrFeNi}$  coating, (e&f) SEM micrographs of  $\text{Al}_{0.5}\text{CoCrFeNi}$  coating, (g&h) EDS mapping of  $\text{Al}_{0.5}\text{CoCrFeNi}$  coating, (i&j) SEM micrographs of  $\text{Al}_1\text{CoCrFeNi}$  coating, (k&l) EDS mapping of  $\text{Al}_1\text{CoCrFeNi}$  coating.

### 4.3 POROSITY ANALYSIS

The porosity value in the percentage of the deposited coatings is a surface property that has an important role to play in case of the development of high-temperature oxidation-resistant coatings. Due to high porosity, the corrosion products could penetrate the top and sub-substrate. Porosity in the deposited coating during thermal spraying is a dominant parameter and is a physical property that differs in the oxidation resistance provided by variants of TSC processes. The mean of five measurements was performed for all deposited coatings and is given in **Table 4.3**. Furthermore, the porosity measurement showed fewer porosity values at the cross-section as compared to the as-sprayed surface of the coatings. The thickness of the deposited coating was kept around 250-300  $\mu\text{m}$ . The thickness was measured by using *Image-J software package* from SEM micrographs taken across the cross-section of the deposited coatings.

**Table 4.3** Average coating roughness, porosity, and thickness for various coatings under investigation.

Coatings	Porosity %
$\text{Al}_0\text{CrCoFeNi}$	$2.5 \pm 0.2$
$\text{Al}_{0.50}\text{CoFeNi}$	$2.1 \pm 0.2$
$\text{Al}_{1.00}\text{CoFeNi}$	$1.5 \pm 0.2$

#### 4.4 EVALUATION OF MICROHARDNESS

In high-temperature hostile environments, coatings may have to withstand the oxidation and erosion attack simultaneously. In these aggressive environments, the softer coatings may be more at risk of this oxidation and erosion attack at elevated temperatures. The microhardness of the deposited coatings was conducted at a 300 gm load with a dwell period of 15 s. The macrographs taken from the microhardness tester equipped with an optical microscope are presented in Fig.4.21. It can be observed from Fig.4.21(d) that the indents were formed on the dark phase, which is corresponding to alumina-based B phase, and it resists deformation. The higher hardness ( $530 \pm 15 \text{ HV}_{0.3}$ ) of  $\text{Al}_1\text{CoCrFeNi}$  coating is attributed to the presence of the BCC phase in this coating.

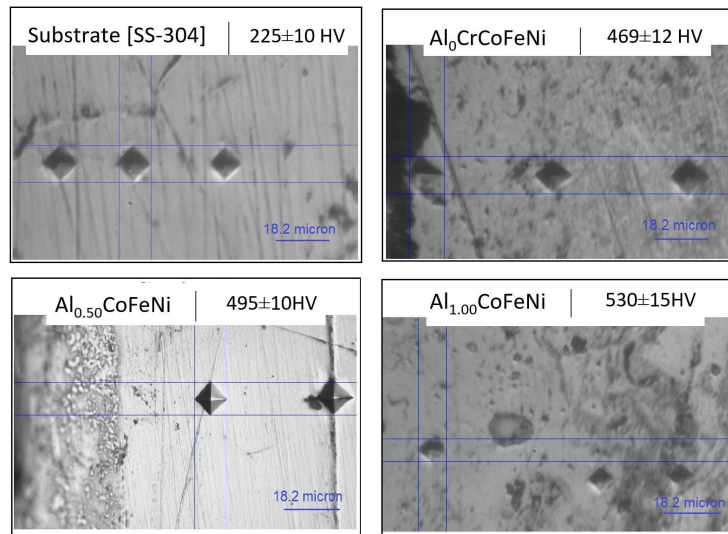


**Fig. 4.21** Microhardness Indents if all coatings.

The average microhardness of as-sprayed coatings is shown in **Table 4.4**.

**Table 4.4.** Average microhardness of as-sprayed & post-processed coatings.

Coating powders	Microhardness (HV <sub>0.3</sub> )
SS-304	225±10 HV <sub>0.3</sub>
Al <sub>0</sub> CrCoFeNi	469±12 HV <sub>0.3</sub>
Al <sub>0.50</sub> CoFeNi	495±10 HV <sub>0.3</sub>
Al <sub>1.00</sub> CoFeNi	530±15 HV <sub>0.3</sub>

The solid solution strengthening mechanism in plasma-sprayed Al<sub>x</sub>CrCoFeNi coatings occurs via the introduction of alloying elements into the crystal lattice structure of the material. This process hinders the movement of dislocations and enhances the material's strength. The inclusion of many elements in solid solution, as seen in high-entropy alloy coatings like Al<sub>x</sub>CrCoFeNi, results in increased strength and hardness [9]. The enhancement of mechanical characteristics in the coatings is a result of the intricate interactions and groupings of atoms inside the crystal structure, which impede the movement of dislocations and reinforce the solid solution. Due increased parentage of Al is responsible for increased hardness (Addition of Al in Al<sub>x</sub>CrCoFeNi with increased content). In addition, the atomic radii of the elements Al (0.143nm), Co (0.135nm), and Cr (0.130nm) in the AlCoCrFeNi high-entropy alloy are larger, while the atomic radii of the other elements Ni (0.124nm) and Fe (0.126nm) are different. This difference in atomic radii can lead to lattice distortion and the presence of an elastic stress field, which in turn hinders the movement of dislocations and results in a solid solution-strengthening effect.

#### 4.5 DISCUSSION

The coating thickness of the deposited coatings has been determined along the cross-sections of samples and the range of 200-230μm has been found, which is near to the desired value for resisting high-temperature oxidation and similar to the analysis noted by Grewal et al. (2013); Espallargas et al. (2008); Roy et al. (2006); and Sidhu et al. (2005B and 2006B) for nickel-based coatings. The surface roughness is also associated with corrosion resistance, as the higher the surface roughness, the higher the possibility of corrosion attacks.

The plasma spray helps to deposit a coating having good inters plat bonding and mechanical anchorage to the substrate. Therefore, plasma spray produces very hard and denser coatings. The mechanical property of the thermal spray coating that is most commonly cited is micro-hardness (Tucker et al., 1994).

The hardness of the coatings was compared with the values noted in the literature. Miguel et al. (2003) noted an average hardness value of 610 for the NiCrSiB coating deposited by the PS coating process. S. Harsha et.al. (2008) found an average value of 511 HV for flame-sprayed coating with NiCrSiB+20%CrC powder. Wang et al. (2009) examine an average micro-hardness value of 410 HV for NiAl + 40% Al<sub>2</sub>O<sub>3</sub> powder deposited by the process of HVOF. Koivuluoto et al. (2009) observed a micro-hardness value of 350 HV for cold spray coating with NiCr + 50% Al<sub>2</sub>O<sub>3</sub> feedstock powder. Hu et al. (2011) observed a maximum micro-hardness of 225HV for Ni+40% Al<sub>2</sub>O<sub>3</sub> powder deposited with the cold spray process, while, Li et al. (2008) reported the highest micro-hardness of 173 HV for the cold sprayed coatings. The AlCoCrFeNi high-entropy alloy (HEA) has garnered considerable interest as a highly promising material for thermal spray coatings. Research has indicated that the versatile phase composition and microstructural features of HEAs allow for the creation of solid solution structures with customized physical properties. The high-velocity oxygen fuel (HVOF) thermal spraying technique is a widely used process in industry for depositing HEA coatings. This technique enables the deposition of coatings with highly desirable characteristics.<sup>8</sup>

Various studies have examined the properties of HVOF-sprayed AlCoCrFeNi HEA coatings, shedding light on their characteristics. The coatings displayed a characteristic lamellar structure with minimal porosity. They consisted of a primary FCC solid solution phase and a blend of oxide inclusions, including Fe<sub>2</sub>O<sub>3</sub>, Fe<sub>3</sub>O<sub>4</sub>, and AB<sub>2</sub>O<sub>4</sub> (where A = Fe, Co, Ni, and B = Fe, Cr).<sup>10</sup> According to the report, the APS and HVOF-sprayed coatings had different oxide content percentages. The HVOF coating, which had a lower oxide content of 12.7%, demonstrated higher wear resistance compared to the APS coating with 47.0% oxide content. In addition, the incorporation of certain elements, such as vanadium, into the AlCoCrFeNi HEA has been discovered to enhance the microstructure of the coating. This results in increased hardness and improved resistance to abrasion. Adding Cr<sub>3</sub>C<sub>2</sub>-Ni<sub>20</sub>Cr particles to the HEA matrix has been demonstrated to enhance the toughness and corrosion resistance of the coating, making it well-suited for use in demanding environments.

Research has also explored the nano- and micro-mechanical properties, along with the corrosion performance, of HVOF-sprayed AlCoCrFeNi HEA coatings. The coatings displayed superior hardness, elastic modulus, and wear resistance in comparison to traditional alloy coatings.<sup>9</sup> In addition, the HEA coatings have shown enhanced resistance to corrosion, especially in environments with high chloride content. In conclusion, the research findings indicate that the HVOF thermal spraying of AlCoCrFeNi HEA powders can create coatings that possess favorable microstructural, mechanical, and corrosion properties. These coatings are highly appealing for a wide range of industrial applications that demand improved surface protection and performance.

In the present study, it could be observed that the hardness of coatings showed much better improvement in the hardness values as compared to the data of hardness for different coatings available in the literature. The higher value of coatings is due to the closely packed splats and eventually the lower porosity content. Moreover, higher hardness is attributed to the coatings deposition with the process of plasma spray as this process is suitable for developing the Ni-based composite coatings.



## CHAPTER 5

### OXIDATION ANALYSIS OF $\text{AlCoCrFeNi}$ COATINGS

This chapter describes the oxidation behaviour of coated specimens that are exposed to the oxidation at  $900^\circ\text{C}$  in the air for 50 cycles. The characterisations of corrosion products are carried out with the help of FE-SEM/EDS and XRD techniques. The results for C1 and deposited coatings are reported under different subheadings in this chapter. In view of the comparison, the weight change data of each coating is plotted along with the bare SS-304. The parabolic rate constants ( $K_p$ ) and thickness of scale for all deposited coatings and C1 substrate have been evaluated after 50 cycles of exposure.

#### 5.1. OXIDATION TEST

The oxidation test of coated, and C1 samples at a high temperature of  $900^\circ\text{C}$  is conducted by using the tube furnace shown in (Figure 5.1 a). Coating the substrate on all six sides helped keep things consistent and cut down on measurement errors.

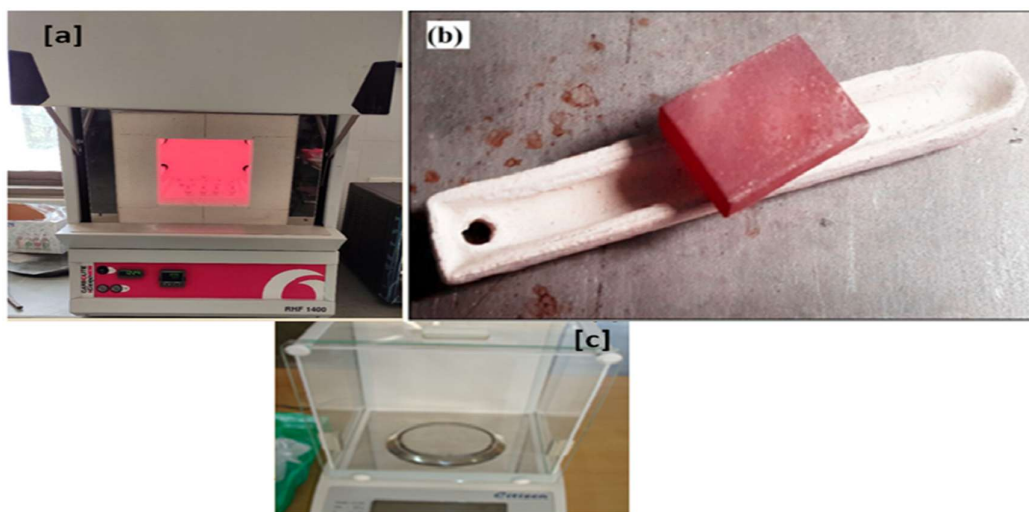


**Fig 5.1** (a) Schematic of tube furnace, and (b) Oxidized sample in  $\text{Al}_2\text{O}_3$  boat (c) weight balance.

The results showed that the oxidation rate increased significantly with each cycle. Fifty cycles are run in this test, with each C consisting of one hour of heating at  $900^\circ\text{C}$  followed by twenty minutes of cooling at ambient temperature. It is created an environment where oxidation might spread quickly. In high-temperature environments, oxidation analysis parameters for coatings are critical for determining the performance and durability of these

coatings. The parameters and methodologies employed may differ contingent upon the material composition, variety of coatings, and testing conditions. Table 5.1 shows typical oxidation analysis parameters in coatings.

**Table 5.1** Analyzing high temperature oxidation requires several parameters.

<b>High temperature oxidation analysis parameters</b>	
Temperature	900 <sup>0</sup> C
Heating Time	1 hr
Cooling Time	20 min
Total cycles	50

The characterization of the efficacy and longevity of coatings and the optimization of their design and materials to withstand oxidation at high temperatures depend on these parameters. Standards and testing protocols may differ according to the industry and application.

## **5.2. VISUAL INSPECTION OF OXIDIZED TBCs SAMPLES**

The evaluation of material oxidation extent is a prevalent method utilized in numerous scientific and industrial domains, which involves the visual inspection of oxidized samples. Visual inspection serves as a beneficial preliminary measure when evaluating the state of oxidized samples; however, further analysis employing specialized methods may be necessary to meet the particular demands and goals of the assessment.

Crucibles made of pure Al<sub>2</sub>O<sub>3</sub> are used to transport the samples to the furnace for the oxidation tests. A single specimen is tested at a time, with the Al<sub>2</sub>O<sub>3</sub> crucibles containing the sample positioned within the furnace along the axis of the tube (Figure 5.1 b) to prevent any possible diffusion or interaction between the samples. The kinetics of the oxidation process are analysed by recording the weight gain or loss after each thermal cycle using data obtained from the thermo-gravimetric analysis. The pictographs of the developed coatings are shown in (Figure 5.2) The pictographs of C2 and C3 reveal some cracks on the surface as compared to the C1 and C4, respectively.

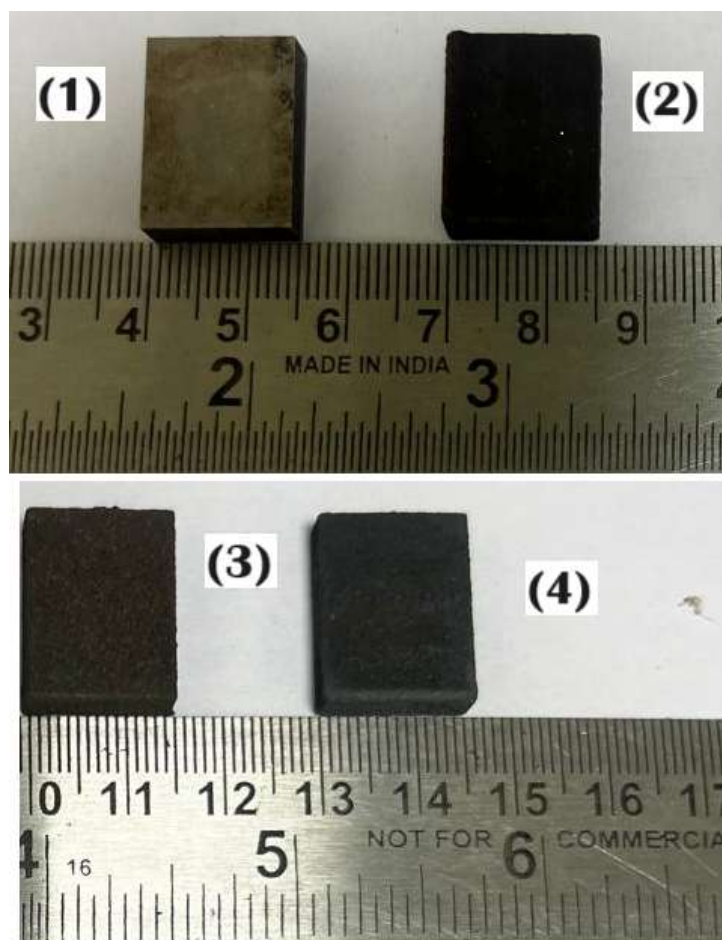


**Fig 5.2** Pictographs of Oxidized coating samples.

### **5.3. SEM-EDS AND XRD ANALYSIS OF OXIDIZED TBCs**

In oxidation test analysis, initial weight gain was observed after completing the 50 cycles. The weight gain for the substrate was  $112\text{mg}/\text{cm}^2$  and for the  $\text{Al}_0\text{CoCrFeNi}$ ,  $\text{Al}_{0.5}\text{CoCrFeNi}$ , and  $\text{Al}_{1.0}\text{CoCrFeNi}$  coatings, it was found to be  $5.6\text{ mg}/\text{cm}^2$ ,  $4.5\text{ mg}/\text{cm}^2$  and  $3.3\text{ mg}/\text{cm}^2$ , respectively. The calculations of the parabolic rate constants ( $K_p$  ( $10^{-4}\text{.mg}^2.\text{cm}^{-1}.\text{s}^{-1}$ )) calculated using a linear least square algorithm ( $\chi^2=K_p t$ ), it was 696.8 for the substrate and for the  $\text{Al}_0\text{CoCrFeNi}$ ,  $\text{Al}_{0.5}\text{CoCrFeNi}$  and  $\text{Al}_{1.0}\text{CoCrFeNi}$  coatings, it was found to be 1.742, 1.125 and 0.605, respectively. Oxidized coatings at  $900^\circ\text{C}$  subjected to 50cycles of oxidation are shown in Fig. 5.4.

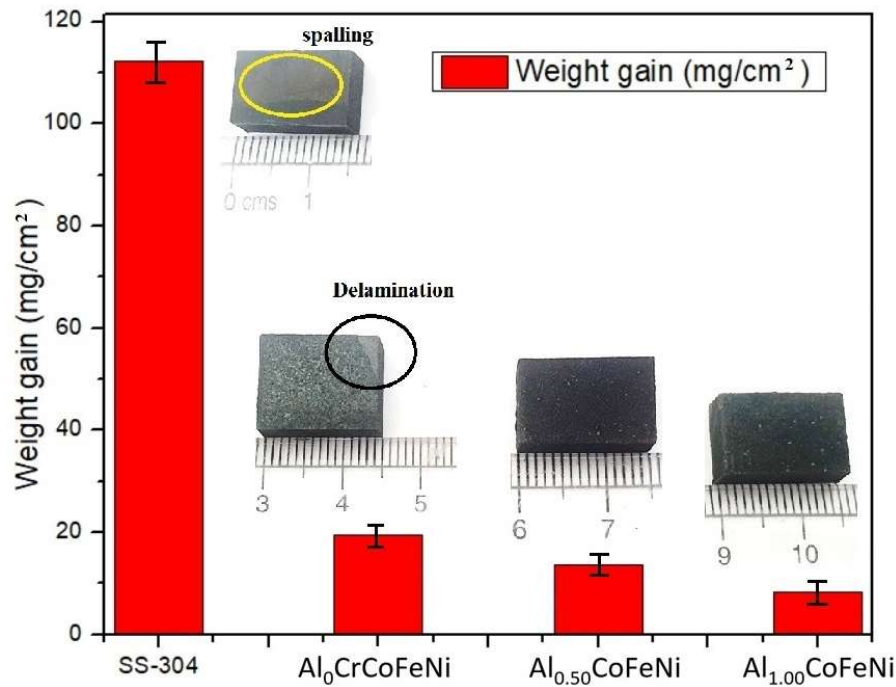


**Fig 5.3.** Oxidized coatings at 900<sup>0</sup>C subjected to 50cycles of oxidation.

The SS-304 has shown intense oxidation on the surface, The granulated scale shows the presence of Fe and O in its composition throughout as shown in Fig .5.4. The EDS has shown the elements present in SS-304 with maximum concentration of Fe, Cr and O as shown in Fig. 5.4 (b).

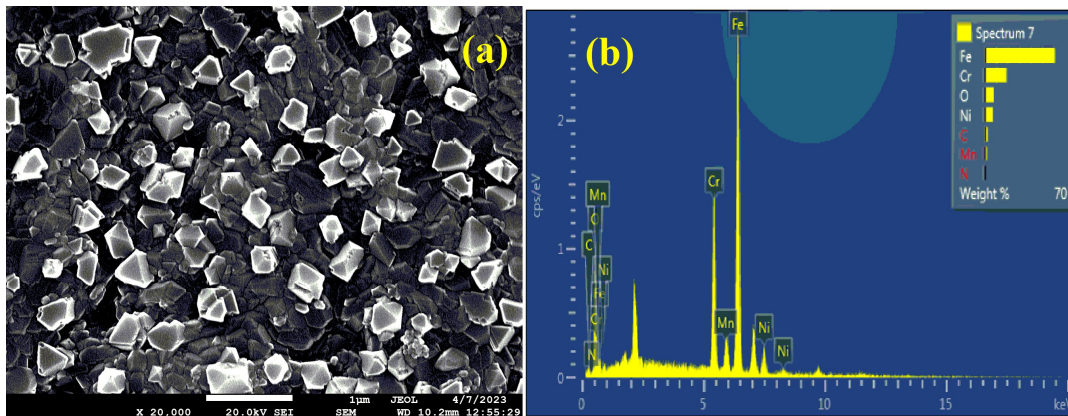


**Fig. 5.4** (a) Oxidized SS-304 substrate at high temperature and b) Area scan EDS of SS-304.

The elemental distribution of the elements present on the oxidized SS-304 surface is presented in Fig. 5.5. The intensity can be observed on the surface in Fig 55(b) for Fe, Cr and O, respectively.

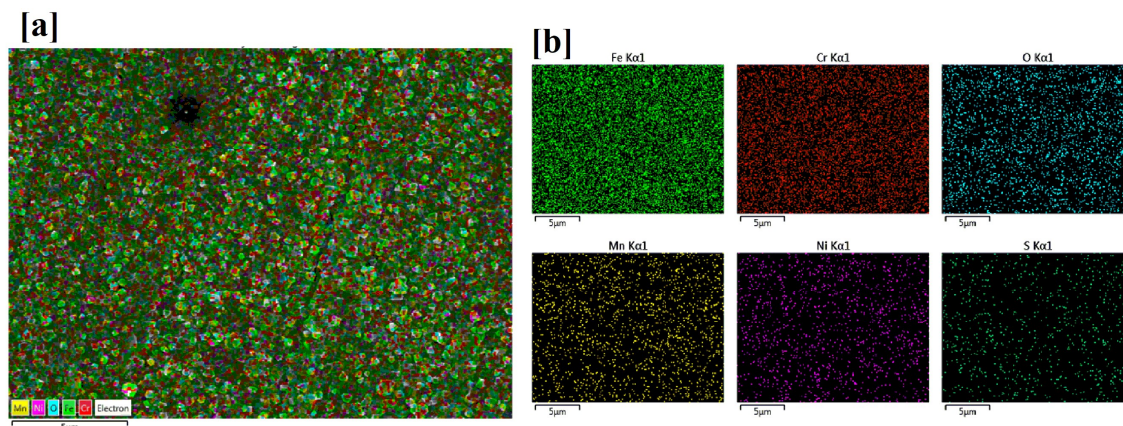
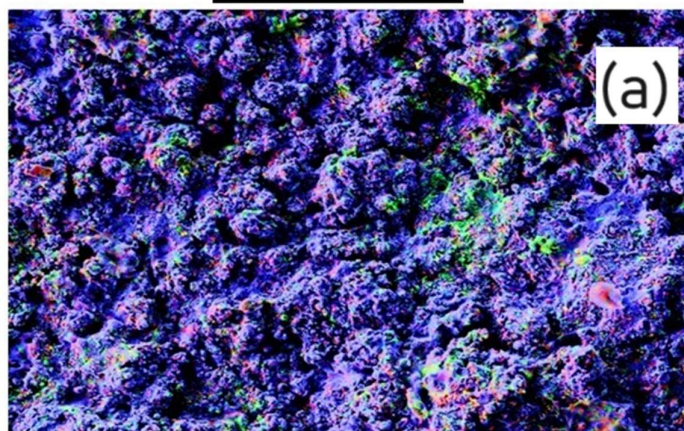


**Fig. 5.5** (a) EDS mapping of Oxidized SS-304 substrate at high temperature and b) elemental distribution of oxidized SS-304.

The AlCoCrFeNi coating undergoes selective oxidation of Al, resulting in the growth of  $\text{Al}_2\text{O}_3$  scales owing to exposure to high temperatures in the air. The exposure of the coatings surface has shown the typical characteristics of thermal spraying i.e., droplet boundaries of metals on all three coatings, which can be observed in Fig 5.6 (c), (d), and (e), respectively. The composition of the black pits is more in the first and second coating with the flat regions, this mismatch may arise from variations in thickness resulting from differing growth rates of  $\text{Al}_2\text{O}_3$  in neighbouring areas. This indicates the development of a thin layer of oxidation on the surface of the coatings. The spinel oxides are formed during the plasma spraying, where Co and Fe are major aggregates of oxides and Cr and Ni are minor aggregates of oxides.

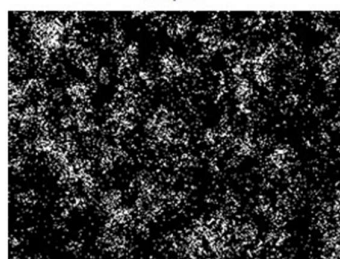


$\text{Al}_0\text{CrCoFeNi}$

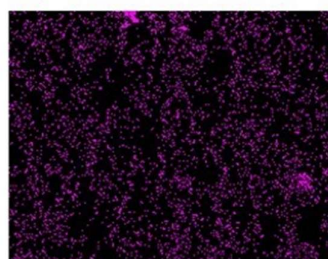


100µm

Mix



Ni Ka1



Al Ka1

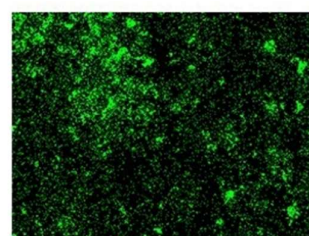
(b)

$\text{Al}_{0.50}\text{CoFeNi}$

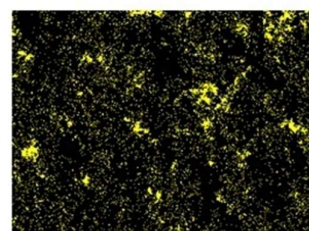


100µm

Mix



Cr Ka1



Al Ka1

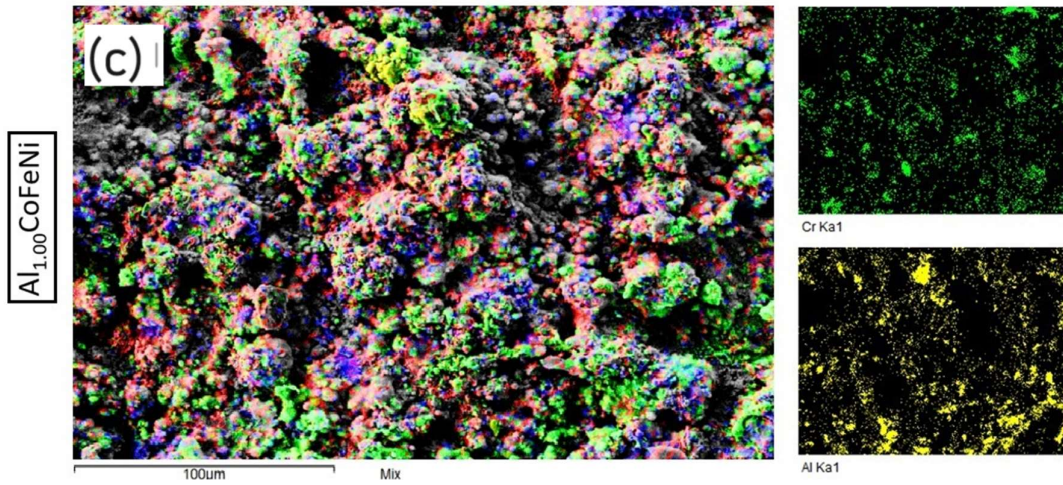


**Fig. 5.6** Oxidized surface of (a) C1, (b) C2 and, (c) C3 coatings.

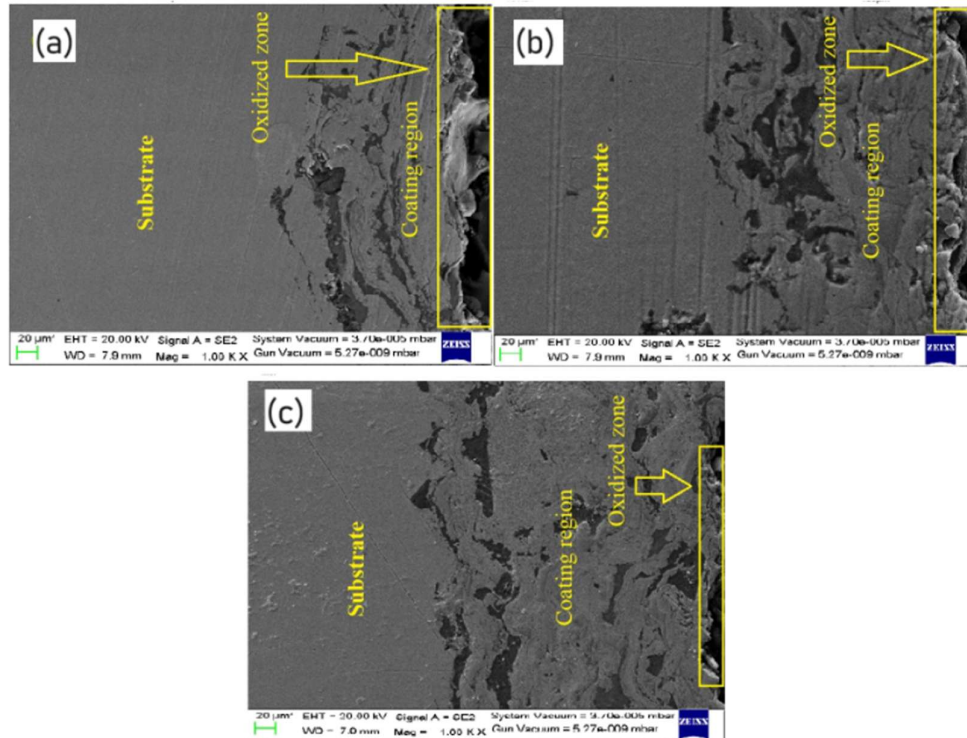


**Fig.5.7.** (a) Weight gain data for oxidized samples, (b) SEM micrograph of SS-304 oxidized surface, (c) SEM micrograph of  $\text{Al}_0\text{CoCrFeNi}$  coatings, (d) SEM micrograph of  $\text{Al}_{0.5}\text{CoCrFeNi}$  coatings, and (e) SEM micrograph of  $\text{Al}_{1.0}\text{CoCrFeNi}$  coatings

The density of the passivation layer of  $\text{Al}_2\text{O}_3$  has increased on the surface of the coatings with an increase in Al content in the  $\text{AlCoCrFeNi}$  coatings. The densest distribution of Al was depicted on the surface of  $\text{Al}_{1.0}\text{CoCrFeNi}$  coatings as shown in Fig. 5.7 (e). This



coating exhibits the presence of irregular  $\text{Al}_2\text{O}_3$  scales and some sudden spinel oxides. According to reference [10], for the oxidation of HEA coatings to occur, Al must first travel through the depletion zone before it can reach the surface and come into contact with O. Because the Al depletion layer has a greater configuration entropy (1.56 R) compared to the definition (1.5 R) of HEA [10], the continuous transportation of internal Al to the surface would be challenging. At elevated temperatures, the phase boundary may serve as the pathway for the diffusion of aluminum (Al) and oxygen (O), facilitating the formation of an aluminum oxide ( $\text{Al}_2\text{O}_3$ ) layer. In general, the inner coating maintains a very consistent structure for Fe, Co, Cr, and Ni, except for Al.

#### **5.4 SUMMARY**

Oxidation test was performed on SS-304, C1, C2 and C3 coatings at  $900^\circ\text{C}$  subjected to 50cycles of oxidation. An increase in the amount of Al present in the AlCoCrFeNi coatings has resulted in an increase in the density of the passivation layer of  $\text{Al}_2\text{O}_3$  that is present on the surface of the coatings. High entropy alloys (HEAs) are a fascinating group of materials that showcase remarkable characteristics, including exceptional hardness, strength, wear resistance, corrosion resistance, and thermal stability. These exceptional qualities have made HEAs a highly desirable choice for thermal spray coatings, ideal for use in challenging conditions and extreme environments. Various thermal spray processes, such as atmospheric plasma spraying (APS), high-velocity oxy-fuel (HVOF), and cold spraying, have been utilized for depositing HEA coatings. The HEA coatings typically exhibit a composite and lamellar microstructure due to the splat bonding and rapid solidification that occurs during the thermal spray process. The microstructure of HEA coatings can exhibit considerable variations based on the chosen thermal spray parameters. Factors like deposition temperature play a crucial role in determining the cooling rate and phase formation. The coatings deposited at lower temperatures usually have a straightforward BCC (body-centered cubic) structure. On the other hand, when coatings are deposited at higher temperatures, they can have more intricate microstructures with multiple phases, such as BCC, FCC (face-centered cubic), and various oxides. Understanding and controlling thermal spray parameters is crucial for optimizing the performance of HEA coatings by customizing their microstructure. In the three developed coatings, there seems to be a higher concentration of black pits in the initial and subsequent coatings, which may be due to variations in thickness caused by different growth rates of  $\text{Al}_2\text{O}_3$  in adjacent areas. It suggests the formation of a thin layer



of oxidation on the surface of the coatings. Spinel oxides are commonly formed through the plasma spraying process, with Co and Fe being the primary components, while Cr and Ni play a smaller role in the oxide formation.

## CHAPTER 6

### HIGH-TEMPERATURE EROSION TEST

The high-temperature erosion behavior of the bare SS-304, as well as plasma sprayed coatings, has been reported in this chapter. The uncoated & coated SS-304 were tested for solid erosion at 900 °C at various impingement angles. The eroded samples were examined using SEM micrographs at varying magnifications. Before erosion testing, the weight of the samples was determined, and the final weight was used to determine the erosive wear rate. After each test, the sample have been weighed and their weight alteration has been determined with a scale with a resolution of 0.01 mg.

#### 6.1 RESULTS AND DISCUSSION

The high-temperature furnace described in the section was used in the present examination to examine the high-temperature erosion behavior of all samples (Chapter 4). The results that were obtained after various characterizations of test specimens are detailed in the following sections.

##### 6.1.1 Uncoated SS-304 and Coated SS-304

###### 6.1.1.1 Erosion Rate

The size and shape of the impression left on both specimens' surfaces during erosion testing could be used to determine the erosion resistance of each specimen. In this chapter, the estimated and reported “erosive wear rates” (g/g) for uncoated SS-304 and Coated SS-304 samples are discussed. Both the plasma-coated samples and the SS-304 substrate were used to calculate the erosive wear rate (g/g), which is the ratio of wear loss of mass in grams to the erodent mass in grams.

The macrographs offer useful data on the process of erosion behavior at 800 °C and of different impingement angles as presented in the upcoming sections. The uncoated SS-304 as well as coated specimens underwent the high-temperature “solid particle erosion” test at 30° & 90° impact angles. **Fig.6.1a-b** displays the optical macrographs for both test angles.

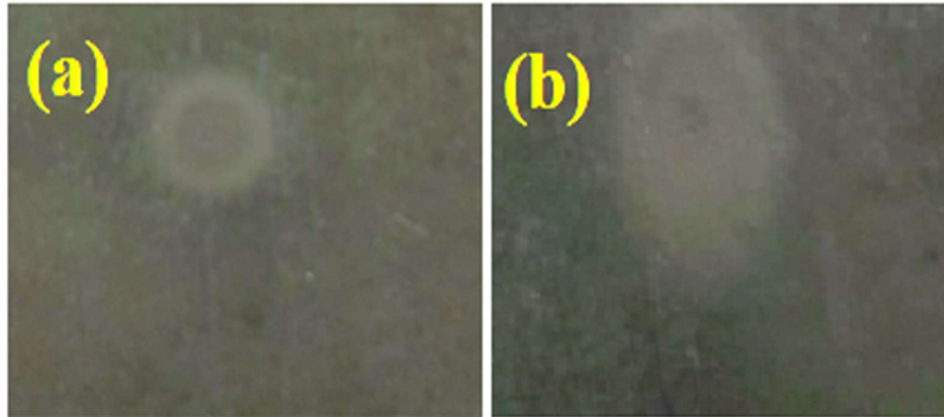


**Fig.6.1.** Macrographs of the SS-304 substrate specimens at (a) 30° and, (b) 90° impact angle.

Due to the existence of small fissures and a few “erodent particles” embedded on the surface at a 90° impact angle, the surface of uncoated SS-304 substrates shows wear in Fig.6.1. SEM picture. These fractures developed as a result of the recurrent fatigue loading brought on by the many erodent effects that led to the SS-304 materials. The surface of the erodent deformed the surface and have grown larger and joined grooves together, pulling material away and causing craters to develop in various places. Therefore, the material removal from the uncoated SS-304 substrate surface is caused by the ductile mode of erosion.

Nevertheless, as seen in **Fig.6.1.**, the uncoated SS-304 substrate has some signs of micro-cutting brought on by the erodent's sharp edges impacting the surface at a grazing angle (at a 30° impact angle) (a). Additionally, at a 30° impact angle, a few tiny craters & cavities also developed on an uncoated SS-304 substrate. These characteristics have developed in a manner that is comparable to that found in the SS-304 sample that underwent erosion testing at a 90° angle of contact. The fatigue stress and production of tiny fractures that result in material pullout are caused by the vertical component of oblique impacts.

The SS-304 substrate formed several craters on its surface after being tested with air-jet erosion at a 30° angle, as illustrated in **Fig.6.1. (a)**. In addition to micro-cutting marks, the cavities following erosion tests are visible on the surface. At a 90-degree impact angle, the SS-304 substrate surface exhibited pull-out and fissures. Because they repeatedly strike the SS-304 substrate at a normal angle, as demonstrated in **Fig.6.1. (b)**, the erodent particles adhere to the surface of the substrate. At a 90° impact angle, the direct

impingement of the erodent particles results in fatigue, which leads to pull-out and the development of cracks from direct impacts.

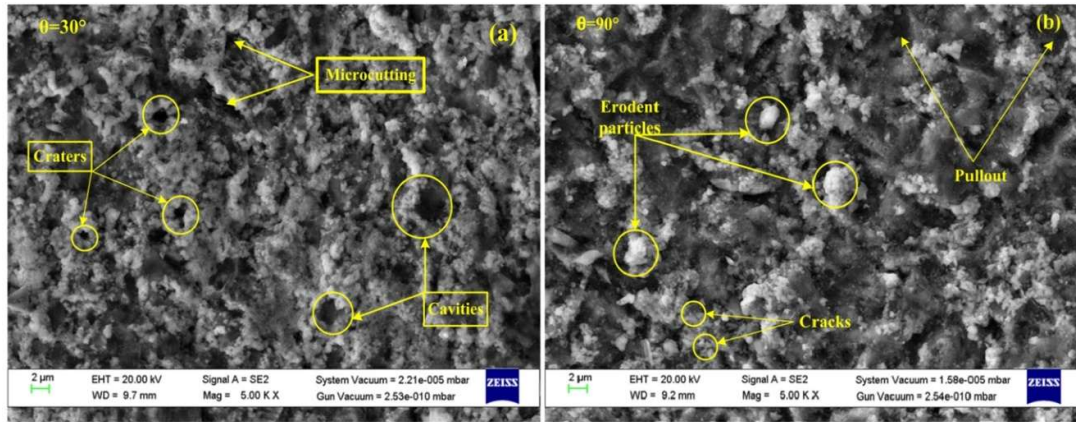


**Fig.6.2.** (a) Eroded surface's SEM micrographs of uncoated SS-304 substrate at 30°, and (b) at 90° angle of impacts.

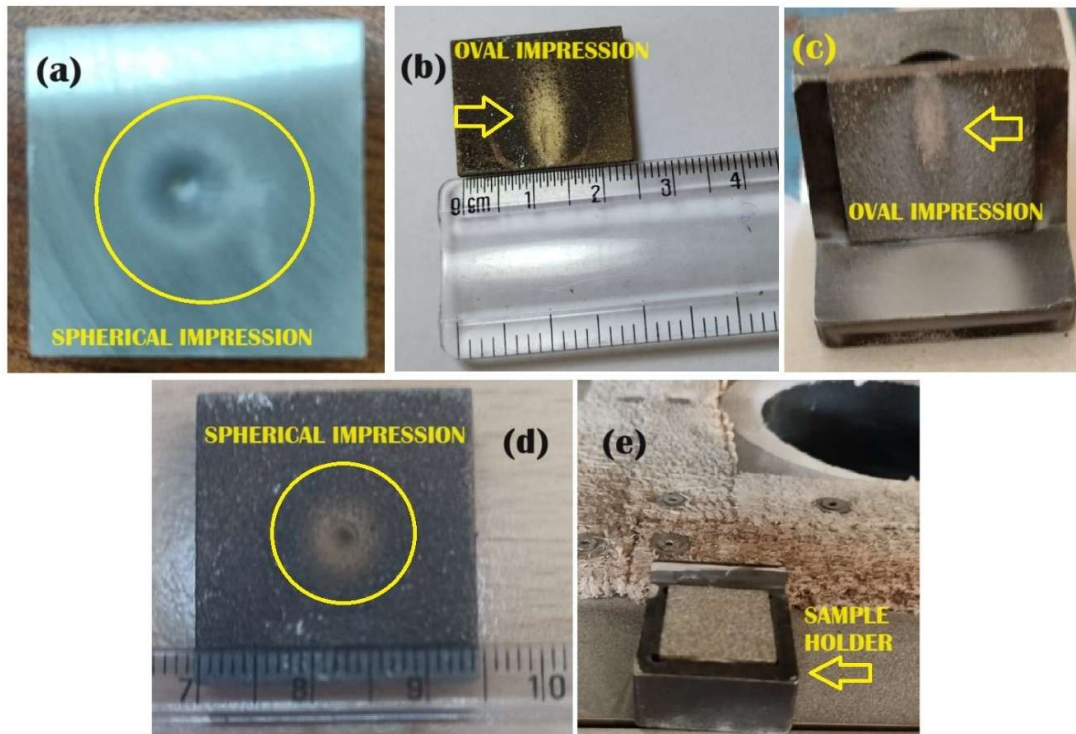


**Fig.6.3.** Photograph of the various C1 coated eroded samples at 30° & 90° angle of impacts (a) C1 obtained after 90°, impact angle, (b) C2 after 30° impact angle, (c) C3 after at 30°, (d) C3 obtained at 90° (e) Sample holder used in erosion testing.

The coatings at a 30° impact angle showed the elliptical mark formed in the erosion test and for a 90° impact angle the round marks were formed.

### 6.1.2 SEM Analysis

However, as shown in **Fig.6.4**, the worn-out surface of C1 coated samples exhibits ploughing as well as plastic deformation of the material. When erosion testing was done at a 30° impact angle, a ploughing or cutting (abrasion) mark could be observed beside the strain-hardened material (lip) and plastically deformed. Therefore, the ploughing or cutting marks might have appeared on the coated surface. Furthermore, the higher erosion rate at a 30° angle of impingement confirms that the Al<sub>0</sub>CoCrFeNi specimen is eroding in ductile mode (Wheeler et al., 2005; Finnie,1995 Finnie,1998). The surface of the Al<sub>0</sub>CoCrFeNi coated sample was subjected to erosive wear tests at a 90° impact angle, which also indicated the development of lip around the edges of the craters. The numerous normal collisions of the erodent particles over the unmelted Al<sub>0</sub>CoCrFeNi powder particles may have fatigued the powder, causing these craters to develop. The development of lips close to cavities demonstrates the splats strain hardening under repeated hits from erodent particles. The Al<sub>0</sub>CoCrFeNi and bare SS-304 substrate showed different impression marks formed during the erosion test at 30° & 90° impact angles. The micro-cutting of the Al<sub>0</sub>CoCrFeNi coating, which was applied using the plasmas spraying technique to a SS-304 substrate, caused the coating to deform plastically. The coating displayed the ductile mode of erosion at a 30° impact angle. As seen in **Fig.6.4(a)**, the higher SEM micrograph demonstrates how the crater edges have developed a lip and distorted splats. When the Al<sub>0</sub>CoCrFeNi coating is hit at a 90° impact angle, impacted sites with deep impressions, and erodent particles are visible, which signifies the erosion ductile mode caused by the repeated impact of erodent during air-jet erosion testing.



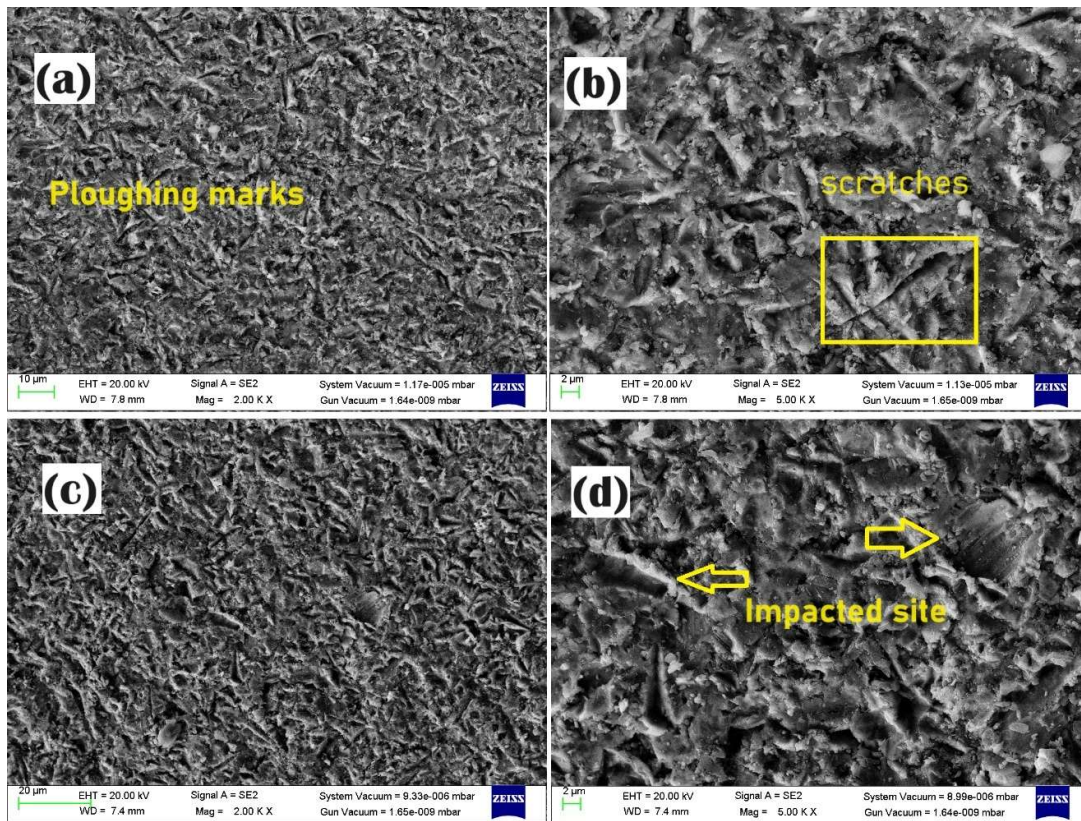


**Fig.6.4.** (a) SEM micrographs of the eroded surface of  $Al_0CoCrFeNi$  (C1) coated SS-304 at 30°, and (b) at 90° angle of impacts.

In remaining two coatings i.e C2 and C3 , Al was mixed with the CoCrFeNi alloy powder before being deposited on the SS-304 substrate using the plasma spraying method. The performance of high-temperature erosion of the  $Al_{0.5}CoCrFeNi$  has been evaluated and presented. The SEM micrograph of  $Al_{0.5}CoCrFeNi$  coatings showed the formation of cutting grooves and lip formation at a 30° impact angle as presented in **Fig.6.5(a)**. The coating showed the pullout and cracks along with erodent particles sticking on the surface at 90° as presented in Figure **Fig. 6.5(b)**.

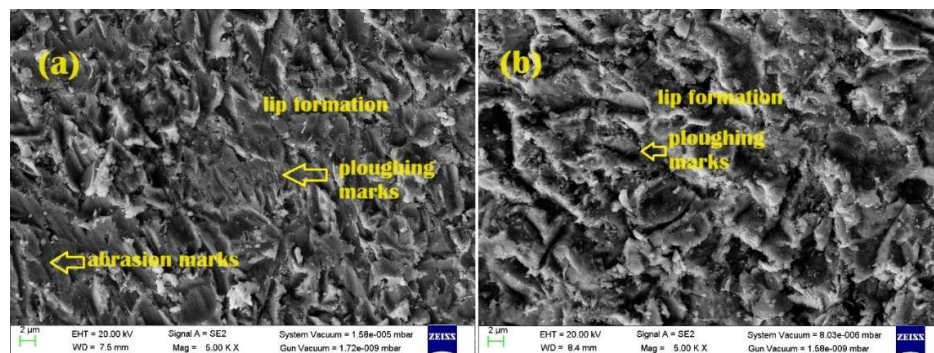


**Fig.6.5.** (a) SEM of eroded micrographs of  $Al_{0.5}CoCrFeNi$  coated SS-304 at 30°, and (b) at 90° angle of impacts.

The SEM micrograph of eroded  $\text{Al}_1\text{CoCrFeNi}$  coating showed ploughing marks and craters when impacted at a  $30^\circ$  impact angle as presented in **Fig.6.6(a)**. The ploughing marks are also present on the eroded coating's surface and a detached splat can be seen. However, the surface morphology of this coating seems in good condition as compared to the  $\text{AlCoCrFeNi}$  and  $\text{Al}_1\text{CoCrFeNi}$  coating. There are fewer cracks and impacted sites formed in  $\text{Al}_1\text{CoCrFeNi}$  coating at a  $90^\circ$  angle of impact as presented in **Fig.6.6(b)**.

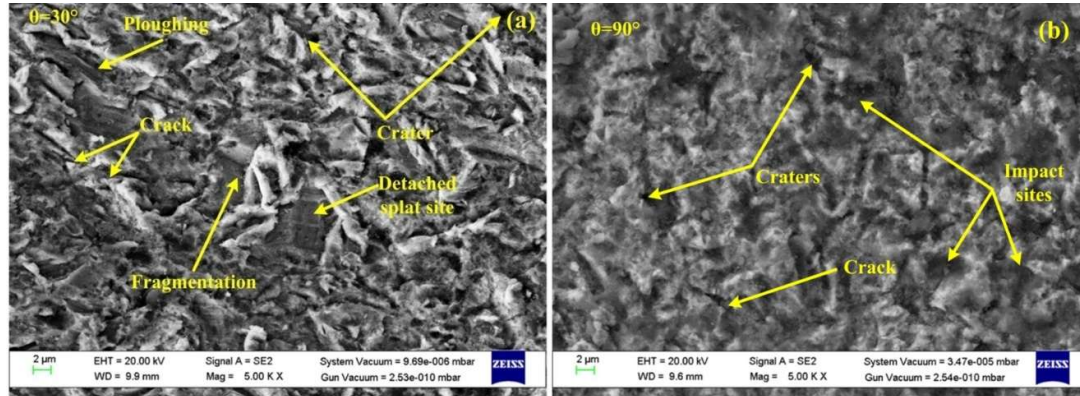


**Fig.6.6.** (a) SEM of eroded micrographs of  $\text{Al}_1\text{CoCrFeNi}$  coated SS-304 at  $30^\circ$ , and (b) at  $90^\circ$  angle of impacts.

The erosive wear rate of the as-sprayed & post-treated coatings are presented in **Table 6.1**.

**Table 6.1.** Erosive wear rate of the as-sprayed  $\text{AlCoCrFeNi}$  coatings.

Substrate/Coatings	Erosion Rate (g/g)	
	$30^\circ$	$90^\circ$
SS-304	$2.1 \times 10^{-3}$	$1.4 \times 10^{-3}$
$\text{Al}_0\text{CrCoFeNi}$ (A1)	$5.0 \times 10^{-4}$	$5.2 \times 10^{-4}$
$\text{Al}_{0.50}\text{CoFeNi}$ (A2)	$5.9 \times 10^{-4}$	$4.1 \times 10^{-4}$
$\text{Al}_{1.00}\text{CoFeNi}$ (A3)	$3.9 \times 10^{-4}$	$3.5 \times 10^{-4}$

The erosive wear rate (g/g) for the coated specimens showed nearly 3.2 times better erosion resistance for  $\text{Al}_{1.00}\text{CoFeNi}$  (A3) coatings when compared with uncoated SS-304

at 30° angle of impacts. On the contrary Al<sub>1.00</sub>CoFeNi (A3) showed 4.7 times better resistance to erosive wear than SS-304 substrate at 90° angle of impacts.

## 6.2 SUMMARY

There are two approaches to understanding the erosion wear process. This involves analyzing the erosion process by considering the type of material used and the angles at which an erodent substance impacts the material's surface. Firstly, the material removal mechanism due to erosive wear considers the ductile and brittle nature of the material. There are two possible processes that can occur during erosive wear, leading to surface deterioration: repeated plastic deformation and cutting. When it comes to ductile materials, the process of material removal is attributed to micro-cutting. After that, the material is removed from its surface. On the other hand, fragile materials can deteriorate when they are repeatedly contacted by an erodent, a process known as fatigue (Wheeler et al., 2005). The particles consistently transfer their energy to the surface, resulting in repeated collisions that can eventually lead to fatigue failure. Due to frequent impacts, the surface develops cracks and the coating becomes more susceptible to debonding, exposing its delicate nature. The impact angle plays a crucial role in determining the material removal method, while the angle at which the erodent particles hit directly affects the erosion mechanism. The impact angle at which the working fluid enters the system and impacts the surface to produce material deterioration of the component's working surface can vary depending on the specific applications, such as gas turbines, rocketry components, heat exchangers, boilers, and hydrodynamic turbines. The material removal method varies based on the impact angles, which can range from low to high. The material is removed through cutting and chip formation, which occurs at low-impact angles. According to a study conducted by Finnie et al. in 1995, it was observed that erosion rates tend to be higher at lower angles of 20° and 30° during the ductile erosion process. At or near an angle of 90 degrees, erosion failure becomes a concern. This involves the creation of lips primarily for materials that deform at a faster rate. Platelets are eliminated through the repeated impact of erodent particles. On the other hand, materials that have the lowest 90-degree erosive wear resistance are classified as brittle mode (Flynn et al., 2001).

The SEM images of SS-304 substrate and coated specimens reveal the craters produced due to impacts and the elongated lips around the periphery of craters. The micro-cutting, micro-plowing, and irregular indentations at 30° could be seen. For a 90° angle of impingement, erodent particles, cracks, and impact sites reveal the plastic deformation.



The erosion process also indicates the elimination of splats at a 30° angle and this is due has caused as the tangential forces act directly by striking of erodent on the splats at the lower impact angle (Ramesh et al., 2011).

The erosive wear rate (g/g) has been computed for SS-304 substrate and coatings at 30° & 90° angles of impact. It displays that the Al<sub>1.00</sub>CoFeNi (A3) coatings exhibited greater erosion resistance as compared SS-304 and other coatings. The erosion rate reduced with an increase in Al content in the case of Al<sub>1.00</sub>CoFeNi coating and on the other hand, Al<sub>0.5</sub>CoFeNi coating alumina showed higher erosion resistance as compared to Al<sub>0</sub>CoFeNi coating. This might be explained by the coating being more ductile. The base metal and as-sprayed coatings have experienced ductile modes of erosion with grooves, lip development, pullouts, and craters as prominent processes. The material takes place at low angles mainly due to micro-cutting caused by striking of erodent and lip formation followed by strain hardening are responsible for ductile fracture (Praveen et al., 2015). The coatings show the maximum loss through erosion at 30° in comparison to the normal angle of impact at 90°.

### CONCLUSIONS AND FUTURE SCOPE

#### 7.1 CONCLUSIONS

The following conclusions were obtained on the basis of experimental results obtained and their analysis in the current work.

1. Plasma-sprayed AlCoCrFeNi coatings with different proportions of Al content have successfully been deposited on SS-304 substrate. The fraction  $x$  was varied from 0 to 1 ( $x=0$ ,  $x=0.5$ , and  $x=1$ ) for Al in the HEAs and three coatings were deposited. The deposited coatings showed homogenous, dense, crack-free, and uniform microstructure.
2. The EDS spectra of different coatings confirm the presence of major elements of feedstock powder used which improved the erosion and oxidation resistance. EDS maps of all coatings showed the proper distribution of Al in the deposited coatings and the incidence of major constituents Co, Fe, Cr, and Ni of feedstock powder. The EDS spectra indicate that their chemical was no change observed in the base metal occurred.
3. The surface of all deposited coatings has shown typical features of plasma spray coatings such as melted, semi-melted and un-melted particles. A coating thickness of 200-250  $\mu\text{m}$  was maintained. A good mechanical bonding can be observed at the interface of substrate and coating and forming a homogenous composite layered structure in all coatings.
4. The increase in the Al concentration can be observed in these XRD patterns. Phase B corresponds to the BCC structure, which has major phases of Fe-Cr and Al-Ni. Phase F corresponds to the FCC structure, with the major phase consisting of Ni-Co-Cr. The phase S corresponds to the spinel's  $\text{NiAl}_2\text{O}_4$ .
5. The microstructure analysis showed that the dispersion of Al particles in plasma sprayed coatings. The porosity level has increased an increase in Al content in the. Maximum porosity in order of 2.5% was observed in  $\text{Al}_0\text{CoCrFeNi}$  coating while the lowest porosity was found in the case of  $\text{Al}_{0.5}\text{CoCrFeNi}$  and  $\text{Al}_1\text{CoCrFeNi}$  coatings on order of 2.1% and 1.5%, respectively.

6. The micro-hardness analysis showed a trend of increased hardness with the addition of Al content in AlCoCrFeNi coatings. A higher hardness of  $530 \pm 15$  HV was found for Al<sub>1</sub>CoCrFeNi coating which is approximately 4.2 times higher than the hardness of uncoated SS-304 ( $225 \pm 10$  HV). On the other hand, in the case of Al<sub>0</sub>CoCrFeNi coatings, the maximum average micro-hardness value of  $469 \pm 12$  HV was obtained for the Al<sub>0</sub>CoCrFeNi, which is about 3.25 times the hardness of the substrate.
7. In oxidation test analysis, initial weight gain was observed after completing the 50 cycles. The weight gain for the substrate was  $112 \text{ mg/cm}^2$  and for the Al<sub>0</sub>CoCrFeNi, Al<sub>0.5</sub>CoCrFeNi, and Al<sub>1.0</sub>CoCrFeNi coatings, it was found to be  $5.6 \text{ mg/cm}^2$ ,  $4.5 \text{ mg/cm}^2$  and  $3.3 \text{ mg/cm}^2$ , respectively. The calculations of the parabolic rate constants ( $K_P$  ( $10^{-4} \cdot \text{mg}^2 \cdot \text{cm}^{-1} \cdot \text{s}^{-1}$ )) calculated using a linear least square algorithm ( $\chi^2 = K_P t$ ), it was 696.8 for the substrate and for the Al<sub>0</sub>CoCrFeNi, Al<sub>0.5</sub>CoCrFeNi and Al<sub>1.0</sub>CoCrFeNi coatings, it was found to be 1.742, 1.125 and 0.605, respectively. The AlCoCrFeNi coating undergoes selective oxidation of Al, resulting in the growth of Al<sub>2</sub>O<sub>3</sub> scales owing to exposure to high temperatures in the air. The density of the passivation layer of Al<sub>2</sub>O<sub>3</sub> has increased on the surface of the coatings with an increase in Al content in the AlCoCrFeNi coatings. The main reason for the enhanced performance is the solid solution strengthening in high-entropy alloys (HEAs) due to a mismatch in atomic size differences among the elements, which is caused by the substantial lattice distortion caused by the higher aluminum content. The oxidation resistance has been observed in the following sequence:

**As-sprayed:** Al<sub>1.00</sub>CoFeNi (A3) > Al<sub>0.50</sub>CoFeNi (A2) > Al<sub>0</sub>CrCoFeNi (A1), A718 > SS-304

8. The erosive wear rate (g/g) for the coated specimens showed nearly 3.2 times better erosion resistance for Al<sub>1.00</sub>CoFeNi (A3) coatings when compared with uncoated SS-304 at 30° angle of impacts. On the contrary Al<sub>1.00</sub>CoFeNi (A3) showed 4.7 times better resistance to erosive wear than SS-304 substrate at 90° angle of impacts. Based on the erosive wear rate, the erosion rates for the investigated coated and uncoated steel at 90° and 30 impact angles can be arranged in the following order:

**As-sprayed:** Al<sub>1.00</sub>CoFeNi (A3) > Al<sub>0.50</sub>CoFeNi (A2) > Al<sub>0</sub>CrCoFeNi (A1), A718 > SS-304

## **7.2 FUTURE SCOPE**

1. The high entropy alloys can be fabricated with other processes such as 3D printing for component design.
2. The post-processing of the high entropy alloys can be done by using heat treatments such as microwave processing and annealing etc to further enhance the performance of the coatings in terms of erosion and corrosion resistance.
3. The electrochemical and hot-corrosion behavior of the coatings may also be performed for particular high-temperature applications like boiler tubes and turbine blades.
4. Other coating techniques such as laser cladding and TIG cladding can be employed on the development of high entropy alloys.

## BIBLIOGRAPHY

1. Akdogan, A.N. and Durakbasa, M.N., (2008), “Thermal cycling experiments for glass moulds surface texture lifetime prediction – Evaluation with the help of statistical techniques” *Measurement*, Vol. 41, pp. 697–703.
2. Bala, N., (2010), “Investigations on the Hot Corrosion Behaviour of Cold Spray and HVOF Spray Coatings on T22 and SA 516 Steels,” Ph.D. Thesis, Mechanical Engineering Department, Punjab Technical University, Jalandhar, India.
3. Bala, N., Singh, H., and Prakash, S., (2009), “High Temperature Corrosion Behavior of Cold Spray Ni-20Cr Coating on Boiler Steel in Molten Salt Environment at 900°C,” *Journal of Thermal Spray Technology*, Vol. 19, pp. 110-118.
4. Bala, N., Singh, H., Karthikeyan, J. and Prakash, S., (2012), “Performance of cold sprayed Ni-20Cr and Ni-50Cr coatings on SA 516 steel in actual industrial environment of a coal fired boiler,” *Vol.14*, pp. 568-580.
5. Bala Ganesh Reddy Majji, Hitesh Vasudev, Amit Bansal. "A review on the oxidation and wear behavior of the thermally sprayed high-entropy alloys" , *Materials Today: Proceedings*, 2021.
6. Bala Ganesh Reddy Majji, Hitesh Vasudev, Amit Bansal. "Application of plasma-sprayed AlxCrCoFeNi High-Entropy alloys for high-temperature oxidation resistance" , *Materials Letters*, 2024
7. Bansal, P., Padture, N. P. and Vasiliev, A., (2003), “Improved interfacial properties of Al<sub>2</sub>O<sub>3</sub>-13wt%TiO<sub>2</sub> plasma sprayed coatings derived from nanocrystalline powders”, *Acta Materialia*, Vol.51, pp.2959-2970.
8. Baskaran, T., & Arya, S. B., (2017), “Role of thermally grown oxide and oxidation resistance of samarium strontium aluminate based air plasma sprayed ceramic thermal barrier coatings”, *Surface and Coatings Technology*, 326, 299–309.
9. Brand, J., Gadow, R. and Killinger, A., (2004), “Application of diamond-like carbon coatings on steel tools in the production of precision glass components” *Surface and Coatings Technology* , Vol.180, pp. 213–217.
10. Cable, M., (1999), “Mechanization of Glass Manufacture” *Journal of the American Ceramic Society*, Vol.82, pp.1093–1112.
11. Callister, W.D., Rethwisch, D.G. and Balasubramaniam, R., (2017), *Materials science and engineering*, Chaudhary press, Delhi, India.

12. Chatha, S.S., Sidhu, H.S. and Sidhu, B.S., (2012A), "High temperature hot corrosion behaviour of NiCr and Cr<sub>3</sub>C<sub>2</sub>-NiCr coatings on T91 boiler steel in an aggressive environment at 750°C," *Surface Coating and Technology*, Vol. 206, No. 19-20, pp. 3839-3850.
13. Chatha, S.S., Sidhu, H.S. and Sidhu, B.S., (2012B), "Characterisation and corrosion-erosion behaviour of carbide based thermal spray coatings," *The Journal of Minerals and Materials Characterization and Engineering*, Vol. 11, No. 6, pp. 569-586.
14. Chen, D., Jordan, E.H. and Gell, M., (2009), "Solution precursor high-velocity oxy-fuel spray ceramic coatings," *Journal European Ceramic Society*, Vol. 29, pp. 3349-3353.
15. Chen, S. F., Liu, S. Y., Wang, Y., Sun, X. G., Zou, Z. W., Li, X. W., & Wang, C. H., (2014), "Microstructure and properties of HVOF-sprayed NiCrAlY coatings modified by rare earth", *Journal of Thermal Spray Technology*, 23(5), 809–817.
16. Chidambaram, D., Clayton, C.R. and Dorfman, M.R., (2005), "Evaluation of the electrochemical behavior of HVOF-sprayed alloy coatings-II" *Surface Coating and Technology*, Vol. 192, No. 2-3, pp.178-283.
17. Choi, I.S. and Park, J.C., (2000), "The corrosion behaviour of TiAlN coatings prepared by PVD in a hydrofluoric gas atmosphere", *Surface Coatings & Technology*, Vol. 131, pp.383-385.
18. Cingi, M., Arisoy, F., Basman, G. and Sesen, K., (2002), "The effects of metallurgical structures of different alloyed glass mould cast irons on the mould performance" *Materials Letters*, Vol. 55, pp. 360–363.
19. Delaunay, F., Berthier, C., Lenglet, M., & Lameille, J., (2000), "SEM-EDS and XPS Studies of the High Temperature Oxidation Behaviour of Inconel 718", *Mikrochimica Acta*, 132(2–4), 337–343.
20. Dent, A.H., Horlock A.J., Cartney D.G. M. and Harris S.J, (2001), "Microstructural characterisation of a Ni-Cr-B-C based alloy coating produced by high velocity oxy-fuel thermal spraying", *Surface Coating and Technology*, Vol. 139, pp. 244-250.
21. Espallargas, N., Berget, J., Guilemany, J.M., Benedetti, A.V. and Suegama, P.H., (2008), "Cr<sub>3</sub>C<sub>2</sub>-NiCr and WC-Ni thermal spray coatings as alternatives to hard chromium for erosion-corrosion resistance," *Surface Coating and Technology*.

Vol. 202, pp. 1405–1417.

22. Fedrizzi, L., Valentinelli, L., Rossi, S. and Segna, S., (2007), “Tribo Corrosion behavior of HVOF Cermet coatings,” *Corrosion Science*, Vol. 49, pp. 2781-2799
23. Feng, Q., Li, T., Teng, H., Zhang, X., Zhang, Y., Liu, C., & Jin, J., (2008), “Investigation on the corrosion and oxidation resistance of Ni-Al<sub>2</sub>O<sub>3</sub> nano-composite coatings prepared by sediment co-deposition”, *Surface and Coatings Technology*, 202(17), 4137–4144.
24. Firestone, G.C. and Yi, A.Y., (2005), “Precision compression moulding of glass micro lenses and micro lens arrays-an experimental study” *Applied Optics*, Vol. 29, pp. 6115-6122.
25. Gao, J., He, Y., & Wang, D., (2010), “Fabrication and high temperature oxidation resistance of ZrO<sub>2</sub>/Al<sub>2</sub>O<sub>3</sub> micro-laminated coatings on stainless steel”, *Materials Chemistry and Physics*, 123(2–3), 731–736.
26. Ghaderi, A. R., Nili Ahmadabadi, M., & Ghasemi, H. M., (2003), “Effect of graphite morphologies on the tribological behavior of austempered cast iron”, *Wear*, 255(1–6), 410–416.
27. Ghriba, T., Tlilib, B., Nouveauc, C., Benlatrech, Y., Lambertin, M., Yacoubi, N. and Ennasr, M., (2009), “Experimental investigation of the mechanical micro structural and thermal properties of thin CrAlN layers deposited by PVD technique for various aluminium percentages” *Physics Procedia*, pp. 1327–1336.
28. Gil, L., and Staia, M.H., (2002), “Influence of HVOF parameters on the corrosion resistance of NiWCrBSi coatings” *Thin Solid Films*, Vol. 420 –421, pp. 446–454.
29. Goswami, D.Y., (2004), *The CRC Handbook of Mechanical Engineering*, CRC Press, New York, USA.
30. Grewal, H. S., Singh, H., & Agrawal, A., (2013a), “Microstructural and mechanical characterization of thermal sprayed nickel-alumina composite coatings”, *Surface and Coatings Technology*, 216, 78–92.
31. Grewal, H. S., Singh, H., & Agrawal, A., (2013b), “Understanding Liquid Impingement erosion behaviour of nickel-alumina based thermal spray coatings”, *Wear*, 301(1–2), 424–433.
32. Griffith, J. D, (1975), United States Patent 1191, 5, 5–10.
33. Guilemany, J.M., De Paco, J.M., Miguel, J.R, Sanchez, J. and Smith, P., (1998), “Corrosion Resistance HVOF Coatings Based Upon TiC+ NiTiC and (Ti,W)C +

- Ni,” Thermal Spray: Meeting the Challenges of the 21st, Century, C. Coddet, Ed., May 25-29, 1998 (Nice, France), ASM International, pp. 57-61.
34. Guilemany, J.M., Espallargas, N., Suegama, P.H. and Benedetti, A.V., (2006), “Comparative Study of  $\text{Cr}_3\text{C}_2$ -NiCr Coatings Obtained by HVOF and Hard Chromium Coatings,” Corrosion Science, Vol. 48, pp. 2998-3013.
  35. Hatate, M., Shiota, T., Takahashi, N., & Shimizu, K., (2001), “Influences of graphite shapes on wear characteristics of austempered cast iron”, Wear, 250–251, 885–889.
  36. Heath, G. R., Heimgartner, P., Irons, G., Miller, R. and Gustafsson, S., (1997), “An Assessment of Thermal Spray Coating Technologies for High Temperature Corrosion Protection,” Material Science Forum, Vol. 251-54, pp. 809-816.
  37. Hecht, R. L., Dinwiddie, R. B., & Wang, H., (1999), “Effect of graphite flake morphology on the thermal diffusivity of gray cast irons used for automotive brake discs”, Journal of Materials Science, 34(19), 4775–4781.
  38. Hemanth, J. (2000), “Wear characteristics of austempered chilled ductile iron” Materials and Design, Vol. 21, pp. 139-148.
  39. Hidalgo, V. H., Varela J. B., Menéndez A. C. and Martýnez S. P., (2001), “High temperature erosion wear of flame and plasma-sprayed nickel–chromium coatings under simulated coal-fired boiler atmospheres”, Wear, Vol. 247, pp. 214–222.
  40. Hidalgo, V. H., Varela, F. J. B. and Rico, E. F., (1997), “Erosion Wear and Mechanical Properties of Plasma-Sprayed Nickel- and Iron-Based Coatings Subjected to Service Conditions in Boilers,” Tribology International, Vol. 30, No. 9, pp. 641-649.
  41. Hidalgo, V. H., Varela, J. B., Calle, J. M. de la and Menendez, A. C., (2000), “Characterisation of NiCr Flame and Plasma Sprayed Coatings for Use in High Temperature Regions of Boilers,” Surface Engineering, Vol. 16, No. 2, pp. 137-142.
  42. Hock, M., Schaffer, E., Doll, W. and Klee, G., (2003), “Composite coating materials for the moulding of diffractive and refractive optical components of inorganic glasses “Surface and Coatings Technology, Vol. 163 –164 , pp. 689–694.
  43. Hocking, M.G., (1993), “Coatings Resistant to Erosive/Corrosive and Severe Environments,” Surface Coating and Technology., Vol. 62, pp. 460-466.



44. Holmberg, k. and Mathews, A., (2009), "Coatings tribology properties, mechanisms, techniques and applications in surface engineering" Elsevier Tribology and interface engineering series , Second edition , 56, Elsevier , Amsterdam, the Netherlands,2009.
45. Hones, P., Consiglio, R., Randall, N. and Levy, F., (2000), "Mechanical properties of hard chromium tungsten nitride coatings" Surface and Coatings Technology, Vol. 125, pp. 179–184.
46. Hu, H. X., Jiang, S. L., Tao, Y. S., Xiong, T. Y., & Zheng, Y. G., (2011), "Cavitation erosion and jet impingement erosion mechanism of cold sprayed Ni-Al<sub>2</sub>O<sub>3</sub>coating", Nuclear Engineering and Design, 241(12), 4929–4937.
47. Ishikawa, K., Seki, M. and Tobe, S., (1993), "Application of Thermal Spray Coatings to Prevent Corrosion of Construction in Japan," Proc. of the 5th Natioanal Thermal Spraying Conference, Anaheim, CA, USA, (1993), pp.679-684.
48. Istikamah, S., Fazira, M. F., & Talib, R. J., (2011), Atmospheric Plasma Spray of NiCrAlY Bond Coat with Different Feed Rates. Solid State Science and Technology, 19(1), 32–39.
49. Jiwang, Y., Takashi O., Tianfeng, Z. and Tsunemoto, K., (2009), "Precision machining of microstructures on electroless-plated NiP surface for moulding glass components", Journal of Materials Processing Technology, Vol.209, pp. 4802–4808.
50. Kalss, W., Reiter, A., Derfingher, V., Gey, C. and Endrino, J.L., (2006), "Modern coatings in high performance cutting applications", International Journal of Refractory Metals & Hard Materials, Vol. 24, pp 399-404.
51. Kamal, S. Jayaganthan, R., Prakash, S. and Kumar, S., (2008), "Hot Corrosion Behavior of Detonation Gun Sprayed Cr<sub>3</sub>C<sub>2</sub>-NiCr Coatings on Ni and Fe-based Superalloys in Na<sub>2</sub>SO<sub>4</sub>-60%V<sub>2</sub>O<sub>5</sub> Environment at 900°C," Journal of Alloys and Compounds, Vol. 463, No. 1-2, pp. 358-372.
52. Kamal, S. Jayaganthan, R., Prakash, S. and Kumar, S., (2009A), "Evaluation of cyclic hot corrosion behaviour of detonation gun sprayed Cr<sub>3</sub>C<sub>2</sub>-25%NiCr coatings on nickel- and iron-based superalloys," Surface Coating and Technology., Vol. 203, pp. 1004-1013.
53. Karaoglanli, A. C., Altuncu, E., Ozdemir, I., Turk, A., & Ustel, F., (2011),

- “Structure and durability evaluation of YSZ+Al<sub>2</sub>O<sub>3</sub> composite TBCs with APS and HVOF bond coats under thermal cycling conditions”, *Surface and Coatings Technology*, 205, S369–S373.
54. Kaur, M. and Singh, H., (2008), “A survey of the literature on the use of high velocity oxy-fuel spray technology for high temperature corrosion and erosion-corrosion resistant coatings,” *Anti-Corrosion Methods and Materials*, Vol. 55, No.2, pp. 86–96.
  55. Kaur, M., Singh, H. and Prakash, S., (2011), “Studies on Role of Detonation-Gun Sprayed WC-Co Coatings to Combat High Temperature Corrosion of Boiler Steel”, *International Journal of Surface Engineering & Materials Technology*, Vol. 01, pp. 33-38.
  56. Kaur, M., Singh, H. and Prakash, S., (2011), “Surface engineering analysis of detonation-gun sprayed Cr<sub>3</sub>C<sub>2</sub>–NiCr coating under high-temperature oxidation and oxidation–erosion environments” *Surface & Coatings Technology*, Vol. 206, pp. 530–541.
  57. Kaur, M., Singh, H. and Prakash, S., (2009A), “High Temperature Corrosion Studies of HVOF Sprayed Cr<sub>3</sub>C<sub>2</sub>-NiCr Coating on SAE-347H Boiler Steel,” *Journal of Thermal Spray Technology*, Vol. 18, No. 4, pp. 619-632.
  58. Kaur, M., Singh, H. and Prakash, S., (2011), “Surface engineering analysis of detonation-gun sprayed Cr<sub>3</sub>C<sub>2</sub>-NiCr coating under high-temperature oxidation and oxidation–erosion environments,” *Surface Coating and Technology*, Vol. 206, pp. 530-541.
  59. Kaur, M., Singh, H., & Prakash, S., (2011), Surface engineering analysis of detonation-gun sprayed Cr<sub>3</sub>C<sub>2</sub>-NiCr coating under high-temperature oxidation and oxidation-erosion environments. *Surface and Coatings Technology*, 206(2–3), 530–541.
  60. Kaur, M., Singh, H., Singh, B. and Singh, B., (2009B), “Studies on the Sliding Wear Performance of Plasma Spray Ni-20Cr and Ni3Al Coatings,” *Journal of Thermal Spray Technology*. Vol. 19, Nos. 1-2, pp. 3378-3383.
  61. Kaur, N., Kumar, M., Sharma, S. K., Kim, D. Y., Kumar, S., Chavan, N. M., Singh, H., (2015), “Study of mechanical properties and high temperature oxidation behavior of a novel cold-spray Ni-20Cr coating on boiler steels”, *Applied Surface Science*, 328, 13–25.

62. Kaushal, G. Singh, H. and Prakash, S., (2011), "High Temperature Erosion-Corrosion Performance of HVOF Sprayed Ni-20Cr Coating in Actual Boiler Environment," Metallurgical and Materials Transactions. A, Volume 42, No. 7, pp. 1836-1846.
63. Kaushal, G. Singh, H. and Prakash, S., (2011), "High Temperature Corrosion Behavior of HVOF- Sprayed Ni-20Cr Coating on Boiler Steel in Molten Salt Environment at 900°C," International Journal of Surface Science and Engineering, Vol. 5, No. 1, pp. 45-53.
64. Kaushal, G. Singh, H. and Prakash, S., (2011B), "Comparative High Temperature Analysis of HVOF Sprayed and Detonation Gun Sprayed Ni-20Cr Coating in Laboratory and Actual Boiler Environments," Oxidation of Metals, Volume 76, No.3-4, pp 169-191.
65. Kaushal, S., Gupta, D., & Bhowmick, H., (2017), "An approach for functionally graded cladding of composite material on austenitic stainless steel substrate through microwave heating", Journal of Composite Materials, (Mmc), 2199831770597.
66. Khanna, A.S., (2002), "Introduction to High Temperature Oxidation and Corrosion," ASM International, Materials Park, Ohio.
67. Khanna, A.S., Kumari, S., Kanungo, S. and Gasser, A., (2009), "Hard Coatings Based on Thermal Spray and Laser Cladding," International Journal of Refractory Metals and Hard Materials, Vol. 27, pp. 485-491.
68. Kim, S., Cockcroft, S., L, Omran, A M. and Hwang, H., (2009), "Mechanical wear and heat exposure properties of compacted graphite cast iron at elevated temperatures' Journal of Alloys and Compounds, Vol. 487, pp. 253–257.
69. Kleer, G. and Doell, W., (1997), "Ceramic multilayer coatings for glass moulding applications" Surface and Coatings Technology, Vol. 94-95, pp. 647-651.
70. Koivuluoto, H., & Vuoristo, P., (2009), "Effect of ceramic particles on properties of cold sprayed Ni–20Cr + Al<sub>2</sub>O<sub>3</sub> coatings", Journal of thermal spray technology, 18, 555–562.
71. Kong, G., Zhang, D., Brown, P.D., McCartney, D.G. and Harris, S.J., (2003), "Microstructural Characterisation of HVOF Thermally Sprayed Stellite 6," Mater. Sci. Technol., Vol. 19, pp.1003-1011.

72. Kuar, N., Kumar, M., Kumar, S., Joshi, S.V. and Singh, H., (2015), "Study of mechanical properties and high temperature oxidation behaviour of a novel cold-spray Ni-20Cr coatings on boiler steels", *Applied surface science*, Vol.328, pp. 13-25.
73. Kumar, M., Singh, H., Singh, N., & Joshi, R. S., (2015), "Erosion-corrosion behavior of cold-spray nanostructured Ni-20Cr coatings in actual boiler environment", *Wear*, 332–333, 1035–1043.
74. Labrecque, C., & Gagné, M., (1998), "Ductile Iron: Fifty Years of Continuous Development", *Canadian Metallurgical Quarterly*, 37(5), 343–378.
75. Lai, G Y, Pub. ASM International (1990) Chapter 3, 15.
76. Lee, C.H. and Min, K.O., (2000), "Effects of heat treatment on the microstructure and properties of HVOF-sprayed Ni-Cr-W-Mo-B alloy coatings", *Surface Coating and Technology*, Vol.132, pp. 49-57.
77. Lee, S.H., (2009), "High-Temperature Corrosion Phenomena in Waste-to-Energy Boilers," Ph.D Thesis, Gradual School of Arts and Sciences, Columbia University.
78. Lembke, M.I., Lewis, D.B. and Munz, W.D., (2000), "Localised oxidation defects inTiAlN/CrN superlattice structured hard coatings grown by cathodic arc/unbalanced magnetron deposition on various substrate materials", *Surface and Coatings Technology*, Vol. 125, pp. 263–268.
79. Leushin, I.O. and Chistyakov, D.G., (2014), "Analysis of Cracking in Glass Moulds Made of Cast Iron" *Russian Metallurgy (Metally)*, Vol.9, pp. 768–771
80. Levy, A.V., (1993), "The Erosion-Corrosion of Tubing Steels in Combustion Boiler Environments," *Corrosion Science*, Vol. 35, Nos. 5-8, pp. 1035-1043.
81. Li, C.J., Li, W.Y., (2003), "Effect of sprayed powder particle size on the oxidation behavior of MCrAlY materials during high velocity oxygen-fuel deposition", *Surface Coating and Technology* Vol.162, pp. 31–41.
82. Li, G.C., Li, C.J., Wang, Y.Y. and Li, W.Y., (2007), "Erosion Performance of HVOF sprayed Cr<sub>3</sub>C<sub>2</sub>-NiCr coatings", *Journal of Thermal Spray Technology*, Vol. 16, No. 4, 557-565.
83. Liang, B. and Ding, C., (2005), "Thermal shock resistance of nano-structured and conventional zirconia coatings deposited by atmospheric spraying", *Surface & Coating Technology journal*, Vol.197, pp.85-192.

84. Limarga, A. M., Widjaja, S., & Yip, T. H., (2005), "Mechanical properties and oxidation resistance of plasma-sprayed multilayered  $\text{Al}_2\text{O}_3/\text{ZrO}_2$  thermal barrier coatings", *Surface and Coatings Technology*, 197(1), 93–102.
85. Lin, M.-B., Wang, C.-J., & Volinsky, A. A., (2011), "High Temperature Oxidation Behavior of Flake and Spheroidal Graphite Cast Irons", *Oxidation of Metals*, 76(3–4), 161–168.
86. Lin, X., Zeng, Y., Ding, C. and Zhang, P., (2004), "Effects of temperature on tribological properties of nanostructured and conventional  $\text{Al}_2\text{O}_3$ -3wt%  $\text{TiO}_2$  coatings", *Wear*, Vol.256, pp. 1018-1025.
87. Liscano, S., Gil, L., Leon, O.A., Cruz, M. and Staia, MH., (2006), "Corrosion performance of duplex treatments based on plasma nitriding and PAPVD TiAlN coating", *Surface Coatings & Technology*, Vol. 201, pp. 4419-4423.
88. Liu, Y., Fischer, T. E. and Dent, A., (2003), "Comparison of HVOF and plasma-sprayed alumina/titania coatings-microstructure, mechanical properties and abrasion behavior", *Surface Coating and Technology* Vol. 167, pp. 68–76.
89. Lugschider, E., Herbst, C. and Zhao, L., (1998), "Parameter Studies on High Velocity Oxy-Fuel Spraying of MCrAlY Coatings," *Surface Coating and Technology*, Vol. 108-109, pp. 16-23.
90. Lyphout, C., Fasth, A., & Nylen, P., (2014), "Mechanical property of HVOF inconel 718 coating for aeronautic repair", *Journal of Thermal Spray Technology*, 23(3), 380–388.
91. Lyphout, C., Nylén, P., & Östergren, L., (2011), "Relationships between process parameters, microstructure, and adhesion strength of HVOF sprayed IN718 coatings", *Journal of Thermal Spray Technology*, 20(1–2), 76–82.
92. Lyphout, C., Nylén, P., Manescu, A., & Pirling, T., (2008), "Residual stresses distribution through thick HVOF sprayed inconel 718 coatings", *Journal of Thermal Spray Technology*, 17(5–6), 915–923.
93. Ma, K.J., Chien, H.H, Chuan, W.H, Chao, C. L. and Hwang, K.C., (2008), "Design of Protective Coatings for Glass Lens Moulding" *Key Engineering Materials*, Vol. 364-366, pp. 655-661.
94. Mahesh, R.A., Jayaganthan, R. and Prakash, S., (2009A), "Microstructural characterization and hardness evaluation of HVOF sprayed Ni–5Al coatings on Ni- and Fe-based superalloys," *Journal of Material Processing and Technology*, Vol. 209, pp. 3501-3510.

95. Mahesh, R.A., Jayaganthan, R., Prakash, S., (2009B), "Microstructural characteristics and mechanical properties of HVOF sprayed NiCrAl coating on superalloys," *Journal of Alloys and Compounds*, Vol. 468, pp. 392-405.
96. Mashloosh, K.M., (2015), "Wear resistance of different types of cast iron used in glass blow mould" *Diyala Journal of Engineering Sciences*, Vol. 08, pp. 3-12.
97. Masud, J., Yan, J., Zhou, T., Kuriyagawa, T. and Fukase, Y., (2011), "Thermally induced atomic diffusion at the interface between release agent coating and mould substrate in a glass moulding press" *Journal of physics*, Vol. 44, pp. 215-302.
98. Matthews, S., Hyland, M. and James, B., (2004), "Long-Term Carbide Development in High-Velocity Oxygen Fuel/High-Velocity Air Fuel  $\text{Cr}_3\text{C}_2$ -NiCr Coatings Heat Treated at  $900^\circ\text{C}$ ," *Journal of Thermal Spray Technology*, Vol. 13, No. 4, pp. 526-536.
99. Matthews, S.J., James, B.J. and Hyland, M.M., (2007), "Microstructural influence on erosion behaviour of thermal spray coatings," *Material Characterization*, Vol. 58, pp. 59-64.
100. Mayrhofer, P.H., Kunc, F., Musil, J. and Mitter, C., (2002), "A comparative study on reactive and non-reactive unbalanced magnetron sputters deposition of TiN coatings" *Thin Solid Films*, Vol. 415, pp. 151–159.
101. Mayrhofer, P.H., Tischler, G. and Mitter, C., (2001), "Microstructure and mechanical/thermal properties of Cr-N coatings deposited by reactive unbalanced magnetron sputtering" *Surface and Coatings Technology*, Vol. 142-144, pp. 78-84.
102. Metals Handbook, (1961), "Properties and Selection of Metals, 8th Edition," Vol. 1, ASM Publication, Metals Park Ohio.
103. Miguel, J. M., Guilemany, J. M., & Vizcaino, S., (2003), "Tribological study of NiCrBSi coating obtained by different processes", *Tribology International*, 36(3), 181–187.
104. Miguel, J.M., Guilemany, J.M., Mellor, B.G. and Xu, Y.M., (2003A), "Acoustic emission study on WC–Co thermal sprayed coatings," *Material Science Engineering A*, Vol. 352, No. 1-2, pp. 55-63.
105. Mishra, S.B., Prakash, S. and Chandra, K., (2006), "Studies on erosion behaviour of plasma sprayed coatings on a Ni-based superalloy", *Wear*, Vol. 260, pp. 422-432.
106. Muhammad, R., Wahab, N. A., & Rakik, R., (2017), "Study on thermal behavior of Inconel 718 thermal cyclic behaviour", *Wear*, 12(6), 1915–1921.
107. Nicholls, J.R., (2000), "Designing Oxidation-Resistant Coatings," *JOM*, pp. 28-35.

108. Nishiyama, S., Takahashi, E., Iwamoto, Y., Ebe, A., Kuratani, N. And Ogata, K., (1996), "Boron nitride hard coatings by ion beam and vapour deposition" *Thin Solid Films*, Vol. 281-282, pp. 327-330.
109. Pawlowski, L., (1995), "The Science and Engineering of Thermal Spray Coatings," Wiley, New York, 1995.
110. Prakash, S., Puri, D. and Singh H., (2005), "Hot Corrosion Behaviour of Plasma Sprayed Coatings on a Ni-Based Superalloy in Na<sub>2</sub>SO<sub>4</sub> -60% V<sub>2</sub>O<sub>5</sub> Environment," *International Surface journal*, Vol. 45, No. 6, pp. 886-895.
111. Prakash, S., Singh, S., Sidhu, B. S. and Madhesia, A., (2001), "Tube Failures in Coal Fired Boilers," *Proc. National Seminar on Advances in Material and Processing*, 9-10th Nov., IIT, Roorkee, India, pp. 245-53.
112. Prasad, A. and Gupta, D., (2013), "Microwave Cladding-Emerging innovative cladding process" *Proc. Of Int. Conf. on Emerging Trends in Engineering and Technology*, pp.506-510.
113. Praveen, A. S., Sarangan, J., Suresh, S., & Siva Subramanian, J., (2015), "Erosion wear behaviour of plasma sprayed NiCrSiB/Al<sub>2</sub>O<sub>3</sub> composite coating.", *International Journal of Refractory Metals and Hard Materials*, 52, 209–218.
114. Priyantha, N., Jayaweera, P., Sanjurjo, A., Lau, K. and K. Krish., (2003), "Corrosion-resistant metallic coatings for applications in highly aggressive environment", *Surface & Coating Technology*, Vol. 163-164, pp. 31-36.
115. Priyantha, N., Jayaweera, P., Sanjurjo, A., Lau, K., Lu, F. and Krist, K., (2003), "Corrosion-Resistant Metallic Coatings for Applications in Highly Aggressive Environments," *Surface Coating and Technology*. Vol. 163-64, pp. 31-36.
116. Provot, X., Burlet, H., Vardayoulias, M., Jeandin, M. and Richard, C., (1993), "Comparative Studies of Microstructures, Residual Stress Distributions and Wear Properties for HVOF and APS WC-Co Coatings of Ti6Al4V," *Proc. NTSC, Anaheim, USA*, pp. 159-166.
117. Ramesh, C. S., Devaraj, D. S., Keshavamurthy, R., & Sridhar, B. R., (2011), "Slurry erosive wear behaviour of thermally sprayed Inconel-718 coatings by APS process", *Wear*, 271(9–10), 1365–1371.
118. Rieser, D., Spie, G. and Manns, G., (2008), "Investigations on glass-to-mould sticking in the hot forming process" *Journal of Non-Crystalline Solids*, Vol.354, pp. 1393–1397.

119. Roy, M., Pauschitz A., Polak R. and Franek, F., (2006), "Comparative evaluation of ambient temperature friction behaviour of thermal sprayed  $\text{Cr}_3\text{C}_2$ -25(Ni-20Cr) coatings with conventional and nano-crystalline grains," *Tribology International*, Vol.39, pp. 29-38.
120. Roy, M., Pauschitz A., Wernisch J. and Franek, F., (2004), "The influence of temperature on the wear of  $\text{Cr}_3\text{C}_2$ -25(Ni20Cr) coating comparison between nanocrystalline grains and conventional grains," *Wear*, Vol.257, pp. 799-811
121. Sarhadi, A., Hattel, J.H. and Hansen, H.N., (2014), "Evaluation of the visco-elastic behaviour and glass/mould interface friction coefficient in the wafer based precision glass moulding" *Journal of Materials Processing Technology*, Vol. 214, pp. 1427-1435.
122. Sidhu, B.S. and Prakash, S., (2003), "Evaluation of the corrosion behaviour of plasma sprayed  $\text{Ni}_3\text{Al}$  coatings on steel in oxidation and molten salt environments at 9000C", *Surface & coatings technology*, Vol.166, pp. 89-100.
123. Sidhu, B.S. and Prakash, S., (2003), "Evaluation of the Corrosion Behaviour of Plasma-Sprayed  $\text{Ni}_3\text{Al}$  Coatings on Steel in Oxidation and Molten Salt Environment at 9000C," *Surface Coating and Technology*, Vol. 166, No. 1, pp. 89-100.
124. Sidhu, B.S. and Prakash, S., (2006G), "Evaluation of the Behavior of Shrouded Plasma Spray Coatings in the Platen Superheater of Coal-Fired Boilers," *Metals and Material Transactio A*, Vol. 37a, pp. 19-27.
125. Sidhu, B.S. and Prakash, S., (2006H), "Evaluation of the Behavior of Shrouded Plasma Spray Coatings in the Platen Superheater of Coal-Fired Boilers," *Metal Material Transaction A*, Vol. 37A, pp. 1927-1936.
126. Sidhu, B.S., Puri, D. and Prakash, S., (2005A), "Mechanical and Metallurgical Properties of Plasma Sprayed and Laser Remelted Ni-20Cr and Stellite-6 Coatings," *Journal of Material Processing and Technology.*, Vol. 159, No. 3, pp. 347-355.
127. Sidhu, H.S., Singh, B.S. and Prakash, S., (2006D), "The Role of HVOF Coatings in Improving Hot Corrosion Resistance of ASTM-SA210 GrA1 Steel in the Presence of  $\text{Na}_2\text{SO}_4$ - $\text{V}_2\text{O}_5$  Salt Deposits," *Surface Coating and Technology*, Vol. 200, No. 18- 19, pp. 5386-5394.
128. Sidhu, T.S., Agarwal, R.D. and Prakash, S., (2006E), "Studies of the metallurgical and mechanical properties of high velocity oxy-fuel sprayed stellite-6 coatings on



- Ni- and Fe-based superalloys,” *Surface Coating and Technology* Vol. 201, pp. 273-281.
129. Sidhu, T.S., Agarwal, R.D., Prakash, S., and Bhagat, R., (2009), “Erosion-corrosion behaviour of Ni-based superalloy Superni-75 in the real service environment of the boiler”, *Surface Coating and Technology*, Vol. 34, No. 2, pp 299-307.
  130. Sidhu, T.S., Agrawal, R.D. and Prakash, S., (2005B), “Hot corrosion of some superalloys and role of high-velocity oxy-fuel spray coatings—A Review,” *Surface Coating and Technology*, Vol. 198, pp. 441- 446.
  131. Sidhu, T.S., Prakash, S. and Agrawal, R.D., (2006), “Hot corrosion performance of a NiCr coated Ni-based alloy”, *Scripta Materialia*, Vol.55, pp.179-182.
  132. Sidhu, T.S., Prakash, S. and Agrawal, R.D., (2006A), “Performance of a High Velocity Oxy-fuel Sprayed Coatings on a Fe-Based Superalloy in Na<sub>2</sub>SO<sub>4</sub>-60%V<sub>2</sub>O<sub>5</sub> Environment at 900 °C, “Part I: Characterisation of the Coatings,” *Journal of Material Engineering and Performance*, Vol. 15, No. 1, pp. 122 -129.
  133. Sidhu, T.S., Prakash, S. and Agrawal, R.D., (2006B), “Characterizations and Hot Corrosion Resistance of Cr<sub>3</sub>C<sub>2</sub>-NiCr Coating on Ni-Base Superalloys in an Aggressive Environment,” *Journal of Thermal Spray Technology*, Vol. 15, No. 4, pp. 811-816.
  134. Sidhu, T.S., Prakash, S. and Agrawal, R.D., (2006C), “Evaluation of hot corrosion resistance of HVOF coatings on a Ni-based superalloy in molten salt environment,” *Material Science Engineering. A*, Vol. 430, pp. 64-78.
  135. Sidhu, T.S., Prakash, S. and Agrawal, R.D., (2006F), “Hot Corrosion Behaviour of HVOF Sprayed NiCrBSi Coatings on Ni- and Fe- Base Superalloys in Na<sub>2</sub>SO<sub>4</sub>-60%V<sub>2</sub>O<sub>5</sub> Environment at 900°C,” *Acta Materialia*, Vol. 54, No. 3, pp. 773-784.
  136. Sidky, P.S. and Hocking, M.G., (1999), “Review of Inorganic Coatings and Coating Processes For Reducing Wear and Corrosion,” *British Corrosion Journal*, Vol. 34, No. 3, pp. 171-183.
  137. Singh, H., Bala, N., Kaur, N., Sharma, S. K., Kim, D. Y., & Prakash, S., (2015), Effect of additions of TiC and Re on high temperature corrosion performance of cold sprayed Ni-20Cr coatings. *Surface and Coatings Technology*, 280, 50–63.
  138. Singh, H., Prakash, S., Puri, D. and Phase, D.M., (2006A), “Cyclic Oxidation Behavior of Some Plasma-Sprayed Coatings in Na<sub>2</sub>SO<sub>4</sub>-60%V<sub>2</sub>O<sub>5</sub> Environment,”

- Journal of Material Engineering and Performance, Vol. 15, No. 6, pp. 729-741.
139. Singh, H., Puri, D. and Prakash, S., (2005A), "Some Studies on Hot Corrosion Performance of Plasma Sprayed Coatings on a Fe-based Superalloy," Surface Coating and Technology, Vol. 192, No. 1, pp. 27-38.
  140. Singh, H., Puri, D. and Prakash, S., (2005B), "Corrosion Behavior of Plasma-Sprayed Coatings on a Ni-Base Superalloy in Na<sub>2</sub>SO<sub>4</sub>-60 Pct V<sub>2</sub>O<sub>5</sub> Environment at 900 °C," Metallic Material Transaction A, Vol. 36A, pp. 1007-1015.
  141. Speidel, M. O., Hyatt, M. V, Speidel, M. O., & Hyatt, M. V., (2005), High-strength aluminum alloys.
  142. Sreedhar, G., Alam, M. M., & Raja, V. S., (2009), "Hot corrosion behaviour of plasma sprayed YSZ/Al<sub>2</sub>O<sub>3</sub> dispersed NiCrAlY coatings on Inconel-718 superalloy. Surface and Coatings Technology, 204(3), 291–299.
  143. Stlinder, R., (1990), "Properties and selection of Irons, Steels and high performance Alloys" ASM Handbook, Ohio, USA.
  144. Sundararajan, G. Sen, D. and Sivakumar., G., (2005), "The Tribological Behaviour of Detonation Sprayed Coatings: The Importance of Coating Process Parameters", Wear, Vol. 258, pp.377-391.
  145. Sundararajan, T., Kuroda, S., Itagaki, T. and Abe F., (2003A), "Steam Oxidation Resistance of Ni-Cr Thermal Spray Coatings on 9Cr-1Mo Steel. Part 1: 80Ni-20Cr," ISIJ Int., Vol. 43, No.1, pp. 95-103.
  146. Sundararajan, T., Kuroda, S., Itagaki, T. and Abe, F., (2003B), "Steam Oxidation Resistance of HVOF Thermal Sprayed Ni-Cr Coatings," Thermal Spray 2003: Advancing the Science & Applying the Technology, (Ed.) C, Moreau and B. Marpie, pp. 495-502.
  147. Sundararajan, T., Kuroda, S., Itagaki, T. and Abe, F., (2004), "Behaviour of Mn and Si in the Spray Powder during Steam Oxidation of Ni-Cr Thermal Spray Coatings," ISIJ Int., Vol. 44, No.1, pp. 139-144.
  148. Taheri, M., Valefi, Z., & Zangeneh-Madar, K., (2012), "Influence of HVOF process parameters on microstructure and bond strength of NiCrAlY coatings", Surface Engineering, 28(4), 266–272.
  149. Tellkamp, V. L., Lau, M. L., Fabel, a., & Lavernia, E. J., (1997), "Thermal spraying of nanocrystalline inconel 718", Nanostructured Materials, 9(1–8), 489–492.

150. Thakur, L., & Arora, N., (2013), "A comparative study on slurry and dry erosion behaviour of HVOF sprayed WC-CoCr coatings", *Wear*, 303(1–2), 405–411.
151. Thomas, A., El-Wahabi, M., Cabrera, J. M., & Prado, J. M., (2006), "High temperature deformation of Inconel 718", *Journal of Materials Processing Technology*, 177(1–3), 469–472.
152. Tsai, Y.C., Hung, C., Hung, J.C., (2008), "Glass material model for the forming stage of the glass moulding process" *Journal of materials processing technology*, Vol. 201, pp. 751–754.
153. Uusitalo, M.A., Vuoristo, P.M.J., Mantyla, T.A., (2002), "High temperature corrosion of coatings and boiler steels in reducing chlorine-containing atmosphere," *Surface Coating and Technology*, Vol. 161, pp. 275-285.
154. Viskanta, R. and Lim, J.M., (2001), "Theoretical Investigation of Heat Transfer in Glass Forming" *Journal of the American Ceramic Society*, Vol. 84, pp.2296–302.
155. W.Y. Li, Zhang, C., H. Liao, J. Li, Coddet, C., (2008), "Characterizations of cold-sprayed nickel–alumina composite coating with relatively large nickel-coated alumina powder", *Surface and coating technology*, 202, 4855–4860.
156. Wadsworth, I., Smith, I.J., Donohue, L.A. and Miinz, W.D., (1997), "Thermal stability and oxidation resistance of TiAlN/KrN multilayer coatings" *Surface and Coatings Technology*, Vol. 94-95, pp.315-321.
157. Wang, B. Q. and Shui, Z.R., (2002), "The hot erosion behavior of HVOF chromium carbide-metal cermet coatings sprayed with different powders," *Wear*, Vol. 253, pp. 550-557.
158. Wang, B., & Lee, S. W., (2000), "Erosion-corrosion behaviour of HVOF NiAl-Al<sub>2</sub>O<sub>3</sub> intermetallic-ceramic coating", *Wear*, 239(1), 83–90.
159. Wang, B.Q. and Shui, Z.R., (2003), "Hot erosion behaviour of carbide-metal composite coatings", *Journal of Material Proceeding Technology*, Vol. 143-144, pp. 87-92.
160. Wang, B.Q. and Verstak, A., (1999), "Elevated Temperature Erosion of HVOF Cr<sub>3</sub>C<sub>2</sub>/ TiC- NiCrMo Cermet Coating," *Wear*, Vol. 233-235, pp. 342-351.
161. Wang, C.J. and Lin, J.S., (2002), "The oxidation of MAR M247 superalloy with Na<sub>2</sub>SO<sub>4</sub> coating," *Materials Chemistry and Physics*, Vol.76, pp. 123-129.
162. Wang, H.T., Ji G.C., Chen Q.Y., Du X. F. and Fu W., (2011), "The Microstructure and Erosion Wear Performance of HVOF-Sprayed Cr<sub>3</sub>C<sub>2</sub>-NiCr Coatings with

- Different Feedstock Powder,” Advanced Materials Research, Vol. 228-229, pp. 809-812.
163. Weck, M. Winterschlade, M. Pfeifer, T. Dorner, D. Brinksmeier, E. Autschbach, L. Riemer, O., (2005), “Manufacturing of Optical Molds using an Integrated Simulation and Measurement Interface” Proc. of SPIE, 5252.
  164. Yang, G.J., Li, C.J., Zhang, S.J., Li, C.X., (2008), “High-Temperature Erosion of HVOF Sprayed Cr<sub>3</sub>C<sub>2</sub>-NiCr Coating and Mild Steel for Boiler Tubes,” Journal of Thermal Spray Technology, Vol.17, No.5-6, pp.782-787.
  165. Yang, Q., Senda, T. and Ohmori, A., (2003), “Effect of carbide grain size on microstructure and sliding wear behavior of HVOF-sprayed WC–12% Co coatings,” Wear, Vol. 254, No. 1-2, pp. 23-34.
  166. Yin, B., Liu, G., Zhou, H., Chen, J. and Yan, F., (2010), “Sliding wear behavior of HVOF sprayed Cr<sub>3</sub>C<sub>2</sub>-NiCr/CeO<sub>2</sub> Composite coatings at elevated temperature upto 8000C,” Tribology Letter, Vol.37, pp. 463-475.
  167. Zafar, S. and Sharma, A.K., (2016), “Abrasive and erosive wear behaviour of nanometric WC–12Co microwave clads”, Wear, Vol.46-47, pp-29-45.
  168. Zafar, S., & Sharma, A. K., (2016), “Abrasive and erosive wear behaviour of nanometric WC-12Co microwave clads”, Wear, 389–400, pp-145-169.
  169. Zhang, Y., Chen, Y., He, R., & Shen, B., (1993), “Investigation of tribological properties of brake shoe materials - phosphorous cast irons with different graphite morphologies”, Wear, 166(2), 179–186.
  170. Zhao, L. and Lugscheider, E., (2002 B), “Influence of the spraying processes on the properties of 316L stainless steel coatings”, Surface Coating and Technology, Vol. 162, pp. 6-10.
  171. Zhao, L. and Lugscheider, E., (2002A), “High Velocity Oxy-Fuel Spraying of a NiCoCrAlY and an Intermetallic NiAl-TaCr Alloy,” Surface Coating and Technology, Vol. 149, pp. 230-235.
  172. Zhao, W.M., Wang, Y., Dong, L.X., Wu, K.Y. and Xue, J., (2005), “Corrosion Mechanism of NiCrBSi Coatings Deposited by HVOF,” Surface Coating and Technology, Vol. 190, pp. 293-298.
  173. Zhao, W.M., Wang, Y., Han, T., Wu, K.Y. and Xue, J., (2004), “Electrochemical Evaluation of Corrosion Resistance of NiCrBSi Coatings Deposited by HVOF,” Surface Coating and Technology, Vol. 183, pp. 118-125.

174. Zhong, D., Mateeva, E., Dahan, I., Moore, J., Mustoe, G.W., Ohno, T., Disamc, J. And Thiel, S. (2000), "Wettability of NiAl, Ni-Al-N, Ti-B-C, and Ti-B-C-N films by glass at high temperatures" Surface and Coatings Technology, Vol. 133-134,8-12.
175. Sharma AK and Krishnamurthy R (2010), "Sliding wear characterization of microwave-glazed plasma-sprayed ceramic composites", Proc.Inst. Mech. Eng. 224 497-51.
176. Zafar S and Sharma AK (2014), "Development and characterisations of WC-12Co microwave clad", Materials Characterization. Vol. 96 pp241-249.
177. Zafar S and Sharma AK (2016), Investigations on flexural performance and residual stresses in nanometric WC-12Co microwave clads, Surface Coating and Technology, Vol. 291 pp.413-22.
178. Sidhu T S, Prakash S and Agrawal R D 2005 State of the art of HVOF coating investigations: a review Mar. Technol. Soc. J. 39 53–64.
179. Lee C H and Min K O 2000 Effects of heat treatment on the microstructure and properties of HVOF-sprayed Ni-Cr-W-Mo-B alloy coatings Surf. Coat. Technol. 132 49–57.
180. Guilemany J M, Fernandez J and Delgado J 2001 Influence of thermal treatments in the corrosion behaviour of HVOF Cr<sub>3</sub>C<sub>2</sub>-NiCr coatings ed C C Berndt and K A Khor Thermal Spray 2001: New Surfaces for a New Millennium, (ASM International: Materials Park, Ohio) 1165-1169.
181. Guilemany J M, Miguel J M, Vizcaino S, Lorenzana C, Delgado J and Sanchez J 2002 Role of heat treatments in the improvement of the sliding wear properties of Cr<sub>3</sub>C<sub>2</sub>-NiCr coatings Surf. Coat. Technol. 157 207-13.
182. Praveen A S, Sarangan J, Suresh S and Subramanian J S 2015 Erosion wear behaviour of plasma sprayed NiCrSiB/Al<sub>2</sub>O<sub>3</sub> composite coating Int. J. Refract. Met. Hard Mater 52 209-218.
183. Grewal H S, Singh H and Agarwal A 2013 Understanding liquid impingement erosion behaviour of nickel-alumina based thermal spray coatings Wear 301 424-433.
184. Bala N, Singh H and Prakash S 2017 Performance of cold sprayed Ni based coatings in actual boiler environment Surf. Coat. Technol. 318 50-61.

185. Afzal M, Ajmal M, Khan A N, Hussain A and Akhter R 2014 Surface modification of air plasma spraying WC–12% Co cermet coating by laser melting technique Opt. Laser Technol. 56 202-206.
186. Sidhu B S, Puri D and Prakash S 2005 Mechanical and metallurgical properties of plasma sprayed and laser remelted Ni-20Cr and stellite-6 coatings J. Mater. Process. Technol. 159 347-355.
187. Zafar S and Sharma A K 2017 Microstructure and mechanical properties of microwave post-processed Ni coating J. Mater. Eng. Perform. 26 1382-1390.

## LIST OF PUBLICATIONS

1. Bala Ganesh Reddy Majji, H. Vasudev, and A. Bansal, "A review on the oxidation and wear behavior of the thermally sprayed high-entropy alloys," *Materials Today: Proceedings*, **Volume 50, Part 5**, 2022, Pages 1447-1451 (Elsevier, Scopus Indexed).

<https://doi.org/10.1016/j.matpr.2021.09.016>



### A review on the oxidation and wear behavior of the thermally sprayed high-entropy alloys

Bala Ganesh Reddy Majji<sup>a,\*</sup>, Hitesh Vasudev<sup>a,\*</sup>, Amit Bansal<sup>b</sup>

<sup>a</sup> School of Mechanical Engineering, Lovely Professional University, Phagwara 144411, India  
<sup>b</sup> IKGPTU, Kapurthala, India

#### ARTICLE INFO

**Article history:**  
Received 26 July 2021  
Received in revised form 29 August 2021  
Accepted 2 September 2021  
Available online xxxx

**Keywords:**  
High entropy alloy  
Thermal spraying  
Feedstock  
Oxidation  
Wear

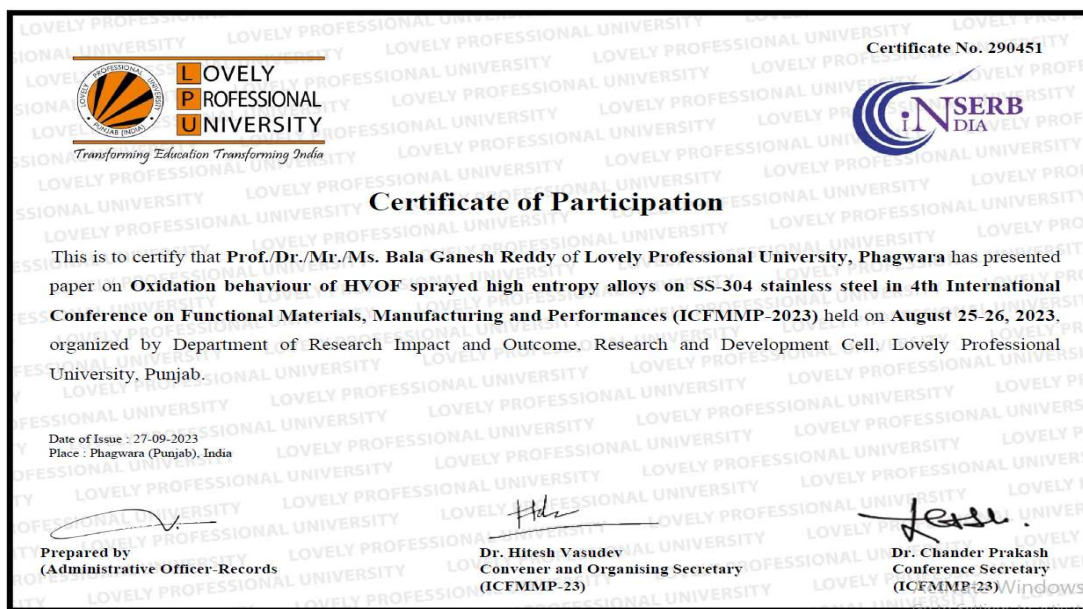
#### ABSTRACT

Several researchers, scientists, and academics have recently become interested in high entropy alloys (HEAs) in order to attain unusual and excellent qualities that are not possible with normal alloys. HEAs are multi-component alloys made up of at least 5 metallic elements which are mixed in unequal or equal molar ratios. In the previous decade, the rapid growth of this discipline has resulted in a large number of research papers. The current paper focuses on the creation of high-entropy alloy-based coatings. The current paper focuses on the thermal spray technique, which is used to combat wear and corrosion in various industrial applications. The mechanical behavior of thermal spray HEA coating is reviewed in electrochemical properties, their oxidation, tribological properties, hardness, and porosity terms as well as their prospective applications are discussed. New evidence that thermally sprayed HEA coatings outperform traditional materials has sparked more research into this area.

Copyright © 2021 Elsevier Ltd. All rights reserved.

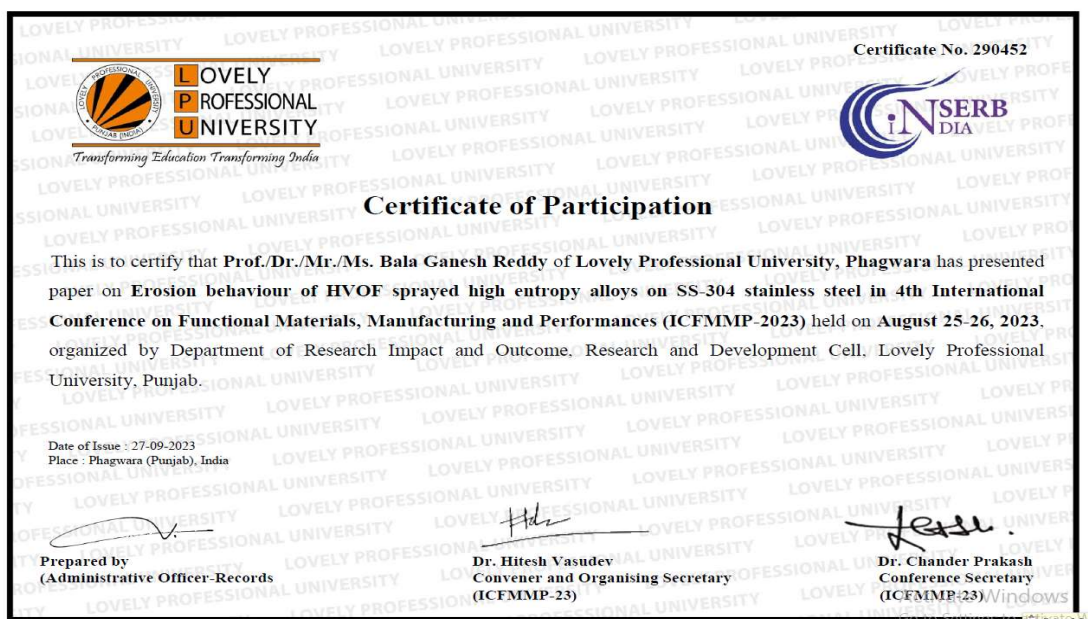
Selection and peer-review under responsibility of the scientific committee of the 2nd International Conference on Functional Material, Manufacturing and Performances

1. Paper presented in International Conference at ICFMMP-2023a at LPU.





2. Paper presented in International Conference at ICFMMP-2023a at LPU.



Bala Ganesh Reddy Majji, H. Vasudev, and A. Bansal, "AIP conference Proceedings Microstructural analysis of high-entropy alloys," 2022 (SCOPUS INDEXED CONFERENCE PROCEEDINGS)





3. Majji, Bala Ganesh Reddy, Hitesh Vasudev, and Amit Bansal. "Application of plasma-sprayed  $\text{Al}_x\text{CrCoFeNi}$  High-Entropy alloys for high-temperature oxidation resistance." *Materials Letters* (2024): 136069. (Impact Factor: 3, Elsevier).

<https://doi.org/10.1016/j.matlet.2024.136069>

Materials Letters 361 (2024) 136069



Contents lists available at ScienceDirect

Materials Letters

journal homepage: [www.elsevier.com/locate/matlet](http://www.elsevier.com/locate/matlet)



## Application of plasma-sprayed $\text{Al}_x\text{CrCoFeNi}$ High-Entropy alloys for high-temperature oxidation resistance

Bala Ganesh Reddy Majji<sup>a</sup>, Hitesh Vasudev<sup>a,c,\*</sup>, Amit Bansal<sup>b</sup>

<sup>a</sup> School of Mechanical Engineering, Lovely Professional University, Phagwara 144411, India

<sup>b</sup> IKGPTU, Kapurthala, India

<sup>c</sup> Research and Development Cell, Lovely Professional University, Phagwara, 144111-India

### ARTICLE INFO

#### Keywords:

High entropy alloys  
Oxidation  
Surfaces  
Thick films

### ABSTRACT

The HEAs were deposited in the form of coatings by using a plasma spraying process on SS-304 substrate material. The fraction  $x$  was varied from 0 to 1 ( $x = 0$ ,  $x = 0.5$ , and  $x = 1$ ) for Al in the HEAs and three coatings were deposited. The high-temperature oxidation test was conducted at 800 °C for 50 cycles. The  $\text{Al}_1\text{CrCoFeNi}$  coating has demonstrated maximum oxidation resistance. The microhardness was found to be maximum in the case of  $\text{Al}_1\text{CrCoFeNi}$  High-Entropy alloy coating ( $540 \pm 11 \text{ HV}_{0.3}$ ). The main reason for the enhanced performance is the solid solution strengthening in high-entropy alloys (HEAs) due to a mismatch in atomic size differences among the elements, which is caused by the substantial lattice distortion caused by the higher aluminum content.